GEORGIA INSTITUTE OF TECHNOLOGY
School of Mechanical Engineering
Atlanta, Georgia

RHEOLOGICAL EFFECTS IN THIN FILM LUBRICATION

NSF Grant GK-31154

by

David M. Sanborn
Assistant Professor

Ward O. Winer
Professor

October 15, 1971 --
September 30, 1974

GEORGIA INSTITUTE OF TECHNOLOGY
School of Mechanical Engineering
Atlanta, Georgia

RHEOLOGICAL EFFECTS IN THIN FILM LUBRICATION

NSF Grant GK-31154

by

David M. Sanborn
Assistant Professor

Ward O. Winer
Professor

October 15, 1971 --
September 30, 1974

GEORGIA INSTITUTE OF TECHNOLOGY
School of Mechanical Engineering
Atlanta, Georgia

RHEOLOGICAL EFFECTS IN THIN FILM LUBRICATION

Ward O. Winer
Principal Investigator

David M. Sanborn
Principal Investigator

Stothe P. Kezios, Director
School of Mechanical Engineering

November, 1974

SUMMARY

The variation of viscosity with pressure, temperature and shear stress has been obtained experimentally for a large group of lubricants at conditions approaching those found in highly loaded (elastohydrodynamic) bearing contacts. It has been shown that many fluids thought to be shear thinning at high shear stresses are, in fact, Newtonian and that apparent viscosity losses can be attributed to viscous heating in the capillary.

The sliding elastohydrodynamic point contact has been studied experimentally in detail, with particular emphasis on the lubricant and bearing surface temperature profiles and the extent of molecular degradation resulting from extreme shear stresses. Temperature rises of 150°C are typical in the lubricant and degradation resulting in up to a 90 percent reduction in molecular weight is possible for high molecular weight fluids.

Analytical investigations applying the lubricant rheological description obtained in the capillary viscometer have resulted in a general solution for rollers and approximate solutions for heavily loaded contacts in general.

APPLICATIONS TO ENGINEERING AND TECHNOLOGY

Because of the extreme importance of bearing reliability and low energy dissipation to the efficient operation of almost every mechanical device, any increase in an understanding of the mechanisms involved and the rheology of the lubricants used will be beneficial. By obtaining a significant amount of rheological data at the extreme conditions typical of bearing operation, less extrapolation of property data will be needed. By obtaining temperature and degradation data in an individual contact for the first time, researchers now know what extreme conditions to expect in these heavily loaded contacts. Finally, through both complete and approximate analytical studies and the resulting dimensionless charts of the results, designers unable to perform individual experiments or comprehensive analyses, can now obtain estimates of the bearing performance.

RESEARCH AND RESULTS

The research conducted was carried out in three phases. The first to be reported are the general rheological investigations of lubricants at extreme levels of pressure and shear stress. The second phase concerns the studies of the behavior of thin film bearings. In this investigation, thin film lubrication has been limited to elastohydrodynamic lubrication. Finally, the third phase of the research consists of attempts to incorporate the rheological findings of phase I to predict the performance of phase II. It is felt that only if the behavior of the lubricated contact can be predicted, can an understanding of the mechanisms and the proper selection of rheological model be assured.

I. Lubricant Rheological Studies at High Pressure and Shear Stress

The lubricant rheology studies were conducted in a high pressure capillary viscometer. The results of these investigations are given in detail in publications 1, 2, 7 and 8 of the Technical Papers prepared under Grant GK-31154 listed below (also attached as Appendix A). The objective of this phase of the research was to determine the effects of pressure, temperature, and shear stress on the viscosity of a wide range of lubricants at conditions as close as possible to those encountered in the elastohydrodynamic bearing contact.

The high pressure capillary viscometer used in these studies had been used in previous investigations, but at lower values of shear stress. In the current investigations the upper limit on pressure was 0.69 GN/m^2 (100 kpsi), with a shear stress range of 30 N/m^2 to 4.8 MN/m^2 and a viscosity range of less than 10^{-3} to more than 10^2 NS/m^2 (.1 to 10^3 Cp). The

temperature of the fluid sample was maintained constant at values ranging from -45 to 232 C. The extreme values of shear stress attainable were a result of using capillaries with very small length-diameter ratios to avoid the viscous heating problem prevalent at high shear stress measurements. By extending the pressure and shear stress capabilities, reliable data can be generated at conditions closed to those found in operating elastohydrodynamic contacts.

In addition to generating pressure-temperature-shear stress-viscosity data, an analytical treatment of the heat dissipation problem in capillary viscometry was also undertaken. This study showed that previous viscosity data obtained at high shear stress for fluids which appeared to be shear thinning, were Newtonian and that the apparent viscosity decreases could be accurately predicted by properly accounting for viscous heating.

The lubricants investigated experimentally included a wide range of typical and experimental lubricants. One class consisted of a series of fourteen siloxane fluids. These fluids were prepared and studied with the objective of determining the influence of the degree of polymerization and the influence of the size and nature of the side radical of siloxanes on the pressure-viscosity behavior. The range of methyl alkyl siloxanes investigated was representative of those most likely to be used as liquid lubricants or mechanical fluids. The viscosity at atmospheric pressure and the viscosity temperature variation both were found to increase as either the degree of polymerization or the number of carbon atoms in the alkyl side radical were increased.

Varying the degree of polymerization or the number of carbon atoms in the alkyl side radicals had little effect (± 10 percent) on the pressure-viscosity coefficient α^* which is believed to be of most importance for elastohydrodynamic lubrication. The range of degree-of-polymerization and size of side radical investigated includes those which might be expected

to be useful for lubrication applications. The pressure-viscosity coefficient α^* can be changed by changing the nature of the side radical on the siloxane chain. Thus if the side radical is hydrogen, as in the methyl hydrogen siloxane, the α^* is reduced and if the side radical is a phenyl group or a trifluoropropyl group the α^* is increased compared with the dimethyl or methyl-alkyl siloxanes. The decrease of the pressure-viscosity coefficient α^* with increasing temperature reported for most of these fluids has been observed for several other fluids.

The other fluids investigated in the capillary viscometer were investigated at extreme shear stress levels. These fluids included a commonly used diester, a 50 cs dimethyl siloxane, a polyalkyl aromatic plus additive, a synthetic paraffinic oil and a blend of paraffinic mineral oil and high molecular weight (2×10^6) polyalkylmethacrylate.

The unblended hydrocarbon lubricants displayed Newtonian behavior up to a shear stress of about 4.8×10^6 N/m^2, (700 psi). This load is only a factor of 3-5 below the average shear stress which is experienced by the lubricant during passage of the high pressure zone of an elastohydrodynamic contact. High shear stress capillary tube viscometry is thus not far from the elastohydrodynamic conditions. The dimethyl siloxane showed shear induced nonliquid behavior at relatively high shear stress levels. The lubricant showed Newtonian properties when liquid behavior was displayed. The polymer blended lubricant showed distinct non-Newtonian properties at low shear, below a stress of 10^4 N/m^2, and shear induced nonliquid behavior at loads above this limit. The nonliquid behavior of the lubricants is possibly of importance for the ability to create a sufficient centerline film thickness in elastohydrodynamic contacts. No significant time dependent effects, for times >4 μsec, were observed in the high shear measurements when the lubricants under investigation showed liquid behavior.

II. Experimental Studies of Elastohydrodynamic Contacts

Studies of thin film lubrication were limited to sliding elastohydrodynamic contacts. This particular configuration was chosen because it is relatively simple to simulate and yet results in perhaps the most severely loaded of bearing contacts. Detailed discussion of the experimental technique, apparatus and results are found in publications 1,3,4 and 5 of the Technical Papers prepared under Grant GK-31154 listed below (see Appendix A). The operating conditions imposed at the bearing contact, formed by a steel sphere rotating and loaded against a sapphire flat, were a 67N load resulting in peak lubricant pressures of 1.0 GN/m^2 and sliding velocities ranging from 0.3 to 12.5 m/s. The objective of these experiments was to determine the temperature distribution within the contact and to measure the extent of molecular degradation of typical lubricants as they passed through such a contact. As part of this work it was also necessary to obtain detailed film thickness and traction measurements.

Temperature measuremtnts were obtained using an infrared microdetector to monitor the radiant energy emitted from the elastohydrodynamic contact. A combination of special filters and different emissivity spheres allowed the radiant energy contributions from the sphere surface and lubricant film to be separated. Once emissivities were determined from calibration experiments, the temperatures could be deduced. The apparatus had a spot size resolution of 36 μm diameter.

Because of the extensive calibration procedures needed for each lubricant studied, a single naphthenic mineral oil was used in all investigations to date. Detailed ball surface and lubricant temperature maps were generated, but the temperatures of primary interest were those along the contact centerline and those at the minimum film thickness location, usually in the side lobe film thickness constriction.

As a function of sliding speed, it was found that the peak ball

surface temperatures along the contact centerline which occur just downstream of the contact center, increase with sliding velocity, but approach an upper limit of approximately 135 C at 12.5 m/s for a lubricant supply temperature of 40 C. The lubricant temperature at this same location varies relatively little with sliding velocity, confined to a range of 175 to 195 C for velocities of 0.3 to 12.5 m/s.

An interesting observation was made in cases in which the local film thickness within the contact approached the composite surface roughness of the contact surfaces. This was usually confined to the side-lobe constriction. (minimum film thickness) and resulted in film temperatures substantially higher than those observed along the centerline. This suggests that some mechanism other than viscous dissipation was acting to cause film temperature as high as 360 C. The most plausible explanation appears to be asperity interaction at these locations, although this has not yet been independently verified.

The extent of lubricant degradation in the same sliding elastohydrodynamic contact has also been investigated. The lubricant was subjected to peak Hertz pressures of approximately 10^9 N/m^2 and average shear rates of 10^6 to 10^7 s^{-1}. Small samples (10^{-8} m^3) of test lubricant were extracted from the entrance and exit regions of the EHD contact. These samples were then analyzed to determine alterations in the molecular weight distribution and viscosity. Depending on the fluid being investigated the molecular alteration was determined by either ionization, infrared absorption or mass spectroscopy or gel permeation or gas chromotography. The alteration in viscosity was detected using a micro-capillary viscometer, specially designed and constructed because of the extremely small lubricant sample size available.

The fluids investigated had also been used in film thickness and traction experiments and had previously been studied in the high pressure

capillary viscometer. They included a paraffinic mineral oil with and without various high molecular weight polymer additives, a diester, a modified polyphenyl ether, and several siloxane fluids. Degradation resulting in up to a 70 percent reduction in viscosity and a 90 percent reduction in average molecular weight was found in fluids which had molecular weights of over 1000 before entering the bearing contact. In addition, a significant degree of correlation was found between molecular weight loss, viscosity loss and the energy dissipated in the contact.

III. Bearing Performance Predication

The objective of this phase of the research was to use the rheological data described in Section I, together with data previously obtained in this laboratory, to predict the operating characteristics of an elastohydrodynamic contact. Because of the analytical complexity of the point contact described in Section II, a complete solution of the problem has been limited to the viscous lubrication of rollers. In the first of these studies (Technical Paper 11, see Appendix A), only rigid cylinders were examined. The flow was assumed isothermal and the lubricant rheology was assumed completely defined by its compressibility as a function of pressure and by its viscosity as a function of pressure and shear stress. An iterative solution technique was developed and solutions covering a range of operating parameters and lubricant properties were obtained. It was found that the shear thinning fluids investigated resulted in a loss in load carrying capacity. The assumption of rigid cylinders was later relaxed. The results of this analysis covered a range of pressure-viscosity coefficients from 0.0 to $29(GN/m^2)^{-1}$. It was found that centerline film thicknesses increase with load over certain ranges of load. As expected, the minimum film thickness decreased. Also, the secondary maximum in the pressure distribution was found at heavy load conditions.

A simplified technique for predicting traction in an elastohydrodynamic contact was developed and results were compared with independent traction measurements (Technical Paper 6, see Appendix A). In order to estimate the traction in a sliding contact the temperature distribution and resulting shear stress distribution, from the rheological model, must be obtained. The solutions are presented in the form of dimensionless design charts, thus allowing traction estimates without obtaining the full iterative solution to the EHD problem. Since the basis of the analysis is the flow between parallel surfaces, accurate results can only be obtained for heavily loaded contacts.

In a subsequent study (Technical Paper 12) the above technique was used to try to predict traction in the contacts described in Section II. As input, the rheology of the lubricant obtained from capillary viscometer data, along with measured film thickness and measured ball surface temperatures, were used. Prediction of the traction was good at high sliding speeds but not as accurate at lower speeds. The effect of variations in lubricant properties on traction was also determined. It was found that traction is strongly influenced by the inlet viscosity and the temperature-viscosity dependence, but only slightly influenced by the pressure-viscosity dependence. In order to make the technique useful to the designer, who usually cannot make film thickness and temperature measuremtnts, the technique has been modified to allow for the use of a film thickness formula and an iterative procedure for determining the ball temperature.

RESEARCH PERSONNEL

WINER, Ward O.,	Professor, Co-Principal Investigator
SANBORN, David M.,	Assistant Professor, Co-Principal Investigator
JAKOBSEN, Jorgen,	Ph. D. granted September, 1973. Research contributions in the area of high shear stress rheological studies.
CARLSON, Stephen F.,	Ph. D. Candidate at grant termination date. Research contributions in the area of analytical treatment of the lubrication of rolling and sliding rigid cylinders.
NAGARAJ, H.,	Ph. D. Candidate at grant termination date. Research contributions in the area of infrared temperature measurements in EHD films.
WALKER, David L.,	M.S.M.E. granted November, 1973. Research contributions in the area of molecular degradation in EHD bearing contracts.
TURCHINA, Valentin A.,	M.S.M.E. granted June, 1973. Research contributions in the area of infrared temperature measurements in EHD films.
KUNZ, Richard K.,	M.S.M.E. candidate at grant termination date. Research contributions in the area of analytical treatment of surface temperatures and traction in elastohydrodynamic lubrication.
AUSHERMAN, Vern K.,	M.S.M.E. candidate at grant termination date. Research contributions in the area of infrared temperature measurements in elastohydrodynamic films.

PUBLICATIONS OF GRANT SUPPORTED RESEARCH

A. Student theses completed and published.

1. Jorgen Jakobsen,
"Lubricant Rheology at High Shear Stress, Ph. D. Thesis, Georgia Institute of Technology, September, 1973.

2. Valentin Alexandru Turchina,
"Pressure and Temperature Measurement Techniques in Elastohydrodynamic Contacts", M.S. Thesis, Georgia Institute of Technology, June, 1973.

3. David L. Walker,
"Polymer Degradation in Sliding Elastohydrodynamic Lubrication", M.S. Thesis, Georgia Institute of Technology, November, 1973.

4. Richard K. Kunz,
"Thermal and Traction Behavior in Sliding Elastohydrodynamic Contacts", M. S. Thesis, Georgia Institute of Technology, expected December, 1974.

B. Student theses in preparation for investigations completed under Grant GK-31154.

1. Stephen F. Carlson,
"The General Viscous Lubrication of Rolling and Sliding Elastic Cylinders", Ph. D. Thesis, Georgia Institute of Technology, expected March, 1975.

2. Vernon K. Ausherman,
"Infrared Temperature Mapping in Elastohydrodynamic Lubrication", M. S. Thesis, Georgia Institute of Technology, expected March, 1975.

C. Technical Papers.

1. Jakobsen, J., Sanborn, D. M. and Winer, W. O., "Simulation of Severe Shear Conditions in Lubrication", Society of Automotive Engineers, SP-382, pp. 59-67, 1973.

2. Jakobsen, J., Sanborn, D. M. and Winer, W. O., "Pressure Viscosity Characteristics of a Series of Siloxane Fluids", Trans. ASME, Journal of Lubrication Technology, Vol. 96, pp. 410-417, 1974.

3. Turchina, V., Sanborn, D. M. and Winer, W. O., "Temperature Measurements in Sliding Elastohydrodynamic Point Contacts", Trans. ASME, Journal of Lubrication Technology, Vol. 96, pp. 464-471, 1974.

4. Walker, D. L., Sanborn, D. M. and Winer, W. O., "Polymer Degradation in Elastohydrodynamic Lubrication", Proceedings of the International Colloquium on Polymers and Lubrication, C.N.R.S., Brest, France, 1974.

5. Walker, D. L., Sanborn, D. M and Winer, W. O., "Molecular Degradation of Lubricants in Sliding Elastohydrodynamic Contacts", ASME Paper No. 74-Lub-35, presented at the 1974 ASME/ASLE Joint Lubrication Conference and to be published in Trans. ASME, Journal of Lubrication Technology.

6. Jakobsen, J. and Winer, W. O., "Traction of Elastohydrodynamic Contacts with Thermal Shearing Flow", ASME Paper No. 74-Lub-28, presented at the 1974 ASME/ASLE Joint Lubrication Conference and to be published in Trans. ASME, Journal of Lubrication Technology.

7. Jakobsen, J. and Winer, W. O., "Dissipative Heating Effects and End Corrections for Viscous Newtonian Flow in High Shear Capillary Tube Viscometry", ASME Paper No. 74-Lub-40, presented at the 1974 ASME/ASLE Joint Lubrication Conference and to be published in Trans. ASME, Journal of Lubrication Technology.

8. Jakobsen, J. and Winer, W. O., "High Shear Stress Behavior of Some Representative Lubricants", ASME Paper No. 74-Lub-41, presented at the 1974 ASME/ASLE Joint Lubrication Conference and to be published in Trans. ASME, Journal of Lubrication Technology.

9. Carlson, S. F. and Winer, W. O., "The Viscous Lubrication of Rolling and Sliding Rigid Cylinders", ASME Paper No. 74-Lub-15, presented at the 1974 ASME/ASLE Joint Lubrication Conference and to be published in Trans. ASME, Journal of Lubrication Technology.

10. Walker, D. L., Sanborn, D. M. and Winer, W. O., "A Micro-Capillary Viscometer", manuscript in preparation; to be submitted as a Technical Brief to Trans. ASME, Journal of Lubrication Technology.

11. Carlson, S. F. and Winer, W. O., "The Viscous Lubrication of Rolling and Slidin g Rigid Cylinders", manuscript in preparation; to be submitted to Trans. ASME, Journal of Lubrication Technology.

12. Kunz, R. K. and Winer, W. O., "Prediction of Traction in Sliding Elastohydrodynamic Contacts", manuscript in preparation.

13. Ausherman, V. K., Nagaraj, H., Sanborn, D. M. and Winer, W. O., "Temperature Measurements in Severely Loaded Elastohydrodynamic Contacts", manuscript in preparation.

RELATED ACTIVITIES

Some of the results of the investigations presented in this report were also presented without publication at the 1972 and 1974 Gordon Research Conferences on Friction, Lubrication and Wear.

On October 19 and 20, 1973 a Tribology Workshop* was held at the Georgia Institute of Technology under the sponsorship of the Industrial Technology Program, Engineering Division, of the National Science Foundation. This workshop was organized by one of the principal investigators (W.O.W.), Professor H. S. Cheng of Northwestern University and Professor F. F. Ling of Rensselear Polytechnic Institute. Although no direct expenses for the Workshop were covered by Grant GK-31154, these two NSF sponsored programs complimented each other. The topics of the workshop included several of the areas under investigation. The laboratory set up under the grant was opened to workshop participants, thus effectively communicating the Grant supported research.

---

*Proceedings of the Tribology Workshop, H. S. Cheng, F. F. Ling, W. O. Winer eds., Sponsored by The Industrial Technology Program, Mechanics Section, Engineering Division, National Science Foundation, April 1974.

APPENDIX A

REPRESENTATIVE PAPERS PUBLISHED

TO DATE

730482

Simulation of Severe Shear Conditions in Lubrication

J. Jakobsen, D. M. Sanborn, and W. O. Winer
School of Mechanical Engineering, Georgia Institute of Technology

ABSTRACT

The importance of high shear conditions in automotive lubrication is discussed with respect to the influence on lubricant rheological properties. The distribution of shearing effects in lubricated components is also discussed. Two methods of simulating high shear conditions—an elastohydrodynamic lubrication simulator and a capillary viscometer—are presented, along with some data obtained from them on polymer containing oils.

N LUBRICATION APPLICATIONS the lubricant is often ıbjected to very high shearing stresses and shearing rates. It as long been known that under these conditions lubricants ay behave differently than is expected on the basis of low ıear kinematic viscosity measurements. Three major effects e expected and have been observed in lubricants under high ıear conditions. These are viscosity decrease due to viscous ating, pseudoplastic viscosity decrease, and irreversible scosity loss due to molecular degradation.

Viscous heating of the lubricant subjected to the high shear nditions of lubricated contacts is to be expected because all e mechanical energy transmitted to the lubricant through lative motion of the solid surfaces is converted into thermal ergy, which increases the lubricant temperature and is conıcted away from the lubricant to the solid surface. Typically, bricants have low thermal diffusivities, but fortunately the ea-to-volume ratio of the film is usually quite high—which creases the heat transfer to the solid. Although the meaırement of the viscosity-temperature behavior of lubricating ls has been a mature field for many years, very little exrimental work has been done to determine the temperatures lubricant films.

Pseudoplastic viscosity decreases associated with high shear es have long been recognized in the lubrication community. ıese are primarily associated with polymer containing bricants such as multigraded motor oils. These materials ıen sheared at constant temperature and pressure exhibit a cosity which decreases from a constant value over a range of v shear rates to another constant value at high shear rates ng what Wright (1)* has called a sigmoid or S-shaped curve. The two constant viscosity values are called the first and second Newtonian, respectively. The first and second Newtonian viscosities and the shear range over which the transition occurs are functions of the temperature, pressure, base oil, polymer type, molecular weight, and concentration. Although most lubricant specifications refer to the first Newtonian viscosity, most high shear lubrication conditions to which the lubricant is subjected are in the second Newtonian range.

Molecular degradation of polymer containing materials invariably decreases the viscosity of the lubricant. The increase in viscosity is dependent on the polymer-base oil solvent interaction, concentration, and molecular weight of the polymer. If the molecular weight of the polymer is decreased due to degradation, the viscosity of the solution is decreased. The degradation can be brought about thermally or mechanically. Our primary concern here is with mechanical degradation resulting from subjecting the solution to high shear lubrication conditions.

Although a number of papers have been published which relate to the high shear behavior of lubricants, only a few will be mentioned. In the area of pseudoplastic behavior of polymer containing lubricants Wright and Crouse (1) present correlations of viscosity with energy input rate showing the effect of polymer concentration and shear rate. Wright and Johnson (2) examined the viscosity-shear rate behavior of new and used multigraded motor oils and automatic transmission fluids (3). They found that the viscometric measurements made on a new fluid bear little relation to its characteristics over the majority of its operating life because of molecular degradation. They also found that is was not unusual for the high shear viscosity of the used oil to no longer meet the oil specifications, and suggest that measurement of the second

*Numbers in parentheses designate References at end of per.

Newtonian viscosity of the used oil might be most definitive of oil behavior in service. Selby and West (4) have also published results on in-service motor oil shear degradation and find the degradation to occur in as little as 400 miles of driving. Unpublished work in our laboratory on commercial motor oil degradation in an engine is in agreement with the findings of Wright and Johnson (2) and Selby and West (4).

Novak and Winer (5, 6) have published data on the viscosity of polymer-containing oils as a function of temperature, pressure, and shear stress. They found the pressure-viscosity characteristics of the second Newtonian to be similar to the first Newtonian.

It has been suggested that the viscosity may be different in two directions in the same flow. That is, the viscosity might be low (second Newtonian) in the direction of primary shear but still be effectively the higher first Newtonian in the direction perpendicular to the primary shear. The argument is that the higher first Newtonian governs the leak rate out the ends of the bearing contact. However, the work of Vinogradov (7) showed that the high shear viscosity controlled the cross flow. His experiment was a concentric cylinder arrangement which also permitted simultaneous axial flow down the annulus. He showed that the viscosity corresponding to the highest shear rate controlled both the circumferencial and axial flows. A similar study by Tanner (8) indicates the same result. He also had Couette shear flow but with one surface oscillating, and again the viscosity corresponding to the highest shear controlled flow in both directions.

The field of mechanical degradation of polymers and polymer solutions has been extensively reviewed by Casale, Porter, and Johnson (9) recently. They show that, although mechanical degradation does occur in polymer solutions, it is a very inefficient process when viewed from energy considerations. In some cases, the energy per mole required to break molecular bonds is as much as a million times the activation energy of C-C bonds.

Many other high shear phenomena in lubricant rheology, in addition to the three discussed above, have been proposed in the lubrication literature, but most are still considered speculative in nature and are not discussed in this paper. The three phenomena discussed here, viscous heating, pseudoplasticity, and mechanical degradation, are known to be significant to lubrication applications.

TYPICAL CONDITIONS IN AUTOMOTIVE APPLICATIONS

Fig. 1 contains a typical viscosity-shear rate curve for a polymer-containing automotive lubricant. The detailed nature of the curve depends on polymer type, concentration, and molecular weight as well as polymer base oil interaction, but this figure will serve the purpose for this discussion. With respect to shear rates, automotive lubrication conditions fall in the three regions marked A, B, and C in Fig. 1. Region A has low shear rates which occur in the oil pump inlet and drainage galleries and corresponds to the shear rates commonly encountered in kinematic viscosity measurements. Typically film thicknesses are large ($\geq$ 1 cm). Behavior in this shear rate range is very important for lubricant circulation particularly at low temperature. This region is discussed extensively in other papers of this symposium and will not be considered further in this paper.

Region B corresponds to what might be called typical hydrodynamic lubrication as occurs in crankshaft journal bearings and other hydrodynamic sleeve bearings in the engine or transmission. Depending on operating speed, the surface velocities range 100-400 in/s and film thickness typically is in the range of 0.001 in (0.002 cm), resulting in shear rates of $1\text{-}5 \times 10^5\ s^{-1}$. Shear stresses will be about $0.3\text{-}2 \times 10^5$ d/cm^2.

Region C corresponds to elastohydrodynamic lubrication (EHD) conditions such as might be expected in gears, cams, tappets, and other concentrated load contacts in the system. These are mechanically the most severe conditions to which the lubricant is subjected in automotive applications. The surface velocities of these contacts are about the same or somewhat lower than those of the journal bearing, but the film thicknesses are typically 100 times smaller, resulting in a shear rate 100 times larger. Shear stresses are not as easily estimated for EHD conditions because the pressures are very high causing an increase in viscosity, but EHD experiments (10) done in our laboratory suggest that average shear stresses are 10^8 dynes/cm^2.

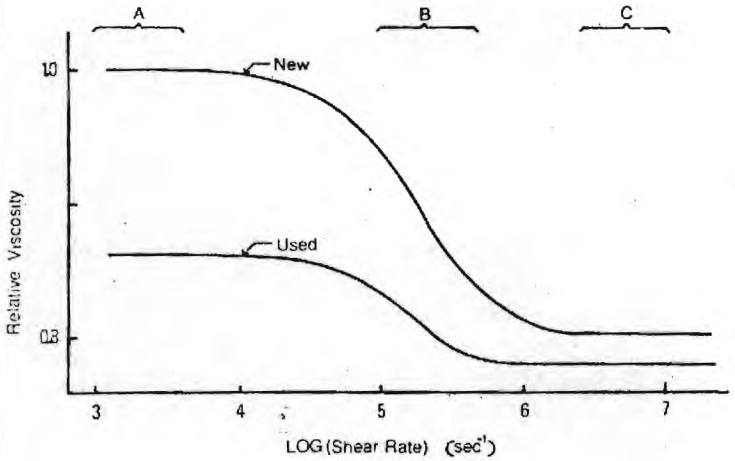

Fig. 1 - Flow curve for a typical polymer containing motor oil

The Casale et al. review article (9) mentioned above indicates that workers have tried to correlate mechanical degradation with shear stress times reciprocal absolute temperature for a given polymer solution. Except for very high molecular weight polymers, not of interest in automotive lubricants, little if any degradation occurs in region A. Mechanical degradation can occur in either region B or C and the extent of degradation depends on many factors. Table 1 compares shear rate, shear stress, and energy inputs for regions A, B, and C in Fig. 1. To calculate the energy input to the fluid a simple model of the lubricated contact is assumed and shown in Fig. 2. The shear stress, shear rate, and thickness (h) of the shaded volume of lubricant have already been discussed for each regime and are entered in Table 1. The energy dissipation rate per unit volume is simply the shear stress times the shear rate and it too is entered in Table 1. However, what is more important for mechanical degradation is the energy dissipated per unit mass of the fluid passing through the volume. This is obtained by multiplying the dissipation rate per unit volume times the volume and divided by the mass flow rate through the volume. Finally, the energy dissipation rate per gram-mole is obtained by multiplying by the molecular weight. Both of these values are entered in Table 1.

Also listed in Table 1 are typical energies per gram-mole of a typical mineral oil and a high polymer used as a polymer thickener. If one recalls that the activation energy for a g mole of carbon-carbon bonds is 80 kcal, it is not surprising that

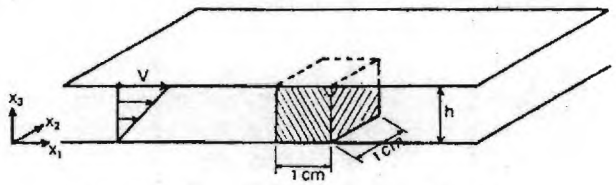

Fig. 2 - Simplified model of a lubricated contact

Table 1 - Typical Conditions in Lubrication Regimes as Relating to Mechanical Degradation of Lubricants

Variable	Regime A Low Shear	Regime B Hydrodynamic Lubrication	Regime C Elastohydrodynamic Lubrication	Units
γ = shear rate	$\leq 10^3$	$1 - 5 \times 10^5$	$2 - 20 \times 10^6$	s^{-1}
τ = shear stress	$\leq 10^3$	$0.3 - 2 \times 10^5$	10^8	$\frac{\text{dynes}}{\text{cm}^2}$
$\tau\gamma$ = energy input rate per volume	$\leq 10^6$	$1 - 10 \times 10^{10}$	$2 - 20 \times 10^{14}$	$\frac{\text{dyne cm}}{\text{cm}^3\text{s}}$
$\frac{2\tau l}{\rho h} = \frac{\text{energy input}}{\text{mass flow}}$	$\leq 10^3$	$0.3 - 2 \times 10^8$	10^{13}	$\frac{\text{dyne cm}}{\text{g}}$
$\frac{2\tau(MW)}{\rho h} = \frac{\text{energy input}}{\text{g} \cdot \text{mole of lub}}$	$\leq (MW) \times 10^3$	$(MW) \times 10^8$	$(MW) \times 10^{13}$	$\frac{\text{dyne cm}}{\text{g} \cdot \text{mole}}$
$\frac{2\tau(MW)}{\rho h} = \frac{\text{energy input}}{\text{g} \cdot \text{mole of lub}}$	$\leq (MW) \times 10^{-7}$	$(MW) \times 10^{-2}$	$(MW) \times 10^3$	$\frac{\text{kcal}}{\text{g} \cdot \text{mole}}$
$\frac{2\tau(MW)}{\rho h} = \frac{\text{energy input}}{\text{g} \cdot \text{mole of lub}}$ (for typical mineral oil of MW 700 awu*)	$\leq 10^{-4}$	7	10^6	$\frac{\text{kcal}}{\text{g} \cdot \text{mole}}$
$\frac{2\tau(MW)}{\rho h} = \frac{\text{energy input}}{\text{g} \cdot \text{mole of lub}}$ (for high polymer MW = 10^5 awu)	$\leq 10^{-2}$	10^3	10^8	$\frac{\text{kcal}}{\text{g} \cdot \text{mole}}$

*MW = molecular weight
awu = atomic weight units

some degradation occurs in region C and possibly even in region B.

In fact, what is surprising when viewed in light of the numbers in Table 1, is that more degradation does not occur. However, in the review paper by Casale et al. (9) several studies on the mechanical degradation of polymers are cited which indicate that mechanical degradation is a very inefficient process, requiring as much as a million times (10^6) more energy than the activation energy for the bond. Clearly, in the EHD areas (regime C) some mechanical degradation is to be expected and it is probably these (EHD) conditions which cause the degradation observed in the engine tests of Wright and Johnson (2, 3) and Selby and West (4).

In automotive applications very small flow rates pass through the EHD contact and then mix with the bulk oil. Also, the fluid is in the EHD contact for a very short time (typically less than 1.0 ms). Automotive applications differ in both of these ways from most polymer degradation studies where homogeneous continuous shear is usually applied.

Further study of the flow rates through the various flow regions in the automotive applications is necessary to understand and model shear degradation in automotive lubricants. With this understanding one should develop an ability to improvise bench tests and appropriate specifications.

ELASTOHYDRODYNAMIC (EHD) SIMULATION OF HIGH SHEAR BEHAVIOR OF LUBRICANTS.

The EHD conditions referred to above as regime C can be simulated in a laboratory apparatus. The schematic of such a device is shown in Fig. 3. This apparatus has been used in our laboratory for several years and details are reported in the literature (10). The system consists of a rotating steel sphere loaded against a stationary sapphire flat with the lubricant entrapped between the sphere and the flat. By optical interference between the sphere and the sapphire, the film thickness can be measured. The traction transmitted between the two surfaces through the lubricant film can also be measured

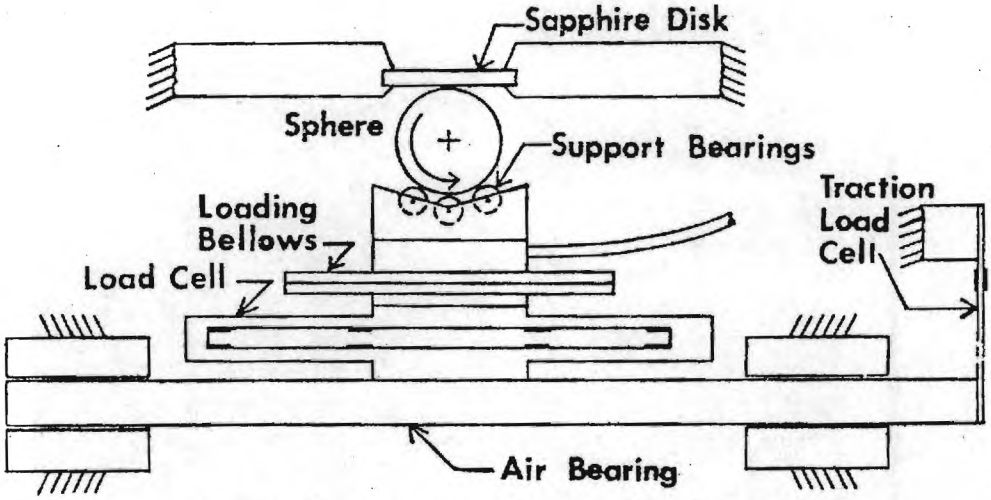

Fig. 3 - Schematic of elastohydrodynamic lubrication simulator

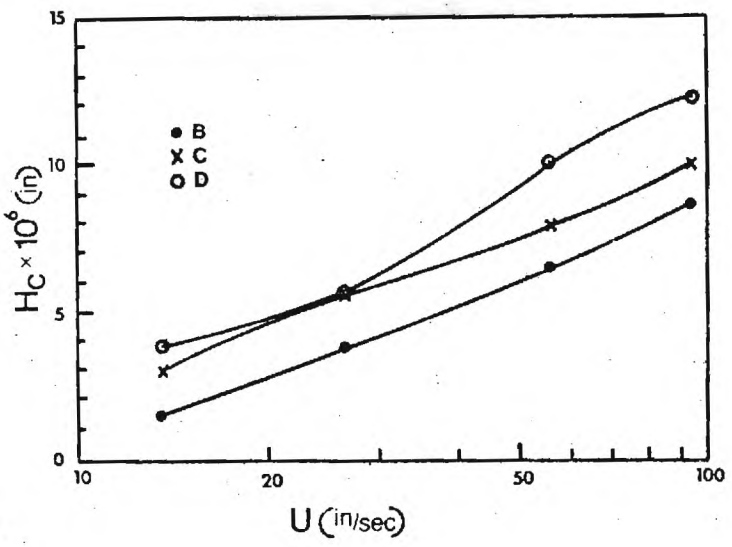

Fig. 4A - EHD film thickness-speed relation for blended oils

as can the load being supported by the film. The conditions to which the lubricant is subjected in this device are very much like those that occur in gears, cams, tappets, and possibly piston rings in automotive applications, and are essentially the conditions listed as region C in Table 1.

Several polymer solutions in mineral oils similar to multigrade motor oils have been examined in this device. Also, several bulk polymers that are used as synthetic lubricants have been examined.

Elastohydrodynamic theory (11) indicates that the only important fluid properties are the atmospheric pressure low shear viscosity, μ_o, and the pressure-viscosity coefficient, α, which is the logarithmic derivative of viscosity with respect to pressure at atmospheric pressure. The film thickness in the center of the contact is expected to vary with the 0.6 power of the product of these two properties and the surface velocity.

Fig. 4A shows measured film thickness as a function of sliding speed for a load of 15 lb for several polymer solutions. The description of the fluids is given in Table 2. This load corresponds to a maximum film pressure of about 150,000 psi. Fig. 4B contains the measured traction coefficients for the same fluids and conditions. The most striking aspect of these data is that neither the film thickness nor the traction are affected by the presence of the polymer in the oil. The behavior of the polymer solutions is essentially that of the base oil from which the solution was made, in spite of the increased kinematic viscosity of the solution over the base oil of as much as five times.

The energy dissipation in these films does not vary greatly with sliding speed and is of the order of 10^8 kcal/g · mole of polymer. Clearly mechanical degradation of the polymer should be expected even though the average fluid particle is in the high shear zone for about 0.6 ms. In fact, the film thick-

Table 2 - Sample Description and Properties

Identification Symbol	Viscosity at Atmospheric Pressure and 100°F, μ_o, cP	Pressure Viscosity Coefficient at Atmospheric Pressure and 100°F,* $\alpha_{oT} \times 10^4$, psi^{-1}	Description
B	29	1.31	Paraffinic base oil
C	65	1.21	B + 4% wt. PAMA (MW = 5.6×10^5 awu)
D	140	1.15	B + 8% by wt. PAMA (MW = 5.6×10^5 awu)
E	105	1.39	B + 4% by wt. polyalkylstyrene (MW = 3.7×10^5 awu)

$$*\alpha \equiv \left.\frac{\partial \ln \mu}{\partial p}\right|_{100°F}$$

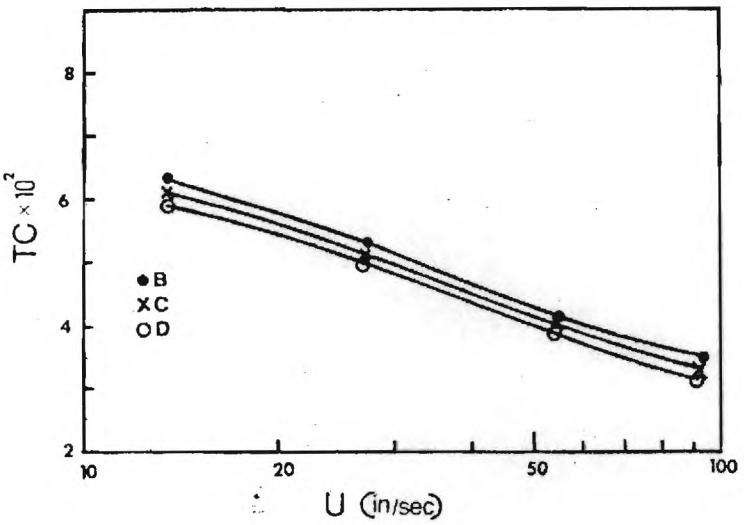

Fig. 4B - EHD traction-speed relations for blended oils

ness and traction measurements suggest that the polymer is of little value in this situation and may be very degraded.

Because of the above results, we have recently undertaken a study which will permit a more detailed study of fluid degradation in EHD contacts. The EHD simulator described above has been modified by putting a 3×10^{-3} in diameter hole in the sapphire surface, which can be moved into the high-pressure region, permitting a sample of the sheared fluid to be removed for analysis. The quantity of fluid passing through the contact is so small that it is difficult to detect degradation

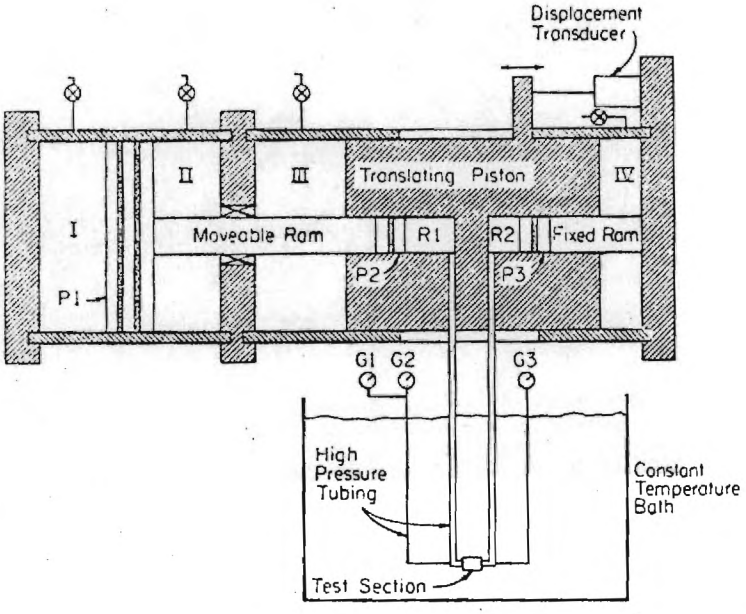

Fig. 5 - Schematic of pressure viscometer

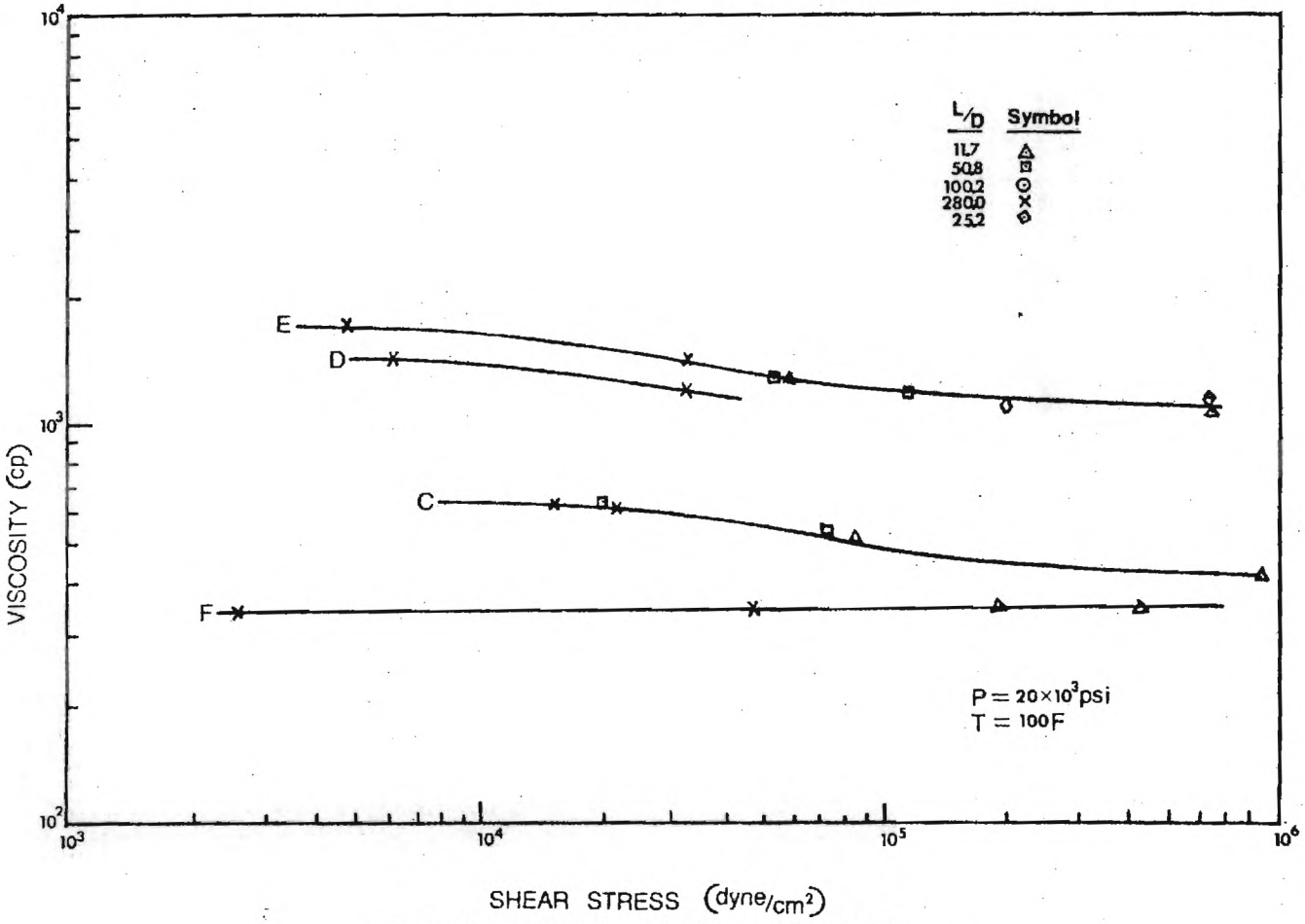

Fig. 6 - Flow curves for base oil and polymer blended oils

in the bulk sample except for very long run times. All the sample removed through the hole has been subjected to the high energy dissipation field and should permit easy detection of mechanical degradation. Thus far, two proprietary materials have been examined. One was of relatively low molecular weight (about 500) which showed no signs of molecular degradation when sheared and unsheared samples were analyzed. The second sample was of higher molecular weight and had a wide molecular weight distribution with peaks at about 16,000 and 40,000 atomic weight units. Upon detailed

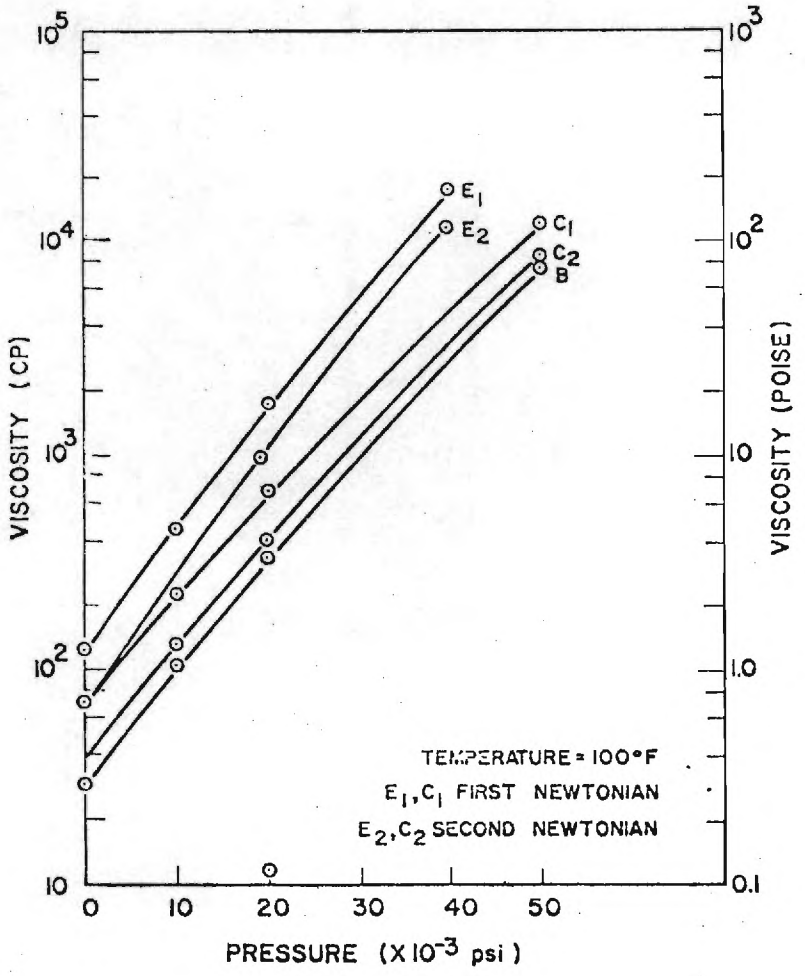

Fig. 7 - Viscosity-pressure relations for two paraffinic based blends

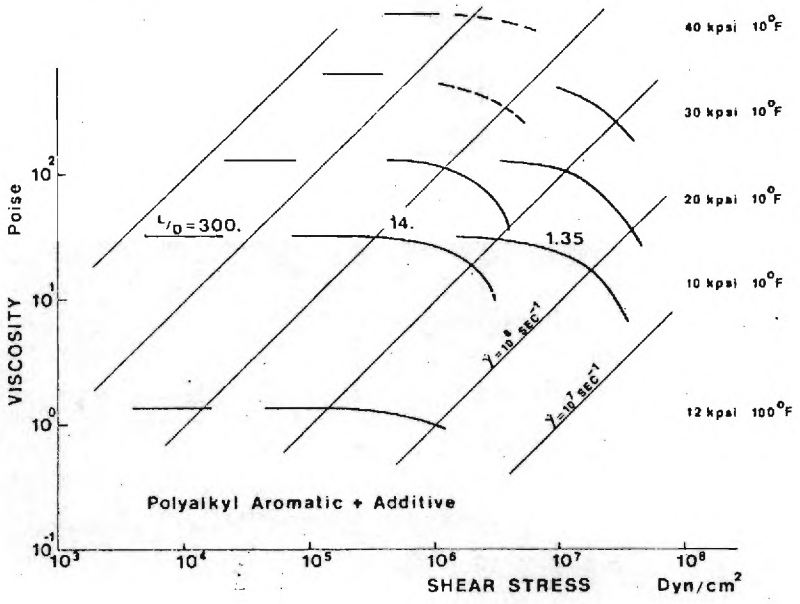

Fig. 8 - Viscosity-shear stress behavior at high shear stress with viscous heating

analysis of the sheared and unsheared sample in this case, it was found that the higher molecular weight peak was gone in the sheared sample suggesting extensive mechanical degradation had occurred. These studies are continuing on other materials some of which are similar to automotive multigraded oils and the results will be published subsequently.

SIMULATION OF HIGH SHEAR IN A CAPILLARY VISCOMETER

The conditions to which the lubricant is subjected in the EHD simulator described above are very nonuniform with respect to pressure temperature and shear stress, and are transient in nature. Consequently, the EHD simulator is not suitable for viscometric determinations. For this reason, a high shear high pressure capillary viscometer was developed in this laboratory (5, 6). The objective of this effort is to simulate the high pressure and high shear stress conditions of the EHD contact in a well-defined viscometric flow so the fluid response to those conditions can be measured. A schematic of the viscometer is shown in Fig. 5. It is a capillary type viscometer with pressure applied to both ends of the capillary. Flow is accomplished by a pressure difference across the capillary which is small compared to the pressure level. The pressure difference is the result of moving the translating piston along the high-pressure pistons. The pressures are measured by strain gage pressure transducers and the flow rates are measured by the displacement of the translating piston along the pressure piston. The capillary is interchangeable to allow different length-to-diameter ratios (L/D) to be used. More details on the instrument can be found in reference 5.

The fluids listed in Table 2 have been investigated in the pressure viscometer. The viscosity of fluids as a function of shear stress are shown in Fig. 6 at a pressure of 20,000 psi. The viscosity pressure data for the base oil, and the first and second Newtonian of the polymer blend are shown in Fig. 7. The pressure viscosity slope at the first and second Newtonian condition is the same, but they depend on the polymer base oil combination. The ratio of first-to-second Newtonian viscosity is nearly constant over the pressure range, as indicated by the curves being parallel in Fig. 7. However, by the same reasoning, the ratio of either first or second Newtonian viscosity to the viscosity of the base oil changes with pressure for the styrene polymer solution.

The viscometer has recently been modified to permit higher shear stresses. By using capillaries with smaller L/Ds, higher shear stresses can be obtained with less viscous heating. By maintaining small Reynolds numbers in the flow, entrance length effects can be minimized. Capillaries of 1.35 L/D have been used with several fluids. Some of the results on one fluid are shown in Fig. 8. The smaller L/D of the capillary permits higher shear stresses before viscous heating reduces the apparent viscosity through an increase in temperature. It is reasonable to conclude that even the apparent viscosity reduction shown in the highest shear stress curve is due to heating because fluids with the largest viscosity-temperature dependence show the greatest reduction and vice versa.

Shear stresses comparable to those in EHD contacts are still 7-10 times those obtained in the viscometric experiments. However, within the high shear stress range that can be measured, it appears that for lubricants viscous heating is more important than non-Newtonian effects in lowering the effective viscosity. For polymer solutions, this shear stress range is already within the second Newtonian range.

Shear degradation probably occurs in the viscometer but is difficult to detect because only a very small fraction of the total sample is subjected to the high energy inputs in the nonhomogeneous stress field of the capillary flow. Low shear rate viscosity which gives a measure of degradation has not been found to change after approximately 100 viscometric measurements on a sample.

Of possible interest to the automotive field are measurements of pressure-viscosity with this instrument on gasoline, a paraffinic oil and a 50-50 mixture of them (12).

DISCUSSION AND CONCLUSIONS

High-shear conditions in automotive lubrication applications play an important role in lubricant rheological behavior. High shear can result in viscosity reductions due to viscous heating, pseudoplastic shear thinning, and irreversible molecular degradation.

We need to learn more about the conditions to which the lubricant is subjected in the system being lubricated with particular emphasis on energy dissipation rates and lubricant flow rates because these will determine the degradation in the lubricant and the rate at which the degraded lubricant will dilute the bulk of lubricant in the system. Only by understanding these factors will it be possible to develop meaningful bench tests and specifications for evaluating lubricants for these applications.

It may be impossible to develop high polymer automotive lubricant additives which do not degrade to some extent under the EHD conditions in some parts of engines and transmissions, but by understanding the factors involved we can develop bench tests and meaningful specifications to aid the user and lubricant developer in avoiding any problems which may arise.

ACKNOWLEDGMENTS

The work in this laboratory has been supported by many organizations over the past few years. We would like to particularly note the support of the Sun Oil Co., Dow Corning Corp., and the National Science Foundation (Grant GK-31154) and NASA Grant (NGR-11-002-133).

REFERENCES

1. W. A. Wright and W. W. Crouse, Jr., "A New Concept in Generalizing Non-Newtonian Fluid Flow Data." ASLE Transactions, Vol. 8 (1965), pp. 184-190.

2. R. H. Johnson and W. A. Wright, "The Rheology of Multigraded Motor Oils." SAE Transactions, Vol. 77 (1968), paper 680072.

3. W. A. Wright and R. H. Johnson, "Rheological Properties of Automatic Transmission Fluid." Paper 680437 presented at SAE Mid-Year Meeting, Detroit, May 1968.

4. J. P. West and T. W. Selby, "The Effect of Engine Operation on the Viscometric Properties of Multigraded Engine Oils." Paper 650445 presented at SAE Mid-Year Meeting, Chicago, May 1965.

5. J. D. Novak and W. O. Winer, "Some Measurements of High Pressure Lubricant Rheology." ASME Trans., Jrl. of Lubrication Technology, Vol. 90 (July 1968), pp. 580-591.

6. J. D. Novak and W. O. Winer, "The Effect of Pressure on the Non-Newtonian Behavior of Polymer Blended Petroleum Oils." ASME Trans., Jrl. Lubrication Technology, Vol. 91 (1969), pp. 459-463.

7. G. V. Vinogradov and A. A. Mamarov, "Flow of Greases Under the Action of Complex Shear." ASME Transactions, Jrl. of Lubrication Technology, Vol. 90 (July 1968), pp. 604-607.

8. R. I. Tanner, "Response of Viscoelastic Fluids in Dynamically Loaded Bearings." ASME Transactions, Jrl. of Lubrication Technology, Vol. 90 (July 1968), pp. 555-560.

9. A. Casale, R. S. Porter, and J. F. Johnson, "The Mechano-chemistry of High Polymers." Rubber Chemistry and Technology, Vol. 44, April 1971.

10. D. M. Sanborn and W. O. Winer, "Fluid Rheological Effects in Sliding Elastohydrodynamic Point Contacts: I–Film Thickness." ASME Trans., Jrl. of Lubrication Technology, Vol. 93 (1971) pp. 262-271, and "Fluid Rheological Effects in Sliding Elastohydrodynamic Point Contacts: II–Traction." ASME Transactions, Jrl. of Lubrication Technology, Vol. 93 (1971), pp. 342-348.

11. D. Dowson and G. R. Higginson, "Elasto-Hydrodynamic Lubrication." New York: Pergamon Press, 1966.

12. W. O. Winer, "A Viscometer for High Pressure Use, and Some Results." ASME Transactions, Jrl. of Basic Engineering, Vol. 94, (September 1972), pp. 586-588.

J. JAKOBSEN
Doctoral Candidate.

D. M. SANBORN
Assistant Professor.

W. O. WINER
Professor.

School of Mechanical Engineering,
Georgia Institute of Technology,
Atlanta, Ga.

Pressure Viscosity Characteristics of a Series of Siloxane Fluids

The viscosity-pressure-temperature behavior of a series of 14 siloxane polymers is reported. The series of fluids includes a range of degree of polymerization and of size and nature of side radicals. The variations span the range of siloxane fluids currently available and considered as possible lubricants. The major conclusion is that the pressure viscosity coefficient considered important to elastohydrodynamic lubrication is only influenced by changing the nature of the side radical and not by the degree of polymerization or the size of alkyl side groups on the siloxane chain.

Introduction

SILOXANE fluids are employed in many mechanical fluid applications and as lubricants. They are used as fluids in dash pots, shock absorbers, liquid springs and hydraulic systems, and as lubricants in rolling element bearings and in some sliding elements systems, depending on the materials involved. They have the desirable characteristics of a wide temperature range of applicability, small viscosity change with temperature compared with most lubricants, and are available in a wide range of viscosities. Dimethyl siloxane fluids, the most common member of the siloxane family, have the disadvantage, when unformulated, of less than desirable performance as a lubricant for highly loaded steel-on-steel sliding contacts. To improve performance of siloxanes under these conditions silicone additive technology has been developed [1][1] and silicone molecular structure changes have been introduced [2, 3, 4, 5].

In highly loaded lubrication applications minimum wear and low friction are best attained when an elastohydrodynamic mode of lubrication is maintained. The most important fluid properties influencing its performance in an elastohydrodynamic lubrication situation are viscosity and the variation of viscosity with pressure and temperature. These characteristics are also important in other applications such as liquid spring systems, shock absorbers, and to some extent hydraulic systems.

The purpose of the study reported in this paper was to determine the relationship between the molecular structure of a series of siloxane fluids and their viscosity variations with pressure and temperature. It is expected that the results will be of value in the synthesis and selection of siloxane fluids for lubrication applications. A series of 14 siloxane polymer fluids, within which both chain length and side radical were varied, investigated in a pressure viscometer. Data on two siloxane fluids previously investigated in our laboratory [6] are included for completeness.

Experimental Fluids[2]

Table I lists the fluids for which data are reported. Fluids 1–15 were made available for this study, while fluids I and J were previously investigated [6]. Fluids 1–10 were specifically synthesized for this study, while fluids 11–15 and *I* and *J* were standard production fluids. "Fluid" 5 was a solid at room temperature and atmospheric pressure and no viscosity data was obtained for that fluid.

All the fluids are siloxane polymers with the general structure shown in Fig. 1.

The nature of the side radical, *R*, and the degree of polymerization (*DP*), *n*, for each fluid are shown in Table I.

From Table I it is seen that the fluids include: (*a*) a series of fluids of constant degree of polymerization (*DP* = 35) with increasing length of side radical; fluids 11, 8, 9, 6, 2, 7, 5, respectively, (*b*) a series with constant side radical, octylmethyl, and increasing *DP;* fluids 1, 3, 10, 4, 9, respectively, (*c*) a series of

[2] The experimental fluids were synthesized, identified and supplied by the Dow Corning Corporation, Midland, Mich.

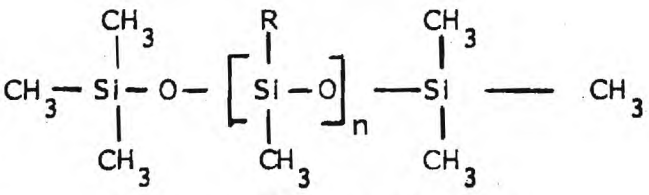

Fig. 1 General structure of fluids investigated

[1] Numbers in brackets designate References at end of paper.

Contributed by the Lubrication Division of THE AMERICAN SOCIETY OF MECHANICAL ENGINEERS and presented at the ASLE-ASME Joint Lubrication Conference, Atlanta, Ga., October 16–18, 1973. Manuscript received by the Lubrication Division, July 2, 1973. Paper No. 73-Lub-33.

Table 1 Definition of experimental fluids

Identification number	Description	Degree of polymerization
1	Octylmethyl siloxane (C_8H_{17}-CH_3)	4 to 5
2	Dodecylmethyl siloxane ($C_{12}H_{25}$-CH_3)	35
3	Octylethyl siloxane (C_8H_{17}-CH_3)	12
4	Octylmethyl siloxane (C_8H_{17}-CH_3)	25
5	Hexadecylmethyl siloxane ($C_{16}H_{33}$-CH_3)	35 (solid)
6	Decylmethyl siloxane ($C_{10}H_{21}$-CH_3)	35
7	Tetradecylmethyl siloxane ($C_{14}H_{29}$-CH_3)	35
8	Hexylmethyl siloxane (C_6H_{13}-CH_3)	35
9	Octylmethyl siloxane (C_8H_{17}-CH_3)	35
10	Octylmethyl siloxane (C_8H_{17}-CH_3)	20
11	Methyl hydrogen siloxane (H-CH_3)	35
12	Dimethyl siloxane (CH_3-CH_3)	43
13	Methyl-phenyl siloxane (CH_3-C_6H_5)	12
14	Methyl-phenyl siloxane (CH_3-C_6H_5)	18
15	Dimethyl siloxane (CH_3-CH_3)	240
I	Dimethyl siloxane (CH_3-CH_3)	70
J	Methyl-trifluoropropyl (CH_3-$C_2H_2F_3$)	30

dimethyl fluids with increasing *DP;* fluids 12, 1, 15, respectively, and (*d*) a set of fluids where the side radical *R* was not an alkyl group, fluids 11, 13, 14, and *J*. But for a small difference in *DP* (43 versus 35), fluid 12 could also be included in the first series above. This set of fluids permits the determination of the effect of the degree of polymerization, and the size and nature of the side radical on the pressure-temperature-viscosity characteristics of siloxane fluids.

Fluid 7 had a viscosity somewhat lower than would be expected for it when compared to the rest of the DP-35 group of fluids. It was found by gas chromatography analysis that this sample had 3 percent unreacted olefin $C_{14}H_{28}$ present. This material was used in synthesizing fluid 7 from a methyl hydrogen siloxane similar to fluid 11 and the unreacted material was not adequately distilled from the sample. This diluent is expected to reduce the 25 C viscosity 500 to 1000 cs (5 to 10 $\times$ 10^{-4} m^2/sec) but have little effect on other physical properties of the sample. It becomes increasingly difficult to remove the unreacted olefins as the size of the side radical increases. Therefore, fluids 2 and 10 [$(C_{12}H_{23}CH_3SiO)_n$ and $(C_{10}H_{21}CH_3SiO)_n$, respectively] were also checked by gas chromatography, but no residual olefins were found in them.

Experimental Apparatus

A high pressure capillary viscometer was employed which has been reported in detail elsewhere [6]. The viscometer is shown schematically in Fig. 2. The upper pressure limit of the device is 6.89 $\times$ 10^8 N/m^2(100 kpsi), the shear stress range is from 30 to 1.2 $\times$ 10^5 N/m^2 (300 to 1.2 $\times$ 10^6 dyne/cm^2) and the viscosity range is from somewhat less than 1 to more than 10^5 centipoise. The temperature of the fluid sample is controlled by a constant temperature bath and can be varied from -45 to 232 C.

Referring to the schematic in Fig. 2, the test fluid is contained in reservoirs R1 and R2 and in the high pressure tubing connecting the two reservoirs to the test section which contains the capillary. The test section is immersed in the constant temperature bath. The fluid in the test section is pressurized by pumping low pressure hydraulic fluid into cavity I and venting cavity II. The high pressure is generated by an intensifier which has a 50 to 1 area ratio between piston P1 and the high pressure piston P2. Flow through the capillary is caused by moving the translating piston along the two high pressure rams. Movement along these rams is measured by a displacement transducer which when recorded as a function of time indicates the volumetric flowrate through the capillary. Care must be taken to insure that no test fluid initially outside the constant temperature bath passes through the capillary during the time measurements are being made.

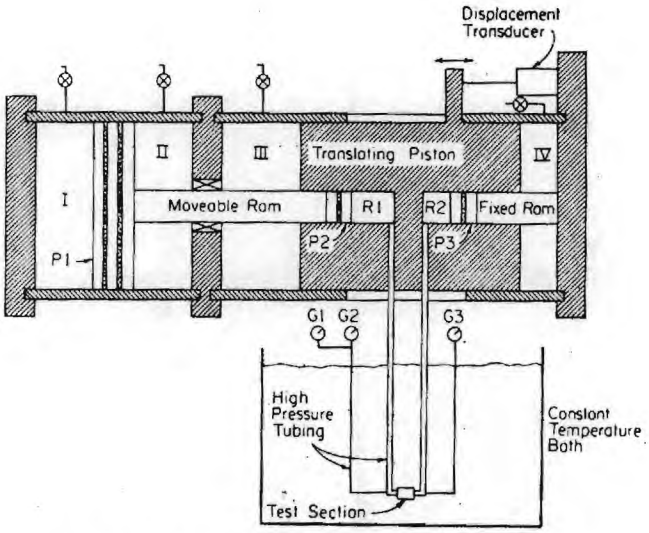

Fig. 2 Schematic diagram of high pressure viscometer

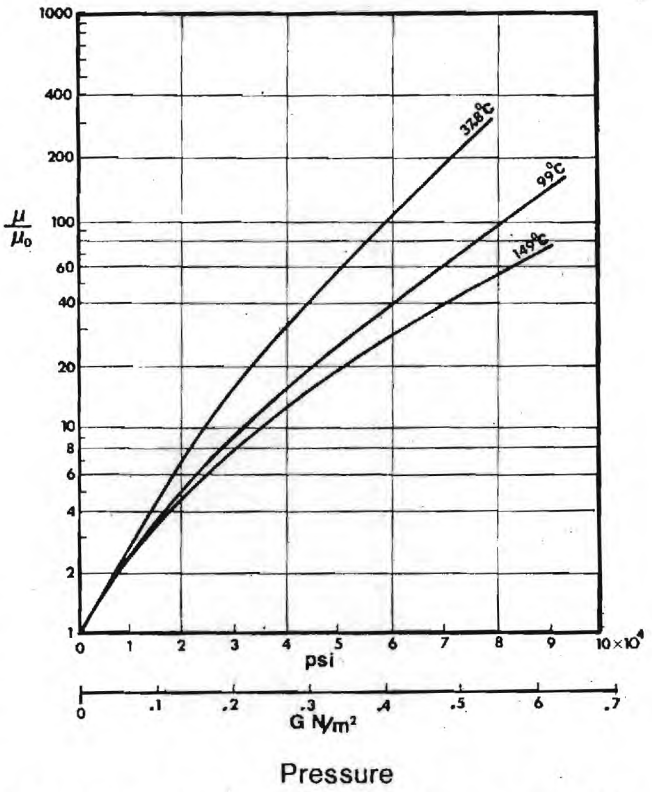

Fig. 3 Reduced viscosity pressure isotherms for octylmethyl fluids [1, 3, 4, 9, 10] at 37.8 C, 99 C, and 149 C

Nomenclature

$$\alpha_{OT} \equiv \left.\frac{\partial \ln \mu}{\partial p}\right|_{T,p=0} \qquad \alpha^* \equiv \left.\left[\mu_0 \int_0^\infty \frac{dp}{\mu(p)}\right]^{-1}\right|_T$$

μ = viscosity

μ_0 = viscosity at atmospheric pressure

Table 2 Measured viscosity and density of experimental fluids at atmospheric pressure

Fluid	Temp[1] (C)	Viscosity[2] $m^2/sec \times 10^6$	Viscosity[2] $N\ sec/m^2 \times 10^3$	Density[3] $kg/m^3 \times 10^{-3}$	Maximum pressure[4] for viscosity measurements $[N/m^2] \times 10^{-7}$
1	25	25.2	22.2	0.880	
	37.8	17.4	15.2	0.871	54.6
	99	5.01	4.15	0.829	51.6
	149	2.73	2.18	0.799	54.0
2	25	8856	7935	0.896	
	37.8	5282	4690	0.888	15.7
	99	1026	870	0.848	18.4
	149	455	372	0.818	21.4
3	25	105	94	0.895	
	37.8	62.1	55	0.886	55.2
	99	15.8	13.4	0.846	48.3
	149	8.24	6.72	0.816	55.3
4	25	770	692	0.899	
	37.8	485	433	0.891	50.4
	99	100	86	0.859	53.4
	149	52	43	0.823	54.0
5	No Data	—	—		
6	25	2390	2153	0.901	
	37.8	1467	1310	0.893	35.8
	99	302.5	258	0.853	47.4
	149	144	118	0.818	48.0
7	25	3390	2983	0.880	
	37.8	2035	1775	0.872	3.6
	99	384	320	0.883	3.6
	149	171	137.5	0.803	3.6
8	25	1895	1743	0.920	
	37.8	1217	1110	0.912	34.7
	99	299	260	0.870	34.1
	149	179	125	0.837	54.3
9	25	1864	1683	0.903	
	37.8	1212	1085	0.895	42.3
	99	274	235	0.856	53.7
	149	131	108	0.825	54.0
10	25	373	337	0.904	
	37.8	239	214	0.896	54.3
	99	55	47	0.856	53.8
	149	26.3	21.65	0.823	54.9
11	25	33	33	0.999	
	37.8	26.6	26.2	0.986	55.2
	99	12.5	11.55	0.925	55.2
	149	8.35	7.31	0.875	53.9
12	25	50	48	0.954	
	37.8	41.5	39.1	0.943	54.4
	99	17.0	15.2	0.894	54.9
	149	8.6	7.31	0.850	56.3
13	25	441	483	1.096	
	37.8	238	259	1.087	14.7
	99	33.0	34.5	1.045	14.2
	149	13.75	13.87	1.009	14.0
14	25	85	89	1.050	
	37.8	58.8	61.2	1.040	27.3
	99	17.5	17.4	0.994	32.7
	149	8.62	8.25	0.957	29.3
15	25	484	470	0.971	27.9
	99	188	170	0.906	27.6
I	25	106	103	0.906	
	37.8	82.7	79.2		56.1
	99	33.8	30.6		49.4
J	25	135	166	1.23	
	37.8	77.2	95.0	1.17	35.4
	99	14.4	16.9		42.8

(1) 25 C = 77 F, 37.8 C = 100 F, 99 C = 210 F, 149 C = 300 F
(2) Multiply m^2/sec by 10^6 to get cs; multiply N sec/m^2 by 10^{-3} to get cp.
(3) Multiply kg/m^3 by 10^{-3} to get gm/cc.
(4) Multiply N/m^2 by 1.45×10^{-4} to get psi.

The test section consists of standard high pressure tubing with a stainless steel capillary tubing pressed into it. The capillary tubing has a nominal I.D. of 2.54×10^{-4}m (0.01 in.). Several interchangeable capillaries of differing lengths were made so that a range of length-to-diameter ratios were available. This permits one to cover a wide range of shear rates and shear stresses with the instrument. The capillary diameters were determined in the usual manner of viscometry by calibration with viscosity standards.

The pressure level and pressure drop across the capillary were measured with commercial strain-gage pressure transducers indicated by G1, G2, and G3, in Fig. 2, respectively. The electrical signals of G2 and G3 were nulled, through electrical balancing, at the pressure level of interest. Then, by amplifying the signals from these transducers through high gain d-c amplifiers small fluctuations of pressure about the pressure level were detected with considerable accuracy.

The signals from the three pressure transducers and the dis-

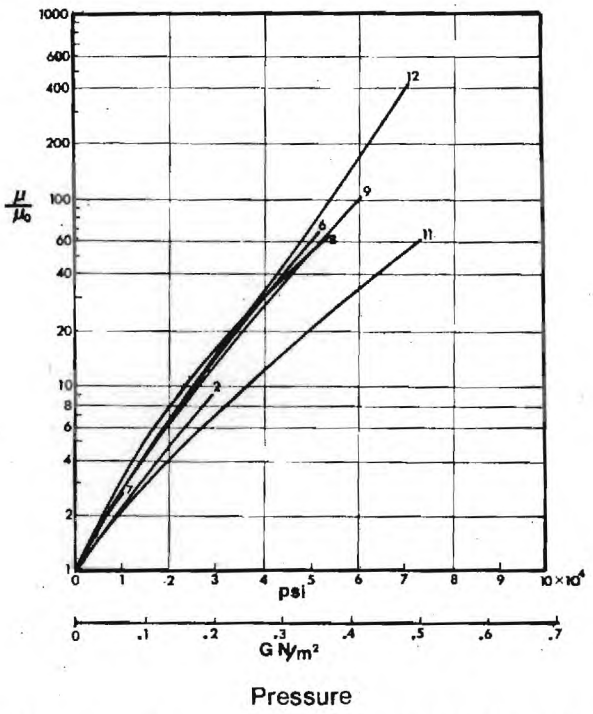

Fig. 4(a) Reduced viscosity pressure isotherms for DP-35 fluids [2, 6, 7, 8, 9, 11, 12] at 37.8 C

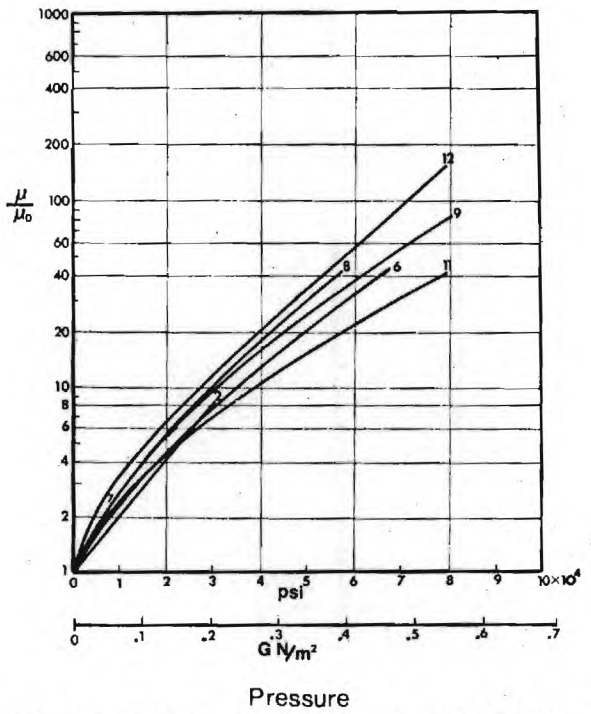

Fig. 4(b) Reduced viscosity pressure isotherms for DP-35 fluids [2, 6, 7, 8, 9, 11, 12] at 99 C

placement transducer were recorded continuously as a function of time. This enables one to use only steady state behavior when deducing the viscosity of a fluid.

A detailed discussion of the calibration procedure, accuracy and viscometric limitation of the apparatus has been published elsewhere [6].

Experimental Measurements Performed

Two types of viscosity data were obtained for each fluid. Viscosity pressure isotherms were obtained at 37.8 C (100 F), 99 C (210 F), and 149 C (300 F). These were all taken at shear stresses of approximately 4×10^3 N/m². The second set of data was taken at 37.8 C (100 F) and pressures of approximtely 6.8×10^7 and 13.8×10^7 N/m² (10 and 20 kpsi) (for fluid 12 these were also made at 20.7×10^7 and 32.4×10^7 N/m² (30, 47 kpsi)) and for varying shear stresses from 4×10^3 to 1.5×10^6 N/m². The first set was to determine the relationship of pressure-temperature viscosity behavior and molecular structure, and the second set was to assess the extent of non-Newtonian pseudoplastic shear thinning at elevated pressure as it relates to molecular structure.

Kinematic viscosity and density at atmospheric pressure and temperatures of 25 C (77 F), 37.8 C (100 F), 99 C (210 F), and 149 C (300 F) we measured according to ASTM Methods D-445-65 and D-1217-54, respectively. These data along with the maximum pressure for which pressure-viscosity data were obtained for each fluid are shown in Table 2.

A very large body of data has been collected and space permits only the presentation of the more significant parts of it.

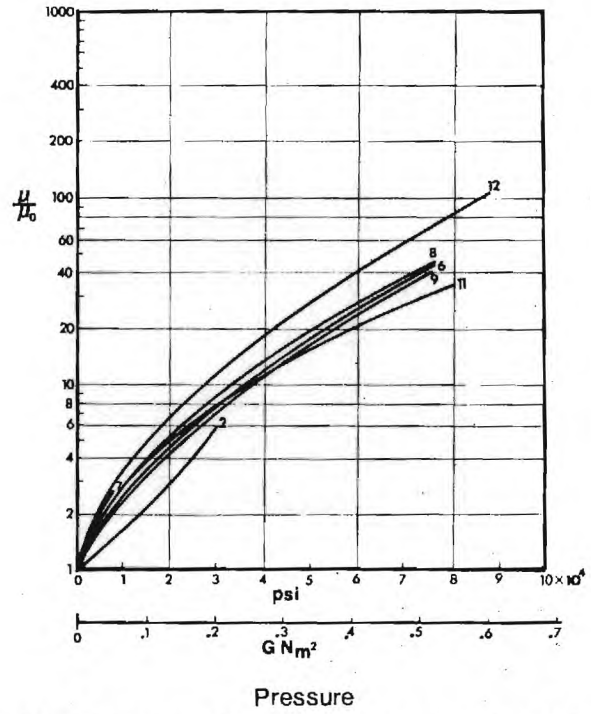

Fig. 4(c) Reduced viscosity pressure isotherms for DP-35 fluids (2, 6, 7, 8, 9, 11, 12) at 149 C

Experimental Results

The experimental pressure viscosity data are presented in several ways. Fig. 3 displays the reduced viscosity $(\mu(p)/\mu_0)$ pressure isotherms for the octylmethyl fluids (1, 3, 4, 9, 10) at 37.8, 99, and 140 C, respectively. The difference between these fluids at each temperature is so small it would be difficult to distinguish between them on these graphs. Fig. 4 (*a,b,c*) and Fig. 5 (*a,b,c*) are similar to Fig. 3 but for the DP-35 fluids and fluids 9, 11, 13, 14, *J* respectively. Figs. 3 and 4 at 37.8 and 149 C are almost identical except for Fluid 11 at 37.8 C and Fluid 12 at 149 C as seen from Fluid 9 which is on each figure for comparison. It is clear from these data that neither the degree of polymerization nor the size of the alkyl side radical have much influence on the low shear rate reduced viscosity pressure behavior even though they do influence the viscosity level, viscosity-temperature dependence, and viscosity-shear dependence. However as seen from Fig. 5 (*a,b,c*) if the nature of the side radial R is changed from an alkyl group to hydrogen, phenyl, or trifluoropropyl the

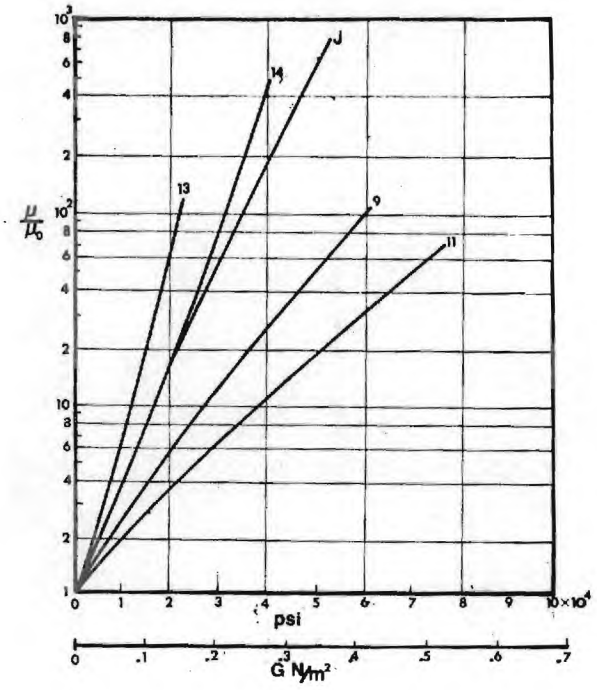

Fig. 5(a) Reduced viscosity pressure isotherms for fluids (9, 11, 13, 14, J) at 37.8 C

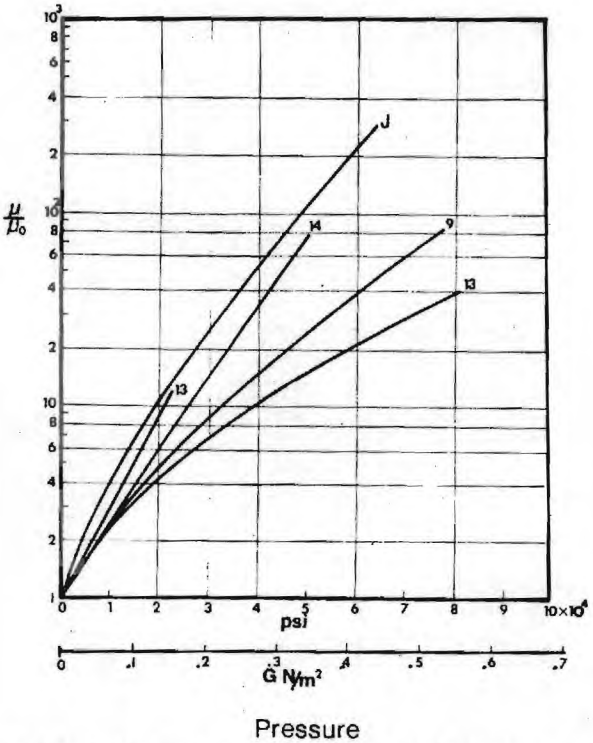

Fig. 5(b) Reduced viscosity pressure isotherms for fluids (9, 11, 13, 14, J) at 99 C

reduced viscosity pressure behavior changes considerably. If the alkyl group is replaced with hydrogen, the effect of pressure and temperature upon viscosity is reduced (i.e., fluid 11). While if the alkyl group is replaced by a bulkier group such as phenyl (fluids 13 and 14) or a trifluoropropyl group (fluid J) the effect of pressure and temperature upon reduced viscosity is considerably increased. The higher phenyl content gives the greater

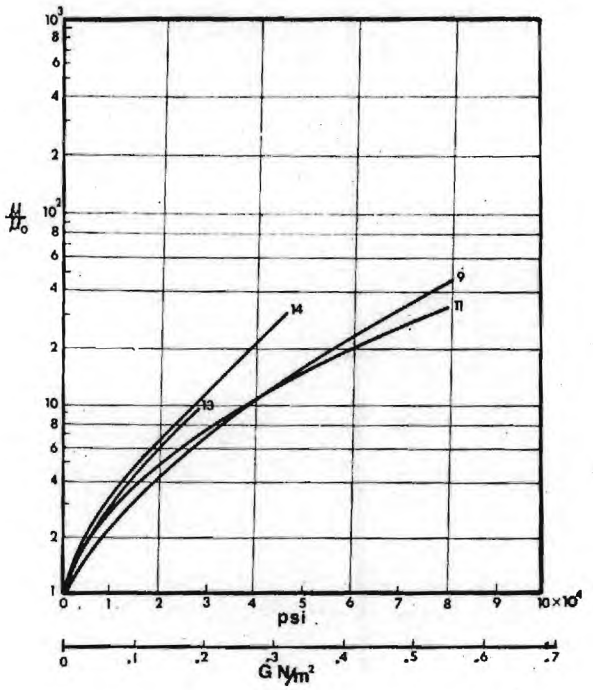

Fig. 5(c) Reduced viscosity pressure isotherms for fluids (9, 11, 13, 14, J) at 149 C

viscosity-pressure dependence (Fluids 13 versus 14). However, as the temperature is increased the pressure dependence of viscosity decreases such that at 149 C there is relatively little difference among any of the 15 fluids for which data was taken at that temperature.

In elastohydrodynamic lubrication the pressure viscosity characteristics are important. However, there is little agreement on a method of expressing this characteristic in a concise and meaningful fashion. There are several methods available. Traditionally the slope of the tangent to the isothermal log viscosity versus pressure curve at atmospheric pressure has been used (α_{OT}). However, there is an increasing interest in α^*. We tend to prefer the latter since it takes the entire pressure-viscosity curve into account. Table III contains these two pressure-viscosity parameters at each temperature for the fluids examined.

α_{OT}, although most commonly used for elastohydrodynamic correlations, is the most difficult to obtain from experimental pressure-viscosity data. To obtain α_{OT} one must differentiate experimental data at one end of the range of experimental data, a procedure which lends itself to considerable uncertainty of the result and which makes the result strongly dependent on the accuracy of only a few data points. α^*, however, is obtained from integrating the experimental data over the entire range of variables, a procedure which lends itself to increased accuracy and makes α^* less dependent on the accuracy of any individual data points. In addition α^* is actually the material property which occurs in an isothermal elastohydrodynamic analysis as pointed out by Blok [7] and Roelands [8] and comes from the Weibull transformation [9], for considering the effect of pressure dependent viscosity in hydrodynamic analysis.

The pressure viscosity coefficients, α_{OT} and α^*, are functions of temperature and almost invariably decrease with increasing temperature. It has been found empirically that a good relationship between temperature and α^* is the ln α^* versus T relationship. Fig. 6 contains plots of ln α^* versus T. The tendency of the pressure-viscosity behavior of all the fluids to approach one another as temperature increases is also seen in Fig. 6. Data for fluid 7 should not be weighed to heavily because it solidified in

the viscometer at 4.9×10^7 N/m² (7 kpsi) and room temperature. Hence the data on fluid 7 is limited to pressures below 4.9×10^7 N/m².

Fig. 7 is a plot of the α^* at 37.8 C as a function of the degree of polymerization (DP). Fig. 7 shows once again that the effect of DP or size of the alkyl side radical on pressure viscosity characteristics of these fluids is small compared to the effect of changing the nature of the side radical on the siloxane chain even though the base viscosities differ by as much as a factor of 330.

When considering the viscosity-pressure dependence as measured by α^* (Fig. 6) we see that fluids 13 and 14 have greater values of α^* at 37.8 C than the other fluids, but at 99 and 149 C they are similar to the other fluids. Because EHD film thickness is dependent on the pressure-viscosity variation of the fluids, we would expect a greater film thickness for comparable viscosity level from fluids 13 and 14 at 37.8 C. These thick films for fluids 13 and 14 relative to the others would not be expected at higher temperatures such as 99 C and 149 C.

An attempt was made to employ Roeland's [8] correlation to describe the pressure-temperature-viscosity behavior of the fluids investigated. However, there were 18 of the 45 isotherms measured where the deviation of the data from the Roeland's prediction was significant. In these cases the deviation from a straight line when plotting the data on a Roeland's chart resulted in measured viscosities as much as ±100 percent different from the value predicted by the best fit straight line through the data. Because of these deviations the constants from the Roeland's correlations for these fluids are not reported. Reasonable estimates of viscosity at a given temperature and pressure can be obtained from the reduced viscosity plots (Figs. 3–5) and the atmospheric pressure data given in Table 2.

The decrease of viscosity with increasing shear stress at elevated pressure is not reported for lack of space but will be discussed. A decrease in viscosity at high shear rate can be the result of pseudoplastic shear thinning (non-Newtonian behavior) or viscous heating in the capillary at high shear stress resulting in a viscosity decrease because of local temperature increases. The maximum reduction in viscosity at 10^8 N/m² was only 40 percent while the average was less than 10 to 15 percent for all the fluids studied. The larger reductions were seen in the higher molecular

Table 3(a) Pressure viscosity characteristics[a] — α_{OT}

	$\alpha_{OT} \times 10^8$ (N/m²)$^{-1}$			
Fluids	23.5 C[b] (75 F)	37.8 C (100F)	99 C (210F)	149 C (300F)
1	2.10	1.96	1.50	1.65
2	1.16	1.12	0.88	0.70
3	1.45	2.60	1.75	1.46
4	1.30	1.47	1.92	1.48
6	2.00	1.60	1.10	1.59
7	1.57	1.52	1.45	1.52
8	1.45	1.63	1.90	1.90
9	1.29	1.23	1.28	1.35
10	1.41	1.44	1.47	1.45
11	0.93	1.05	1.48	1.48
12	1.86	1.97	2.22	2.22
13	3.05	2.49	1.56	1.67
14	3.05	2.47	1.43	1.67
I	1.38	1.51	2.09	—
J	1.99	2.06	2.32	—
15	2.18		2.17	

(*a*) To obtain pressure viscosity coefficient in [psi]$^{-1}$, multiply the entry in the table by 6.894×10^3.
(*b*) Extrapolated Data except for 15.

Table 3(b) Pressure viscosity characteristics[a] — α^*

	$\alpha^* \times 10^8$ (N/m²)$^{-1}$			
Fluids	23.5 C[b] (75 F)	37.8 C (100 F)	99 C (210F)	149 C (300F)
1	1.44	1.37	1.07	0.96
2	1.20	1.17	1.01	0.87
3	1.38	1.32	1.12	0.98
4	1.30	1.31	1.15	0.95
6	1.62	1.32	0.97	1.00
7	1.55	1.52	1.45	2.18
8	1.37	1.36	1.20	1.08
9	1.29	1.25	1.04	0.94
10	1.32	1.29	1.08	0.97
11	0.89	0.91	0.98	1.02
12	1.42	1.40	1.39	1.38
13	2.77	2.60	1.60	1.43
14	2.54	2.20	1.29	1.26
I	1.23	1.25	1.42	—
J	2.04	1.96	1.67	—
15	1.95		1.73	

(*a*) See footnote (*a*) in Table 3(*a*).
(*b*) Extrapolated data except for 15.

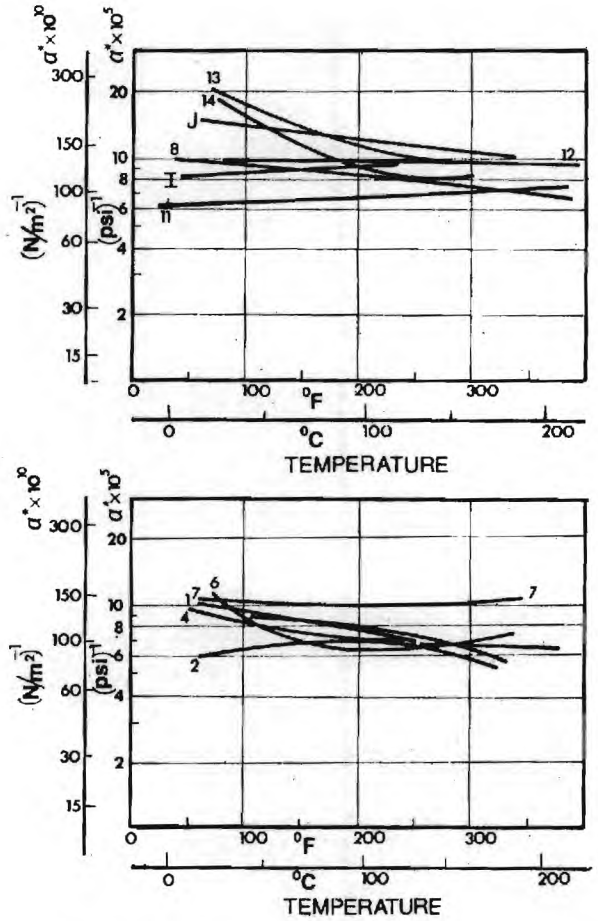

Fig. 6 Temperature dependence of pressure-viscosity coefficient α^*

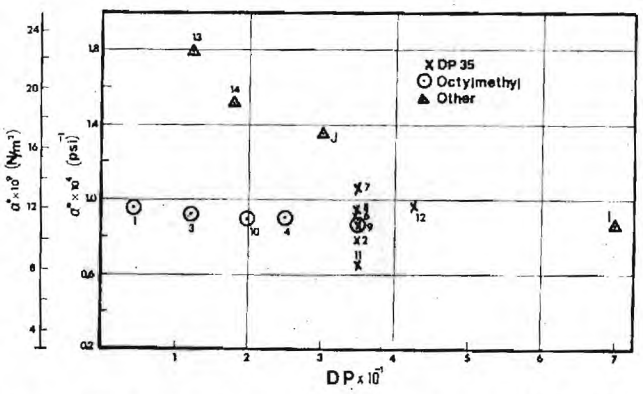

Fig. 7 Pressure viscosity characteristic α^* as a function of *DP* at 37.8 C

Table 4 Pressure viscosity characteristics from a Bridgman's data [10] and ASME [11]

Siloxane fluid(b)	Temp. (C)	Atm. pressure viscosity μ_0 Nsec/m² × 10³	α_{OT} × 10⁸ [N/m²]⁻¹	α^* × 10⁸ [N/m²]⁻¹	Source ref.
Trimer	25	0.847	1.25	0.98	10
Tetramer	25	1.307	1.56	1.12	10
Hexamer	25	2.38	1.62	1.17	10
Octamer	25	3.57	1.42	1.14	10
500–1.00 cs	25	0.82	1.59	1.01	10
500–2.00 cs	25	1.74	1.46	0.89	10
500–12.8 cs	25	12.03	1.54	1.30	10
200–10.0 cs (100 cs)	25	97.0	1.33	1.20	10
53	25	170	2.46	2.83	11
	37.8	115	1.96	2.22	
	99	21	1.75	1.45	
55	25	91	1.96	1.65	11
	37.8	70	2.22	1.65	
	99	26.5	2.15	1.52	

(a) See footnote (a) Table 3(a).
(b) Fluid designations employed here are those used in the original publications. All the fluids except 53 are dimethyl siloxane polymers. Fluid 53 is a phenylmethyl siloxane polymer. The fluid 200-10.0 cs in the Bridgman reference was mislabeled and was actually a 100 cs dimethyl fluid (private communication from Dr. A. J. Barry of Dow Corning, November, 1970).

weight materials which would be expected to be more likely to exhibit shear thinning and to have greater viscosity-temperature dependence. The separation of the two effects is difficult and is the subject of another research program in this laboratory.

Bridgman [10] reported pressure-viscosity data at 25C on series of eight dimethyl silicones (Trimer, Tetramer, Hexamer, Octamer, and blends with base viscosities of 1, 2, 12.8, and 100 cs each). The pressure viscosity characteristics as described by α_{OT}, and α^* for these fluids at 25 C are shown in Table 4. Also shown in Table 4 are two siloxane fluids reported in the 1953 ASME Pressure Viscosity Report [11]. Fluid 53 is a methylphenyl siloxane fluid similar to our fluids 13 and 14 while fluid 55 is a dimethyl siloxane with the same base viscosity as our fluid 1 and Bridgman's 200-100cs fluid. When considering the α_{OT} data, that of Bridgman is less reliable than that of either ASME or our own because of the much larger pressure increments used by Bridgman. The α^* data are more reliably compared between the three sources. When comparing the α^* data from the three sources for the dimethyl fluids (1, 55, 200-100cs) we see that our data and Bridgman's are within 2 percent and the ASME data is consistently higher than ours over the entire temperature range. The ASME data is about 30 percent higher at 25C and only 7 percent higher at 99C. Although not exactly the same, ASME fluid 53 is similar to our fluids 13 and 14 with respect to viscosity and methyl/phenyl content ratios. When comparing the α^* data for the three fluids the agreement in level and temperature dependence for the ASME fluid is very similar to our fluid 14, which has the same phenyl content as the ASME fluid but a lower molecular weight.

Conclusions

The range of methyl alkyl siloxanes investigated was representative of those most likely to be used as liquid lubricants or mechanical fluids. The viscosity at atmospheric pressure and the viscosity temperature variation both were found to increase as either the degree of polymerization or the number of carbon atoms in the alkyl side radical were increased. Shear thinning at high shear stress (10^5 N/m²) also apparently increases with increases in molecular size although a clear distinction between shear thinning and viscous heating could not be made. The total reduction in apparent viscosity from both viscous heating and shear thinning was never more than 40 percent, even for the highest molecular weight material investigated, and was more commonly less than 10 to 15 percent.

Varying the degree of polymerization or the number of carbon atoms in the alkyl side radicals has little effect (±10 percent) on the pressure-viscosity coefficient α^* which is believed to be of most importance for elastohydrodynamic lubrication. The range of degree-of-polymerization and size of side radical investigated includes those which might be expected to be useful for lubrication applications.

The pressure-viscosity coefficient α^* can be changed by changing the nature of the side radical on the siloxane chain. Thus if the side radical is hydrogen, as in the methyl hydrogen siloxane (fluid 11), the α^* is reduced and if the side radical is a phenyl group or a trifluoropropyl group (as in fluids 13, 14, *J*) the α^* is increased compared with the dimethyl or methyl-alkyl siloxanes. However, the differences of α^* between the methyl alkyl siloxanes and fluids 11, 13, 14, and *J* are reduced as temperature is increased such that there is little difference between them at 99 C and 149 C. The methyl phenyl siloxane (fluid 14) has an α^* 80 percent greater than α^* for the dimethyl fluid 12 at 25 C but at 99 C and 149 C the α^* of fluid 14 is 6 and 10 percent less than that of fluid 12 at the same temperature respectively.

The decrease of the pressure-viscosity coefficient α^* with increasing temperature reported for most of these fluids has been observed for several other fluids.

Acknowledgments

The authors wish to acknowledge the support of the Dow Corning Corporation for supplying the fluids and for a grant-in-aid to help support the work, and of a grant (GK-31154) from the National Science Foundation, which also helped support this research.

References

1 Quaal, G. J., and Groenhof, E. D., "Recent Advances in Silicone Oil Lubricants," *An Assessment of Lubrication Technology*, ASME, 1972.

2 Schiefer, H. M., Awe, R. W., and Whipple, C. L., "Extending the Utility of Silicone Lubricants Through Structural Modifications," *Journal of Chemical and Engineering Data*, Vol. 6, No. 1, Jan. 1961.

3 Brown, E. D., "Methyl Alkyl Silicones. A New Class of Lubricants," *Trans. ASLE*, Vol. 9, No. 1, 1966, pp. 31–35.

4 Schiefer, H. M., "Trifluoropropyl Halophenyl Substituted Silicone Copolymers—A New Class of Wide Temperature Range Lubricants," *Trans. ASLE*, Vol. 9, No. 1, 1966, pp. 36–46.

5 Smith, R. E., Groenhof, E. D., and Winer, W. O., "The Behavior of Fluorosilicones as Lubricants," Synthetic Lubricants Symposium, AIChE Conference, Atlanta, Ga., February 18, 1970.

6 Novak, J. D., and Winer, W. O., "Some Measurements of

High Pressure Lubricant Rheology," JOURNAL OF LUBRICATION TECHNOLOGY, TRANS. ASME, Series F, Vol. 90, No. 3, July 1968, pp. 500–591.

7 Blok, H., "Inverse Hydrodynamics," *Proceedings of the International Symposium on Lubrication and Wear*, edited by Muster and Sternlicht, McCutehan Publishing Corp., Berkeley, Calif., 1964, pp. 1–151.

8 Roelands, C. J. A., "Correlational Aspects of the Viscosity-Temperature-Pressure Relationship of Lubricating Oils," doctor ingenieur dissertation, Technische Hogeschool te Delft, 1966 (also OP Books Program, University Microfilm, Ann Arbor, Mich.).

9 Weibull, W., "Slidlagerteori med variabel viskositet," (Plain Bearing Theory With Variable Viscosity), *Teknisk Tidskrift*, Mekanik, Vol. 55, 1925, pp. 164–167.

10 Bridgman, P. W., "Viscosities to 40,000 Kg/cm^2," *Proceedings of the American Academy of Arts and Sciences*, Vol. 77, 1949, pp 117–128.

11 ASME Pressure Viscosity Report Vol. I, II, ASME, New York, 1953.

DISCUSSION

Robert L. Johnson[3]

The siloxane series of fluids offers unique opportunities to observe the influence of structural variations on rheological properties of interest in thin film lubrication. There is always danger in overgeneralization, but the results of this paper offer tempting guidelines for speculating on the behavior of other fluid types in concentrated contacts. Can the authors indicate the extent to which such generalization might hold up?

One of the anomalies of concentrated contact lubrication has been the general acceptance of the importance of pressure–viscosity coefficients in analytical studies but the inability to demonstrate that effect experimentally. The observation in the present paper is that differences in pressure–viscosity coefficient disappear at higher temperatures (e.g., 149 deg C), which are still modest for many applications. When we add to the high ambient temperatures the very substantial transient increases in fluid temperature in the contacts [12], it becomes apparent that our real knowledge of lubricant conditions in concentrated contacts is very weak. We hope that IR analysis methods will allow a much better definition of fluid state in concentrated contacts in the near future.

The authors have pointed out the deficiency of Roelands' chart for correlating pressure-temperature-viscosity behavior of fluids. Are there alternate correlation methods that are more accurate or otherwise more useful than that of Roelands?

Several years ago, two of the authors obtained some pressure–viscosity data at relatively high shear stresses for NASA-Lewis with fluids of interest in our lubrication research program. At that time we were concerned about viscous heating in the capillary as the potential origin of non-Newtonian behavior, as mentioned by the present authors. Data on the same fluids obtained with an oscillating crystal method at the University of Oklahoma Research Institute (NASA CR-120786) gave similar results. Both evaluation methods showed non-Newtonian effects, and the oscillating-crystal method was not subject to the capillary viscous heating influence.

The structural rearrangements of the present paper deal with side chain effects and polymeric chain lengths, but without modification to the structure of the chain. Can the authors provide general guidelines as to the effects of other type of structures (e.g., aromatic) in the molecules backbone on pressure viscosity.

Additional References

12 Turchina, V., Sanborn, D. M., and Winer, W. O., "Temperature Measurements in Sliding Elastohydrodynamic Point Contacts," JOURNAL OF LUBRICATION TECHNOLOGY, TRANS. ASME, Series F, Vol. 96, No. 3,

[3] National Aeronautics and Space Administration, Lewis Research Center, Cleveland, Ohio.

F. W. G. Fearon[4]

The authors are to be congratulated on a careful piece of work that is a significant contribution to our understanding of the behavior of silicone fluids.

Data presented clearly indicate that chemical composition is the dominant factor governing the pressure–viscosity characteristics of these materials. However, it appears to this discusser that the significant differences observed between alkylmethyl, phenylmethyl trifluoropropylmethyl, and methylhydrogen polysiloxanes probably reflect basic differences in intermolecular interactions, rather than mere differences in bulk of the substituent as the authors suggest. If size of the substituent alone were the governing factor, greater differences might be expected between dimethylpolysiloxane and decylmethylpolysiloxane than are actually observed.

The conclusion that degree of polymerization has little effect on the pressure–viscosity behavior was arrived at by considering a series of octylmethylpolysiloxanes endblocked with trimethylsiloxy moieties in which the minimum degree of polymerization was four to five. This conclusion may not hold for shorter chains when the trimethylsiloxy groups become a significant portion of the molecule.

Edward Brown

This paper is a welcome addition to the literature at a time when silicone fluids are being used in mechanical applications to a much greater degree. Several of the fluids tested have been checked in our laboratories and by Wolveridge. The agreement is well within the experimental error.

From a practical standpoint, we find it interesting that there is very little correlation between pressure–viscosity and sliding-friction lubricity. This is quite clear as we notice that the authors find no difference in viscosity–pressure characteristics as the alkyl group increases in length, but all authors (Tabor, Archard, Brown, etc.) find a sharp decrease in friction and wear when the alkyl side group reaches 6 to 8 carbons in length. Likewise, the materials with the greatest viscosity–pressure dependence (phenyl fluids) have the poorest lubricity.

Since the same characteristics hold in a disk tester, we must conclude that pressure–viscosity alone has little effect on lubricity, except in homologous series.

The data presented by the author, coupled with lubricity experience with the fluids, should serve as a starting point for most interesting studies.

[4] Dow Corning Corp., Midland, Mich.

V. TURCHINA
Graduate Student.

D. M. SANBORN
Assistant Professor.
Assoc. Mem. ASME

W. O. WINER
Professor.

Georgia Institute of Technology, School of Mechanical Engineering, Atlanta, Ga.
Mem. ASME

Temperature Measurements in Sliding Elastohydrodynamic Point Contacts

Techniques using the infrared radiation emitted by a sliding EHD point contact to measure oil film and surface temperature are discussed. Temperature distributions in the EHD contact are presented for a naphthenic mineral oil at 1.04 × 10^9 N/m^2 (150,000 psi) Hertz pressure and several sliding velocities. Film temperatures as high as 360 C are reported at locations near the points of minimum film thickness in the contact side lobes.

Introduction

EHD has been one of the major developing areas in lubrication in the last decade. Some of the significant unanswered questions in this field are related to the rheological behavior of the lubricant in the EHD contact and to the criteria for failure limits in EHD contacts. The rheological behavior of the lubricant is not only a function to the appropriate constitutive equation relating the stress and strain rate in the lubricant, but also to the thermodynamic state as defined by the pressure and temperature of the lubricant as it passes through the conjunction region. Because large amounts of mechanical energy are dissipated in the EHD film, particularly in contacts where there is some relative velocity between the surfaces, temperatures of the lubricant and the solid surfaces may be quite different from the ambient. The temperatures in the contact are important because the viscosity, which is probably the most important mechanical property of the lubricant in the contact, is a strong function of temperature. The viscosity decrease with increasing temperature becomes larger at elevated pressures such as those occuring in EHD contacts. Temperature increases in the inlet region may influence the minimum film thickness whereas temperature increases in the high pressure region will influence traction and surface shear stresses. The surface stresses in turn are an important factor in bearing surface failure. Several attempts at defining a failure criteria through a thermal analysis of lubricant films have been made the most notable of which is Blok's flash temperature theory [1].[1] Because of the importance of surface and film temperature in EHD films, the program described next was undertaken.

Most analytical research has assumed an isothermal fluid film, thereby greatly reducing the complexity of the mathematical model dealt with. Notable exceptions to this are the works of Crook [2], Cheng and Sternlicht [3], Dowson [4], and Archard [5 and 6]. In all of these investigations it was not only necessary to assume mechanical and thermal constitutive equations for the lubricant, but also to assume thermal boundary conditions for the film.

Relatively little experimental research has been directed toward the determination of temperatures in the EHD contact. Cheng and Orcutt [7] used a platinum film gauge on a glass disk to measure a surface temperature, and Hamilton and Moore [8] used a nickel film gauge on a glass disk to determine temperature. Both of these studies were for rolling contacts and limited to low Hertz pressures because a glass disk was used as one of the bearing surfaces. Because of these conditions, the measured temperature rises in the contact were small ($\leq$3 deg C).

In this paper a technique is described for measuring temperatures in the EHD contact. The technique is based on the emitted infrared radiation from the contact area. Through an appropriate set of measurements the local steel ball surface temperature and a local lubricant temperature averaged through the film can be determined.

Because the surfaces used for the EHD contact are steel and sapphire, the pressures in the contact are in the range of current design practice. The maximum Hertz pressure is 1.034 × 10^9 N/m^2 (150,000 psi) for the data reported. This data is for a sliding contact. For a given set of conditions the ball surface temperature reaches a maximum of 115 C and average fluid temperature reaches a maximum of 360 C, both occurring near the side lobes. The experiment is performed in a room temperature environment.

The temperature distributions obtained, along with film thickness and traction data from the same apparatus, can be used to evaluate lubricant constitutive equations. More importantly from a design point of view, they can be used to detect the onset of lubricant film failure and thereby evaluate or establish limiting design criteria for lubricated contacts.

[1] Numbers in brackets designate References at end of paper.

Contributed by the Lubrication Division of The American Society of Mechanical Engineers and presented at the ASLE-ASME Joint Lubrication Conference, Atlanta, Ga., October 16–18, 1973. Manuscript received by the Lubrication Division, July 9, 1973. Paper No. 73-Lub-23.

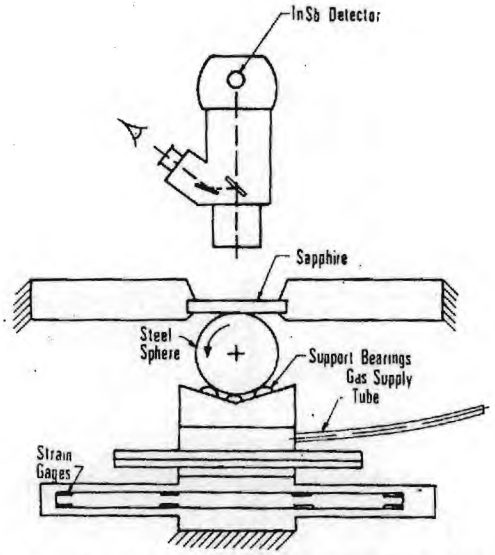

Fig. 1 Schematic diagram of the experimental equipment

Experimental Equipment and Technique

The sliding EHD point contact is formed using a 3.18×10^{-2} m (1.25 in.) diameter steel ball rotating and loaded against a 1.52×10^{-3} m (0.060 in.) thick sapphire flat. The system has been used previously in extensive investigations of film thickness [9] and traction [10]. As is shown in Fig. 1, the visual microscope used to observe interference fringe patterns for film thickness measurements has been replaced by an infrared radiometric detector (Barnes Engineering Company, Model RM-2A). The purpose of this detector is to measure the infrared radiation emitted from the contact and, therefore, allow contact temperatures to be deduced.

The radiometric detector has been equipped with a 15× reflecting objective which allows spot size resolution of 3.56×10^{-5} m (0.0014 in.). The radiation from this spot plus that from a related solid angle (Fig. 1) between this spot and the objective, is focused onto a liquid nitrogen cooled indium antimonide detector. This detector has a spectral response of 1.8 to 5.5×10^{-6} m (1.8 to 5.5 microns). The sapphire has a transmissivity of 0.90 over this same range, thus allowing the steel ball and oil film radiation to reach the detector. The visible light also collected by the objective is separated from the IR and is directed toward a visual eyepiece. The visual and IR systems are parfocal. The area covered by the detector is located in the center of the visual field of view and indicated by intersecting cross hairs. This allows one to focus on the oil film by visually searching for the interference fringe pattern characteristic of the EHD contact. The detector will then respond to radiation from the 3.56×10^{-5} m (0.0014 in.) diameter oil film and steel ball surface plus a volume of the sapphire disk (see Fig. 1). Since the temperatures of the lubricant film and the bearing surfaces are desired separately, rather than an average contact temperature,

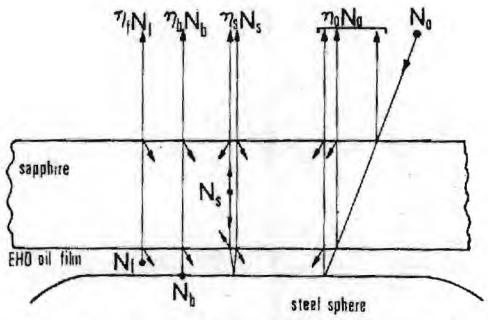

Fig. 2 Radiation incident on the detector (angles exaggerated for clarity)

experimental techniques have been devised to isolate the radiation contributions from the sapphire, lubricant film, and steel ball.

Fig. 2 shows the components of the radiation received by the In-Sb detector. There are four sources of areal radiant intensity: N_o—due to reflected ambient background radiation, N_s—due to emission from the sapphire, N_b—due to emission from the steel ball, and N_f—due to emission from the lubricant film. There is an attenuation factor associated with each of these components. Under the conditions listed below, these factors are:

$$\begin{aligned} \eta_o &= 0.082 + 0.683\,\rho_b \\ \eta_s &= 1.0 + 0.830\,\rho_b \\ \eta_b &= 0.830 \\ \eta_f &= 0.830 \end{aligned} \tag{1}$$

based on

1 Fresnel reflection losses of 0.076 at the sapphire—air interface and 0.0064 at the sapphire-oil interface [11].

2 Sapphire transmissivity of 0.90 for the 1.52×10^{-3} m (0.060 in.) thick disk [11].

3 The sapphire radiates to both hemispheres and a portion of the radiation initially directed toward the oil film is reflected back to the detector.

4 Absorptivity of the oil film is negligible due to its thickness of approximately 2.54×10^{-7} m (10^{-5} in.).

5 Although the oil film also radiates to both hemispheres, the effect has been accounted for in the value of emissivity assigned to the film.

The IR radiometric detector contains a black body source at ambient temperature. A mechanical chopper in the detector alternately exposes the detector to the total incident radiation and then to the black body reference. The output signal, therefore, is a function of the difference between these values

$$E = k(N_{\text{TOTAL}} - N_0) \tag{2}$$

where k is a known instrument constant. It can be seen from Fig. 2 that the total incident areal radiant intensity is given by

$$N_{\text{TOTAL}} = \eta_f N_f + \eta_b N_b + \eta_s N_s + \eta_0 N_0 \tag{3}$$

Nomenclature

E = microscope output signal—volts
f = traction force—N
h = film thickness—m
k = instrument constant
N = areal radiant intensity—watts/cm²-steradian
N^{BB} = black body areal radiant intensity
N_0 = black body areal radiant intensity at ambient temperature
T = temperature—deg C
t = transmissivity
U = sliding velicity—m/s
α = absorptivity
α^* = pressure viscosity coefficient—$\text{m}^2/\text{N} = \left[\int_0^\infty \frac{\mu_0 dp}{\mu(p)}\right]^{-1}$
ϵ = emissivity
η = an attenuation factor
ρ = reflectivity

Subscripts

b = steel ball
b_1 = steel ball of emissivity 0.28
b_2 = steel ball of emissivity 0.47
F = filter
f = EHD oil film
s = sapphire

Therefore, combining equations 1–3,

$$E/k = 0.830(N_f + N_b) + (1.0 + 0.830\,\rho_b)\,N_s + (0.683\,\rho_b - 0.912)\,N_0 \quad (4)$$

The reflectivity of the ball surface ρ_b can be measured with the radiometric detector. The quantity N_0 is dependent on the ambient temperature only and can be evaluated. The individual areal radiant intensity values N_f, N_b, and N_s are known functions of the source emissivity and temperature.

The 1.52×10^{-3} m (0.060 in.) thick sapphire is expected to have a large temperature gradient and radiation is emitted from throughout the thickness rather than just at a surface. Because the temperature distribution of the sapphire is unknown a sapphire surface temperature has not been determined thus far.

Since the steel ball is opaque, a surface emissivity and temperature can be associated with N_b. The emissivity of the ball surface has been determined at several temperatures using the radiometric detector. The technique is to paint a small spot of flat black paint ($\epsilon \simeq 0.95$) on the ball surface, heat the ball to an elevated temperature and then compare values of areal radiant intensity at adjacent points on the ball surface—one on and one off the painted section. This technique gave a surface emissivity of 0.28 for the 52100 chrome steel ball. This value was reproducible at several temperature levels.

The emissivity of the oil film must be determined before a film temperature can be calculated. Since the oil film is an absorbing medium with anticipated high temperature gradients, the temperature which will be assigned to the oil film will be an average temperature across the film. Because the areal radiant intensity is related to the fourth power of temperature, however, this average value will be skewed toward the maximum temperature in the film. In general, the emissivity of the oil film is a function of oil chemistry, wavelength and film thickness. The emissivity, therefore, must be determined for the lubricant being used with the same detector to be used in temperature measurements. Once the dependence on film thickness is known, film thickness profiles previously obtained [9] can be used to obtain a local emissivity value. McMahon [12] presents a relation between effective emissivity and film thickness of a semi-transparent material. For a lubricant film thickness h, the relation is

$$\epsilon = \frac{(1 - \rho^*)\,(1 - e^{-\lambda h})}{(1 - \rho^* e^{-\lambda h})} \quad (5)$$

where λ is an absorption coefficient for the oil film and ρ^* is the effective reflectivity of the oil film. In a separate experiment in which a stationary ball was placed in a constant temperature bath of the test lubricant with the sapphire resting on top of the ball, the areal radiant intensity was measured near the contact between the surfaces. An oil film occupied the space between the ball and sapphire. Since the dimensions of the gap can be determined from geometry alone, the radiation data at a known fluid temperature can be transformed into a local emissivity value. The data obtained resulted in an emissivity of 0.352 for a film thickness of 5.08×10^{-5} m (0.002 in.). Solving equation (5) for λ yields $\lambda = 9.43 \times 10^3$ m^{-1} (240 in^{-1}). For EHD film thicknesses on the order of 10^{-7} m (10^{-6} in.), the quantity λh is of the order 10^{-3}, allowing equation (5) to be accurately approximated by

$$\epsilon_f = \lambda h \quad (6)$$

For a given experiment, temperature is a function of only areal radiant intensity and emissivity, therefore,

$$T_b = f(N_b, \epsilon_b) \quad (7)$$

$$T_f = f(N_f, \epsilon_f) \quad (8)$$

Since the film thickness at any point in the contact can be determined using the optical interference technique [9], ϵ_b and ϵ_f can be found. However, there remain three equations (4), (7), (8) with five unknowns (N_f, N_b, N_s, T_b, T_f). Clearly, two additional independent relations must be found. This has been done by the following two alterations to the experiment described thus far.

In order to determine the ball surface temperature, the EHD experiment was repeated under identical conditions, but with a similar ball having an emissivity of 0.47 compared with that of 0.28 used in the first experiment. A comparison of film thickness values taken using each ball indicated that the conditions in the contact were identical regardless of which ball was used. The authors have shown through an order of magnitude analysis (see Appendix A) that the increased radiation from the ball surface will have a negligible effect on the film and surface temperatures. Therefore, for a given point in the contact, the data from the two experiments using a low and high emissivity ball

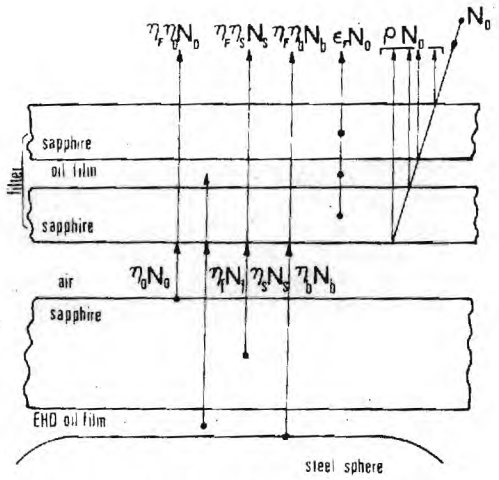

Fig. 3 Oil film filter (not to scale)

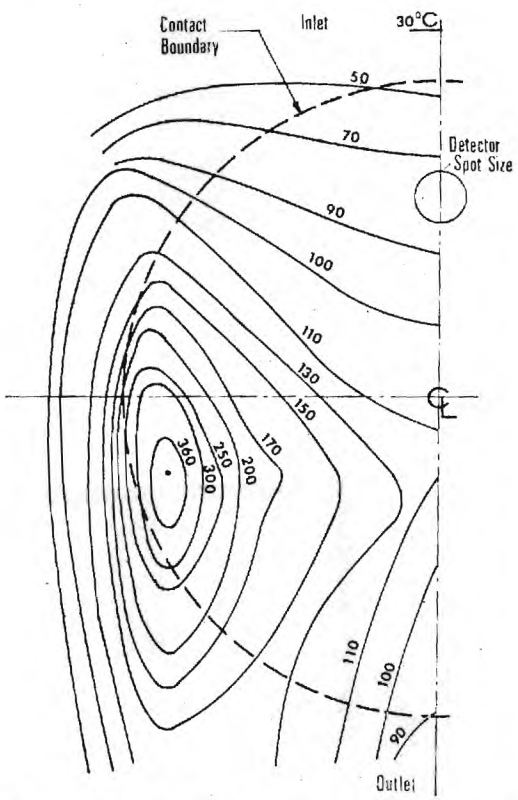

Fig. 4 Steady state film temperatures in the EHD contact at 1.39 m/sec (54.9 ips) sliding speed

will result in two different output signals E_1 and E_2. Since the transmissivity of the ball is zero [13]

$$\rho_b + \alpha_b = 1 \tag{9}$$

but at equilibrium [13]

$$\alpha_b = \epsilon_b \tag{10}$$

therefore

$$\rho_b = 1 - \epsilon_b \tag{11}$$

Equation (4) may now be rewritten for the low and high ball emissivity experiments

$$E_1/k = 0.830(N_f + N_{b1}) + 1.598\,N_s - 0.426\,N_0 \tag{12}$$

$$E_2/k = 0.830(N_f + N_{b2}) + 1.440\,N_s - 0.556\,N_0 \tag{13}$$

where the subscript 1 refers to the low emissivity ($\epsilon_{b1} = 0.28$, $\rho_{b1} = 0.72$) and 2 refers to the high emissivity ball ($\epsilon_{b2} = 0.47$, $\rho_{b2} = 0.53$). Subtracting equation (12) from (13)

$$\frac{E_2 - E_1}{k} = 0.830\,(N_{b2} - N_{b1}) - 0.158\,N_s - 0.130\,N_0 \tag{14}$$

The black body areal radiant intensity N^{BB} is a function of temperature only with

$$N = \epsilon N^{BB} \tag{15}$$

Since the ball surface temperatures are assumed equal in cases 1 and 2, equation (14) may be rewritten as

$$\frac{E_2 - E_1}{k} = 0.158N_b{}^{BB} - 0.158N_s - 0.130N_0 \tag{16}$$

With an ambient temperature of 24 deg C, $N_0 = 3.7 \times 10^{-3}$ watts/cm²-ster. A conservative estimate of N_s (see Appendix B) is on the order of 0.4×10^{-3} watts/cm²-ster or about 2 percent of $N_b{}^{BB}$ and has, therefore, been neglected. The value of $N_b{}^{BB}$ is typically of the order 20×10^{-3} watt/cm²-ster. The only unknown in equation (16) is $N_b{}^{BB}$. The temperature can be obtained from the black body areal radiant intensity, through the calibration curve supplied with radiometric detector.

Although the two experiments described above allow the determination of the ball surface temperature they are not sufficient to allow the film temperature to be deduced. The technique devised to isolate the film radiation consists of an experiment in which the low emissivity ball is used. The detector output signal E_1 is then compared with the signal E_3 obtained with a filter placed between the upper sapphire surface and the detector objective (see Fig. 3). The filter consists of a sandwich of two sapphire disks and a 5×10^{-5} m (0.002 in.) thick film of oil identical in composition to that being used in the EHD contact. Hence the radiation from the EHD oil film is absorbed by the oil in the filter. As can be seen from Fig. 3, those contributions other than $\eta_f N_f$ shown in Fig. 2 have been attenuated by a filter attenuation factor η_F. Because of a strong absorption band (C-H bond) in the naphthenic oil at 3.4 μ, the EHD oil film will emit primarily at this wave length. Since a much thicker film of the same oil at ambient temperature is used in the filter, the filter will absorb the entire contribution $\eta_f N_f$ from the EHD oil film. Fig. 3 also shows that the filter itself is emitting at T_0 and that some of the background radiation is also reflected from the filter. The total areal radiant intensity received in this third experiment is, therefore,

$$(N_{\text{TOTAL}})_3 = \eta_F\,(\eta_{b1}N_{b1} + \eta_s N_s + \eta_0 N_0) + \epsilon_F N_0 + \rho_F N_0 \tag{17}$$

Substituting equations (1) and (17) into equation (2) we get,

$$E_3/k = \eta_F\,(0.830N_{b1} + 1.598N_s + 0.574N_0) - (1 - \rho_F - \epsilon_F)\,N_0 \tag{18}$$

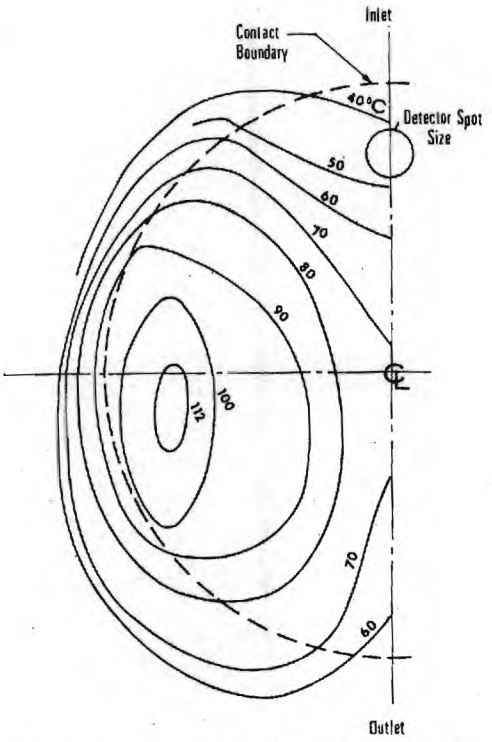

Fig. 5 Ball surface temperatures in the EHD contact at 1.39 m/sec (54.9 ips) sliding speed

Since for a transparent medium (13)

$$t_F + \rho_F + \epsilon_F = 1 \tag{19}$$

the last term in equation (18) may be written as $t_F N_0$. The transmissivity of the filter t_F can be related to the attenuation factor η_F which includes transmission and reflection losses

$$\eta_F = (1 - \rho_F)t_F = 0.850t_F \tag{20}$$

where the reflection losses are calculated Fresnel reflections at the sapphire-air and sapphire-oil interfaces. Substitution of equation (20) into (18) and subtracting from equation (12) yields,

$$\left(E_1 - \frac{E_3}{\eta_F}\right)\frac{1}{k} = 0.830N_f + 0.176N_0 = 0.830\epsilon_f N_f{}^{BB} + 0.176N_0 \tag{21}$$

The quantities E_1 and E_3 are the output signals, and k and N_0 are known. The film emissivity ϵ_f can be obtained from equation (6) since the film thickness profile has also been obtained throughout the contact (14). The filter attenuation factor has been found experimentally by placing the filter between the detector objective and a calibrated black body source (Barnes, Model RM 121).

Experimental Results

The lubricant used during this investigation is a naphthenic mineral oil used in previous EHD studies [9, 10, 14] and viscometric studies [15] in this laboratory. The fluid has been shown to be Newtonian [15] at shear rate and pressure levels approaching those anticipated in the EHD contact. The atmospheric pressure viscosity is 0.0217 Ns/m²(21.7 cp) at 37.8 C and 0.0032 Ns/m²(3.2 cp) at 98.9 C and the pressure-viscosity characteristic α^* is 2.32×10^{-8} m²/N(1.60×10^{-4} in²/lbf).

All data was obtained with a peak Hertz contact pressure of 1.034×10^9 N/m² (150,000 psi). Sliding velocities of 0.35, 0.69 and 1.39 m/s (13.7, 27.4 and 54.9 in/sec) were used in the investigation.

Using the optical techniques developed in the previous section, contour maps of the steady state film and ball surface tempera-

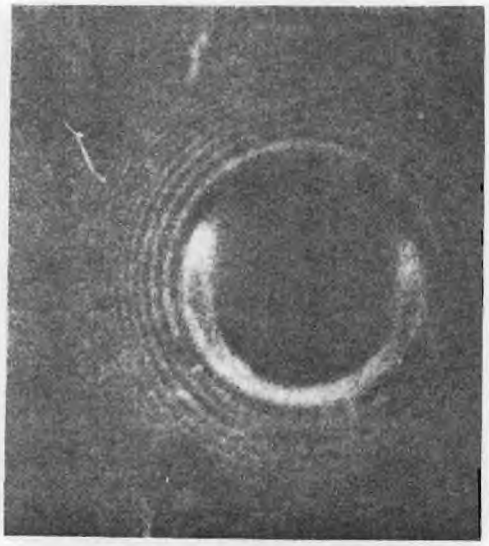

Fig. 6 Interference fringe pattern of the EHD contact at 1.39 m/sec (54.9 ips) sliding speed

tures have been obtained and are shown in Figs. 4 and 5 for the maximum sliding velocity. Fig. 6 shows the interference fringe pattern for the same conditions (1.39 m/s, 1.034×10^9 N/m^2) as used in Figs. 4 and 5.

In all these figures, the lubricant is entering the contact at the top of the figure. Referring to Fig. 4, it can be seen that along the contact center line, the lubricant is at 30 C just ahead of the contact inlet and increases in temperature to almost 50 C as it crosses the Hertzian contact boundary. The film reaches a maximum of 115 C just beyond the contact center and exits from the contact region at 75 C. The most striking feature about Fig. 4, however, is the fact that the maximum film temperature ($\simeq$ 360 C) occurs at the minimum film thickness location (see Fig. 6) in the EHD side lobe constriction. Based on previous measurements [14] the film thickness at this location is only 6.35×10^{-8} m (2.5×10^{-6} in.).

Fig. 5 is a plot of the ball surface temperature distribution. The ball surface temperature is less than 40 C at the contact inlet, rises to over 70 C just beyond the contact center and exits the contact at just under 60 C. As is the case for T_f, the maximum ball surface temperature occurs in the side lobe constriction. The maximum values of T_f and T_b do not appear to be at precisely the same locations, however. The maximum ball temperature is only 115 C compared with 360 C for the lubricant film.

The temperature contours shown in Figs. 4 and 5 were the maximum steady state values obtained during the investigation. Figs. 7(a) and (b) show the variation with sliding velocity of steady temperature, T_f and T_b along the contact center line. It can be noted that at each position in the contact and at each speed, the mean film temperature is substantially higher than the ball surface temperature. This is consistent with the fact that there is internal heat generation in the film due to viscous shear and that conduction to the boundaries is a primary heat transfer mechanism.

Finally, Fig. 8 is a plot of maximum ball surface temperature in the contact as a function of sliding velocity. As was mentioned above, the maximum temperature is found in the EHD side lobe constriction. Fig. 8 also shows the film temperature variation with sliding velocity at the same contact location where the maximum ball temperature was found.

The most significant possible error is in the emissivity assigned to the oil film. From equation (6) it is seen that the emissivity is proportional to film thickness. Unfortunately, the error in film thickness is an absolute quantity (depending on fringe order interpretation (see Fig. (6)) rather than a percentage of the film thickness. This yields a maximum relative error at points of minimum film thickness, which are located at the points of maximum film temperature. The maximum error in film thickness has been assessed at $\pm 1.8 \times 10^{-8}$ m (0.7×10^{-6} in.). At the point of maximum film temperature (360 C) this $\pm 1.8 \times 10^{-8}$ m error in minimum film thickness (6.4×10^{-8} m) results in an error in temperature of ± 30 deg C. At all other locations within the contact, this error is substantially less.

The detector has been calibrated over the temperature range of interest using a radiometric calibration source (Barnes Model RM-121). The detector resolution under the conditions of the experiment is 0.5 C, according to manufacturer's specifications. Because of this relatively high resolution, the accuracy of the temperature data reported is primarily a function of the emis-

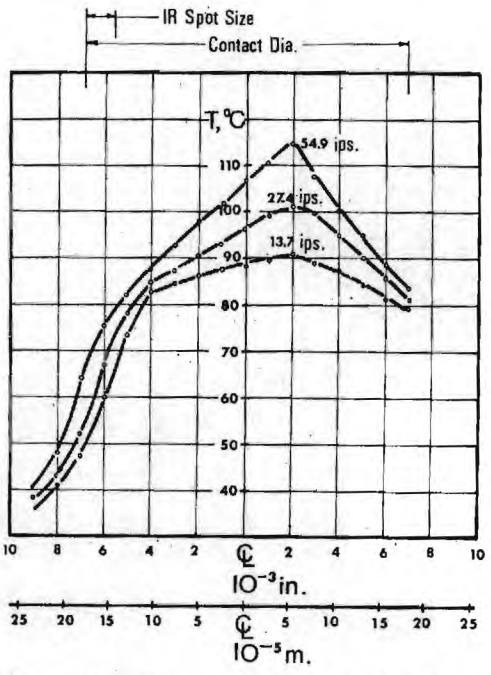

Fig. 7(a) Steady state film temperature distribution along the contact center line as a function of sliding speed

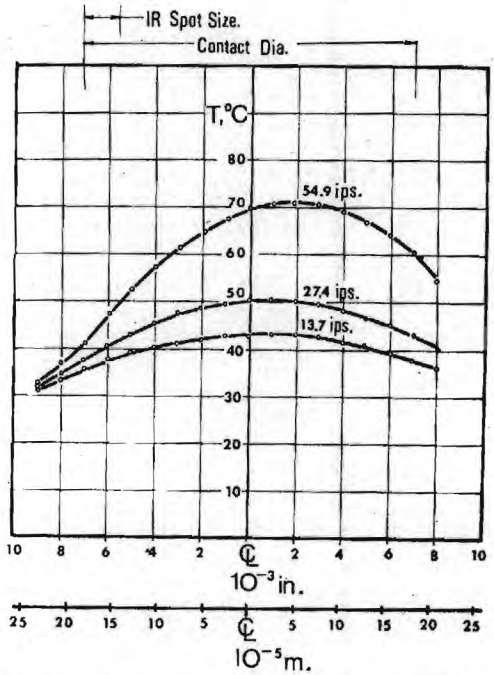

Fig. 7(b) Ball surface temperature distribution along the contact center line as a function of sliding speed

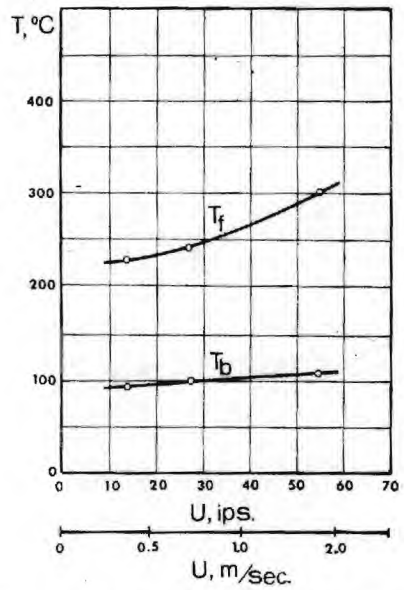

Fig. 8 Maximum ball surface temperature and film temperature as a function of sliding speed

sivity values and the proportion of received radiance assigned to each source in equations (15), (16), and (21). The measured emissivity values for the ball surface used are believed to be correct to well within 10 percent. If this ±10 percent error is carried through the above equations it amounts to an error in ball temperature of ±4 deg C at the maximum contact temperature of 115 C. At locations where the temperature is less than this maximum the error will be lower. Also, if any of the calculated coefficients in equations (16) and (21) are in error by ±10 percent, a similar error in ball temperature will result.

Conclusions

The authors have presented a technique for mapping the temperature distribution in a sliding EHD contact. Both the ball surface temperature and a fourth power average lubricant film temperature have been obtained at points throughout the contact. Under a specific set of experimental conditions, ball temperatures as high as 115 C and average fluid film temperatures as high as 360 C have been reported. Both temperature peaks were found to occur in the contact side lobes where the film thickness is a minimum. It was also observed that at each point in the contact, both temperatures increased significantly as the sliding velocity was increased.

Although only a limited amount of data was collected, it is sufficient to show that the technique reported can be useful in obtaining detailed temperature data in the EHD contact. In addition, it also suggests additional experiments using the IR microdetector; namely extensions to rolling contact experiments, to a determination of the sapphire surface temperature, to a spectral analysis of the materials in the contact, to aid in evaluating lubricant constitutive equations under EHD conditions, and to an investigation of the mechanisms leading to film failure.

Acknowledgments

The authors wish to acknowledge the support of NASA Grant NGR 11-002-133 and the encouragement of Mr. R. L. Johnson of NASA-Lewis in connection with this research.

APPENDIX A

The Effect of Ball Radiation Change on Film Temperature

The energy dissipation rate in the EHD contact can be determined from film thickness and traction measurements previously obtained [9, 10]. For the most severe conditions imposed in this investigation (1.39 m/s velocity and 67 N normal load) the traction force was observed to be 4.7 N. This results in an energy input rate ($f\,U$) of 6.53 watts.

From radiation measurements made with each of the two balls, the change in ball radiation is of the order 10^{-2} watts/cm² steradian for a 3.6×10^{-5} m diameter spot size. For radiation to one hemisphere ($2\,\pi$ steradians) and for an EHD contact diameter of 3.6×10^{-4} m, the radiation heat transfer rate is of the order 10^{-5} watts. Therefore the heat transfer through the film due to ball radiation is negligible compared to the 6.53 watts dissipation rate. The effect of different ball surface emissivity on film temperature should therefore be negligible.

APPENDIX B

Relative Contribution of Sapphire Radiation

As an order of magnitude approximation it has been assumed that the upper sapphire surface is at ambient temperature (25 deg C) and that the lower surface is at a temperature equal to that of the average fluid temperature (115 deg C). These temperatures correspond to black body areal radiant intensity values of 3.7×10^{-3} and 40×10^{-3} watts/cm²-ster, respectively. These data represent the maximum temperature condition on the contact center line. The radiation characteristic of the sapphire should be less than the average of the surface radiation values, due to the fourth power relation between temperature and areal radiant intensity. For an average N_s^{BB} of 22×10^{-3} watts/cm²-ster and a sapphire emissivity of 0.018, N_s becomes 0.4×10^{-3} watts/cm²-ster, which is 2 percent of N_b^{BB} shown in equation (16). The 2 percent maximum error resulting from omitting the contribution from the sapphire will result in an error in ball temperature of less than 2 deg C.

References

1 Blok, H., "General Discussion on Lubrication," *I. Mech. E.*, Vol. II, London, 1937, p. 14.

2 Crook, A. W., "The Lubrication of Rollers,—II, III," *Phil. Trans. Roy. Soc. London*, Series A, 1961, Vol. 254, p. 223.

3 Cheng, H. S., and Sternlicht, B., "A Numerical Solution for the Pressure, Temperature and Film Thickness Between Two Infinitely Long, Lubricated Rolling and Sliding Cylinders Under Heavy Load," *Journal of Basic Engineering*, TRANS. ASME, Series D, Vol. 87, No. 3, Sept. 1965, pp. 695–707.

4 Dowson, D., and Whittacker, A. V., "A Numerical Procedure for the Solution of the Elastohydrodynamic Problem of Rolling and Sliding Contacts Lubricated by a Newtonian Fluid," *Proc. I. Mech. E.*, Vol. 180, Part 3B, 1965–1966, pp. 57–71.

5 Archard, J. F., "The Temperature of Rubbing Surfaces," *Wear*, Vol. 2, No. 6, 1959, p. 438.

6 Wolveridge, P. E., and Archard, J. F., "Temperature Distributions in Elastohydrodynamic Films: A New Analytic Solution," *I. Mech. E.*, Tribology Meeting, 1972 (to be published).

7 Cheng, H. S., and Orcutt, F. K., "A Correlation Between the Theoretical and Experimental Results on the Elastohydrodynamic Lubrication of Rolling and Sliding Contacts," *Proc. I. Mech. E.*, Vol. 180, Part 3B, 1965–1966, pp. 158–168.

8 Hamilton, G. M., and Moore, S. L., "Deformation and Pressure in an Elastohydrodynamic Contact," *Proc. Royal Society Lond.*, 322A, 1971, pp. 313–330.

9 Sanborn, D. M., and Winer, W. O., "Fluid Rheological Effects in Sliding Elastohydrodynamic Point Contacts With Transient Loading: I—Film Thickness," JOURNAL OF LUBRICATION TECHNOLOGY, TRANS. ASME, Series F, Vol. 93, No. 2, Apr. 1971, pp. 262–271.

10 Sanborn, D. M., and Winer, W. O., "Fluid Rheological Effects in Sliding Elastohydrodynamic Point Contacts With Transient Loading: II- Traction," JOURNAL OF LUBRICATION TECHNOLOGY, TRANS. ASME, Series F, Vol. 93, No. 3, July 1971, pp. 342–348.

11 Kebler, R. W., *Optical Properties of Synthetic Sapphire*, Linde Company, N. Y., N. Y.

12 McMahon, H. O., "Thermal Radiation From Partially Transparent Reflecting Bodies," *Journal of the Optical Society of America*, Vol. 40, No. 6, 1950, pp. 376–380.

13 Kreith, F., *Principles of Heat Transfer*, International Textbook Company, 1964, pp. 177–180.

14 Sanborn, D. M., *An Experimental Investigation of the Elastohydrodynamic Lubrication of Point Contacts in Pure Sliding*, PhD dissertation, University of Michigan, December 1969 and University Microfilms, Inc., Ann Arbor, Mich.

15 Winer, W. O., and Novak, J. D., "Some Measurements of High Pressure Lubricant Rheology," JOURNAL OF LUBRICATION TECHNOLOGY, TRANS. ASME, Series F, Vol. 90, No. 3, July 1968, pp. 580–591.

DISCUSSION

P. M. Ku[2]

The work reported here is a milestone in experimental elastohydrodynamic lubrication. It ranks in importance with Crook's film thickness measurements, which gave the EHD theory the first tangible verification, and Archard's application of optical interferometry, which opened the way for the mapping of the film thickness distribution in an EHD conjunction. However, in terms of the difficulty of the task and the ingenuity of the experimental technique, this work has no peer.

As the authors have indicated, their technique permits the mapping of the lubricant-film and surface temperature distributions in an EHD conjunction, so that these can be related to the film thickness distribution and hopefully lead to an elucidation of the rheological behavior of the lubricant in the conjunction and the impact of the latter on traction behavior. This is a monumental task, but the technique does appear to hold great promise.

One of the intriguing problems in gears and similar sliding-rolling machine elements is associated with rubbing wear and scuffing failures. There seems to be general agreement among investigators of gear failures [16–18] that the breakdown of the EHD film, while it is a sufficient condition for the occurrence of wear, is only a necessary but insufficient condition for scuffing to occur. In other words, in order for wear to advance to scuffing, another condition believed to be thermal in character must also be met. This additional necessary condition is apparently strongly influenced by the chemical interfacial action involved. If this view of scuffing is true, it appears that the maximum temperature in the conjunction may be related to the chemical nature of the lubricant and metal surface, as well as to whether the atmosphere is oxidative or inert. Perhaps the authors' technique may be employed to provide a direct insight into the problem.

Additional References

16 Blok, H., "The Postulate About the Constancy of Scoring Temperature," *Interdisciplinary Approach to the Lubrication of Concentrated Contacts*, P. M. Ku, editor, NASA SP-237, 1970.

17 Bell, J. C., and Dyson, A., "The Effect of Some Operating Factors on the Scuffing of Hardened Steel Discs," *Elastohydrodynamic Lubrication, 1972 Symposium*, IMechE, London, 1972.

18 Ku, P. M., "Tribology of Gears," *Proceedings of a Forum on Gear Manufacture and Performance*, ASM, 1973.

William R. Jones, Jr.[3]

The authors should be complimented on tackling an extremely difficult problem area—that of surface and film temperature measurements in elastohydrodynamic contacts. The importance of such measurements has been adequately spelled out in the paper.

The basic principles involved in determining local temperatures from emitted infrared radiation are fairly straightforward. However, because of the complexity of the system and the number of unknowns involved, the ability to produce local temperature maps from measured radiance data requires a great deal of imaginative and innovative thought.

Nevertheless, as impressive as these results are, they appear to be anomalous. For instance, the location of the maximum film temperature in the side lobe region is unexpected. The minimum film thickness and thus the maximum shear rate does occur in this region. However, the local pressures (and thus the local shear stresses) should be considerably less than those at the contact center. Therefore, one would expect the maximum heat generation due to viscous shear (and thus the maximum film temperatures) to occur at or near the contact center. And, indeed, this has been predicted in analytical studies.

Of course, these analytical studies only considered heat generation due to viscous shear. Obviously, in this paper the possibility of asperity interactions between the ball and disk surfaces cannot be discounted. At the highest sliding speed (54 ips) the measured minimum film thickness at the side lobes is only 2.5 μ in. This should be well within the surface roughnesses of the two surfaces. If surface interactions are occurring, the side lobe temperatures are easily explained. But then another apparent anomaly appears in Fig. 8. Why does T_f (the film temperature measured at the location of maximum ball temperature) decrease with decreasing sliding speed? As speed decreases, the minimum film thickness at the side lobes also decreases, and one would expect increased asperity interactions and therefore higher film temperatures.

Further studies should clear up this point of conjecture. Temperature measurements can be performed on thicker films where the possibility of asperity interactions can be ruled out. Furthermore, if solid contact is occurring, one would expect some surface distress to be observed on the ball and disk. Therefore, a technique that might be of value here is Ferrographic analysis [16] of the lubricant. If any metallic debris is generated during asperity interactions, it should be detectable using this technique.

Finally, a few questions come to mind concerning the analysis of the radiance data. Can the absorption coefficient (λ) in equation (6) really be assumed constant for very thin films? Does film emmissivity (ϵ_f) vary with temperature as well as film thickness? Can interference effects of the infrared radiation such as those observed by Wedeven [17] be completely discounted?

Additional References

16 Seifert, W. W., and Westcott, V. C., "A Method for the Study of Wear Particles in Lubricating Oil," *Wear*, Vol. 21, 1972, pp. 27–42.

17 Wedeven, L. D., "Preliminary Study of the Use of Infrared Radiation to Reveal Lubrication Behavior," NASA TM X-67883, July 1971.

G. Dalmaz and D. Berthe[4]

We wish to congratulate Prof. W. O. Winer, V. Turchina, and Dr. D. M. Sanborn on having mastered the technique of obtaining both oil and ball temperatures with infrared measurement. We will not comment on the technique other than to say that having obtained equivalent results in mixed friction, where data interpretation is simpler [18], we fully appreciate the difficulty of the problem and thus the contribution that was made.

Going directly to the results, the authors have shown that in pure sliding and under relatively high loads temperatures of 360 deg C were reached. Under these conditions thermal effects are dominant, isoviscous fluids or even piezoviscous fluids alone cannot be considered.

In an attempt to get a better understanding of the problem, we have calculated the pressure distribution in a point contact knowing the contact geometry, which had been determined experimentally with interferometric techniques [19]. These calculations show that:

1 For small loads (a and b in Fig. 9) the piezoviscous law $\mu = \mu_0 \exp(\alpha p)$ gives acceptable results.

2 For loads that correspond to the onset of the elastohydrodynamic regime (c in Fig. 9) infinite pressure are obtained. This is of course unacceptable.

3 For these same loads, the substitution of isoviscous to piezoviscous fluids give satisfactory results for the pressure. The load calculated from that pressure distribution is very close to the applied load.

The drop in effective viscosity can be explained by considering the pressure-viscosity relaxation time discussed by Trachman

[2] Southwest Research Institute, San Antonio, Texas.

[3] National Aeronautics and Space Administration, Lewis Research Center, Cleveland, Ohio.

[4] Laboratoire de Mécanique des Contacts, Institut National des Sciences Appliquées de Lyon, Villeurbanne, France.

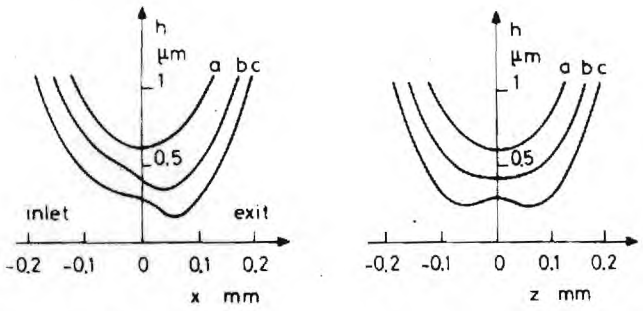

Fig. 9 Variation of film shape for a given speed u = 8 cm/sec with load ω = *(a)* 1.5 N; *(b)* 3 N; *(c)* 4.6 N; viscosity μ_e = 1.3 PI

[20] and the local rise in temperature observed by the authors.

We believe that the authors are in a privileged situation to evaluate at least qualitatively the relative importance of both these effects. Film thickness, temperature, and thus viscosity μ_0 are known all over the contact. If these values are introduced point by point into the Reynolds equation the pressure distribution can be calculated and compared to the applied load. This could give a fairly solid base for discussion. We would also like to know if the authors have observed any correlation between temperature and either the minimum film thickness or the energy dissipated locally. Such a correlation would help immensely, as it would allow us to get practical theoretical results directly without having to solve the energy equation.

Additional References

18 Deyber, P., and Godet, M., "Contact Temperature in Mixed Friction," *Tribology*, Vol. 4, No. 3, Aug. 1971, pp. 150–154.

19 Dalmaz, G., and Godet, M., "An Apparatus for Simultaneous Measurement of Load, Traction and Film Thickness in Lubricated Sliding Point Contacts," *Tribology*, Vol. 5, No. 3, June 1972, pp. 111–117.

20 Trachman, E. G., and Cheng, H. S., "Thermal and Non-Newtonian Effects on Traction in Elastohydrodynamic Contacts," *Proc. IME, Elastohydrodynamic Lubrication* 1972, *Symposium*, pp. 142–148.

J. L. Lauer

The Barnes infrared microdetector used is a radiation pyrometer accepting, without discrimination, radiation over a wide band width from everywhere within it angle of acceptance. The authors therefore designed a number of calibration experiments and essentially subtracted their results from the total radiometer readings to obtain film emissivities relatable to film temperatures. In one of these experiments a layer of cold fluid is used to reabsorb the radiation emitted by the hot fluid in the contact so that the latter radiation can be isolated from the background. This procedure is excellent, but since an emission band is generally wider than an absorption band at lower temperature, the cold film must be—and the authors reported it to be—much thicker than the hot one. Furthermore, there can be a polarization effect, for the C–H dipole from the fluid in the contact can, conceivably, be oriented; and if this orientation depended on shear velocity, the reflectivities associated with the hot and cold film surfaces might become variables. Such an effect—if it exists—can be checked easily with an infrared polarizer. Much of the radiation emitted by the film may not be associated with the C–H dipole; e.g., phase changes and conformational changes can be envisaged. However, a cursory calculation by this reviewer using the data given in the paper gave values for the energy input in the contact region that were well below those required for the mechanical rupture of C–H bonds. Both reflectivities and transmissivities are, in general, temperature-dependent.

Since a sapphire window had to be used to transmit radiation in the radiation pyrometer region—which is always on the high-frequency side of the Planck peak—the heat-flow pattern under the experimental conditions will necessarily be different from that in an all-metal situation. The heat conductivity of sapphire at ambient temperature is about one order of magnitude poorer than that of of iron, although the difference is much less at elevated temperature where the conductivity of iron is much lower. The heat conductivity of a diamond window is nearly that of iron and is almost independent of temperature, but diamond would not be suitable in this wavelength region.

While there are, therefore, limitations to this approach, the authors deserve bouquets for an excellent beginning on an important aspect of a most important problem.

Authors' Closure

The authors wish to thank the discussors for their comments. Since the research reported employs a new technique, the comments and suggestions are particularly useful in the development of this tool.

The questions raised by Mr. Jones concerning the occurance of the temperature peak in the contact side lobe are understandable. The mechanism of asperity contact appears to be the most reasonable explanation, but further research is needed on this point. The decrease of film thickness in the side lobes with sliding speed does not seem unreasonable, however, since the "film thickness" probably changes very little after initial asperity contact. This being the case, the local energy dissipation rate will be reduced. The temperature and film thickness dependence of the film emissivity needs additional research. In trying to establish the feasibility of the infrared temperature measurement technique, a rather simple model was selected. In future work, the emissivity should be used as a function of temperature, film thickness and wavelength. It is doubtful that interference of infrared rays was a problem in this experiment since the wavelengths are long compared to the film thickness and they are not from a coherent source.

We agree with the comments of Messers Dalmaz and Berthe on the importance of obtaining a pressure profile through the Reynolds equation, or even a shear stress distribution which could be checked against the traction in the contact. Although approximations can be made, detailed solutions require that the temperature distribution across the film be known. At the present time only an averaged film temperature and ball surface temperature have been determined. Although a distribution through the film seems difficult to obtain, reasonable approximations could be made if the sapphire surface temperature could be determined. Such a measurement could be obtained with an additional experiment.

The discussions of P. M. Ku and J. L. Lauer are greatly appreciated. We agree with the desirability of extending the technique to gears and more realistic bearing surfaces although this task appears formidable.

74-Lub-35

D. L. Walker
Grad. Student;
(presently, E. I. Dupont de Nemours & Co, Kinston, N. C.)

D. M. Sanborn
Asst. Professor.

W. O. Winer
Professor.

Georgia Institute of Technology, School of Mechancial Engineering, Atlanta, Ga.

Molecular Degradation of Lubricants in Sliding Elastohydrodynamic Contacts

The extent of lubricant degradation in a sliding elastohydrodynamic contact has been investigated. The lubricant was subjected to peak Hertz pressures of approximately 10^9 N/m^2 and average shear rates of 10^6 to 10^7 s^{-1}. Hydrocarbon lubricants, bulk polymers and polymer containing hydrocarbon solutions were examined. Small samples ($10^{-8}m^3$) of test lubricant were extracted from the entrance and exit regions of the EHD contact. These samples were then analyzed to determine alterations in the molecular weight distribution. In addition, a microcapillary viscometer was developed to determine viscosity changes. Degradation resulting in up to a 70 percent viscosity loss was found in fluids which had molecular weights of over 1000. High degrees of correlation were found between molecular weight loss, viscosity loss and the energy dissipated in the contact.

Introduction

The increasing use of high molecular weight synthetic lubricants by industry in locations where stable, clean fluids are required has created a need for more information on the stability of these fluids when subjected to mechanical shearing. The most extreme conditions of mechanical shearing that a lubricant must withstand are those found in elastohydrodynamic lubrication. These conditions result in energy input rates into the fluid greater than 10^{15} J/kmol. This can be compared to an activation energy of less than 10^8 J/kmol of carbon-carbon bonds. Although the fluid is usually subjected to these conditions for only a short period of time (less than 1.0 ms) some degradation should be expected.

In previous studies the problem of mechanically induced molecular degradation has been approached in either of two ways: (1) attempts have been made to simulate actual conditions on laboratory apparatus, or (2) tests have been done using production equipment. By testing on specially designed equipment, the conditions under which the degradation takes place are usually well defined. However, the lubricant is not subjected to the combined high pressure-high shear stress state that is characteristic of the EHD contact [1–4].[1] To reproduce these extreme conditions on the lubricant, studies using production equipment, such as automotive engines, have been undertaken [5, 6]. However, in this type of experiment, the stress conditions imposed on the lubricant are difficult to establish. These conditions range from EHD lubrication at the cam followers and gears to low shear stirring in the sump with temperature ranges from ambient at the start of the test to over 95degC after warmup.

The objective of this study was to subject a variety of fluids to conditions that are found in EHD lubrication and determine the extent of degradation. The test fluids were subjected to pressures of 10^9 N/m^2 and shear rates of approximately $10^6 - 10^7$ s^{-1}. Samples of the fluids were collected and analyzed to determine if degradation had occurred. The viscosity of the sheared fluids was measured and the viscosity average molecular weight was calculated using available empirical equations [7, 8]. If this method resulted in an indication of degradation, further analysis was done using gel permeation chromatography [9], flame ionization spectroscopy and other analytical methods.

Test Lubricants

The lubricants selected for examination were chosen so that a wide range of molecular weights and fluid types could be tested. Detailed descriptions of the test fluids are given in Appendix A and summarized in Table 1.

As representative examples of the hydrocarbon type fluids, a paraffinic base oil and three solutions of high molecular weight polyalkylmethacrylate (PAMA) were chosen. Two of these solutions used a PAMA additive with a viscosity average molecular weight (MW_v) of 560,000 atomic units (au) with concentrations of 4 percent and 8 percent. The third solution used a PAMA additive with a MW_v of 1,650,000 au and a concentration of 4 percent. In this manner variations with concentration and MW could be studied. The paraffinic base oil with an average MW of 404 was also tested as a control.

Six synthetic fluids were tested. A commercially available silicone diffusion pump fluid with a MW of 546 au was tested be-

[1] Numbers in brackets designate References at end of paper.

Contributed by the Lubrication Division of THE AMERICAN SOCIETY OF MECHANICAL ENGINEERS for presentation at the ASME-ASLE Joint Lubrication Conference, Montreal, Canada, October 8–10, 1974. Manuscript received by the Lubrication Division, June 26, 1974. Paper No. 74-Lub-35.

Copies will be available until June, 1975.

cause of its very narrow MW distribution. Because of this property, small variations in MW could be detected. Another commercially available silicone lubricant which had a bimodal MW distribution centered around molecular weights of 16,000 and 47,000 was tested. The results obtained with this fluid led to tests of two silicone blends with widely dispersed MW distributions. Stable lubricant films could not be generated with either fluid, however. In addition, a sebacate diester (MW=426) and a modified polyphenyl ether (MW=423) were examined.

Experimental Technique

The experimental equipment is a slight modification of the apparatus used to study EHD film thickness and traction and previously reported in this literature [10, 11]. The equipment is shown schematically in Fig 1. The sliding EHD point contact is formed by rotating a 31.8-mm-dia steel sphere which is loaded against a sapphire disk. The sphere has a surface finish of 0.038 μm. Optical interference techniques were used to measure the EHD film thickness and the air bearing and traction load cell system allowed direct traction measurements to be obtained.

The technique used for extracting a lubricant sample from the contact entrance and exit involved introducing a hole in the sapphire flat into the desired region. This orifice was then allowed to fill up with the lubricant. Most of the data was taken using a sapphire disk 7.87 mm in dia, 1.52 mm thick and with a conical hole having a minimum diameter of approximately 50 μm at the oil interface. A micrometer screw adjustment mechanism (Fig. 1) allowed the orifice in the sapphire to be positioned at the desired location. Both the hole and EHD contact could be observed through the microscope.

Fig. 2 shows the orifice in the sapphire in relation to the EHD contact. The dark area surrounding the minimum hole diameter is a result of the conical shape of the orifice. When the orifice was moved up to the exit edge of the contact, the flow of lubricant into the cone could be observed. When a sufficient amount of oil had collected on the sapphire, two 10^{-8} m^3 samples were extracted using disposable syringes. In order to compare changes in molecular weight and viscosity, samples were also taken from the fluid reservoir and the original sample container.

The experimental conditions for each test are given in Table 2. Also listed are the centerline film thickness and the traction coefficient (TC). Table 3 is a summary of the average conditions experienced by the fluid in the EHD contact. An average shear rate $\dot{\gamma}$ is determined from the relative velocity of the bearing surfaces divided by the film thickness. The average shear stress τ is calculated by dividing the traction force by the contact area. The energy dissipation rate per unit volume (E) is given by the product of the shear stress and the shear rate. Finally, the energy dissipation rate per mole of polymer (ϵ) is determined from the product of E, the contact volume and MW divided by the product of average mass flow rate and polymer weight concentration.

In calculating the energy dissipated per mole of polymer ϵ, the contact volume is assumed to be the product of the centerline film thickness and the Hertz contact area. The average mass flow rate is obtained from the product of the lubricant density, one half the sliding velocity, the centerline film thickness, and the Hertz contact diameter. For the silicone blends, the concentration is taken to be 100 percent and the molecular weight is 546 for the single species S5 and the weight averaged value of 45,600 for S6.

Table 1 Test fluids

Designation[1]	Fluid description[2]
P1	Paraffinic base oil (R-620-12)
P2	P1 + 4 percent polyalkylmethacrylate (PL-4521)
P3	P1 + 8 percent polyalkylmethacrylate (PL-4521)
P6	P1 + 4 percent polyalkylmethacrylate (PL-4523)
S1	Diester- bis-2-ethyl hexyl sabacate (PL-5159)
S5	Pentaphenyltrimethyltrisiloxane (DC-705)
S6	Dimethylsiloxane (DC-200)
S7	Dimethylsiloxane Blend (E1923-48)
S8	Dimethylsiloxane Blend (E1923-49)
S9	Modified Polypenyl Ether (MCS-418)

[1] The fluid designations correspond to designations used in previous studies on these fluids [10].

[2] Manufacturer's designation is shown in parentheses. See Appendix A for detailed description.

A variety of techniques were used to analyze the samples obtained from the EHD contact. The viscosity of most of the fluids was measured in a microcapillary. Where possible and necessary, further analysis was done using ionization spectroscopy, infrared absorption spectroscopy and mass spectroscopy. The micro-capillary was made from a glass tube with a capillary section 60 mm long by 75 μm inside diameter [12]. The capillary was used in a constant temperature bath and the pressure differential was applied using a water manometer. After a calibration constant had been determined from a test on a viscosity-standard fluid, viscosities were determined by measuring the time for the miniscus to travel between two prescribed points. Measurements were highly repeatable in both flow directions through the capillary. As a

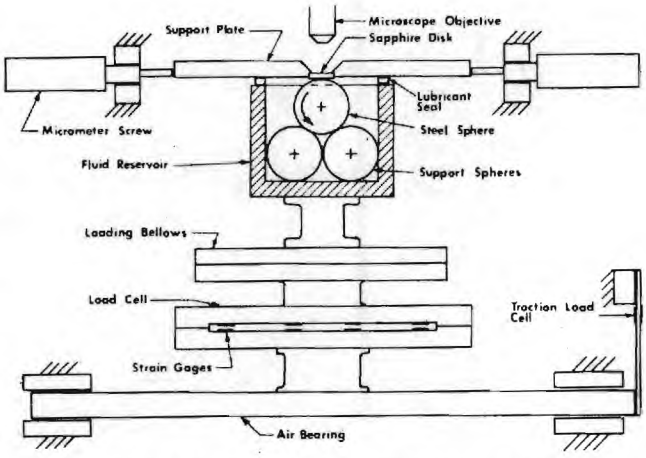

Fig. 1 Schematic diagram of experimental equipment

Nomenclature

E = energy dissipation rate per unit volume, W/m^3

h_c = centerline EHD film thickness, μm

MW = molecular weight, au

S = apparent viscosity loss from film thickness data

S_P = permanent viscosity loss due to degradation

TC = traction coefficient

$\dot{\gamma}$ = shear rate, s^{-1}

ϵ = energy dissipated per mole of polymer, J/kmol

μ = viscosity, N s/m^2

τ = shear stress, N/m^2

Subscripts

e = effective value from film thickness data

N = number average

o = unsheared; atmospheric pressure value

s = sheared value

v = viscosity average

w = weight average

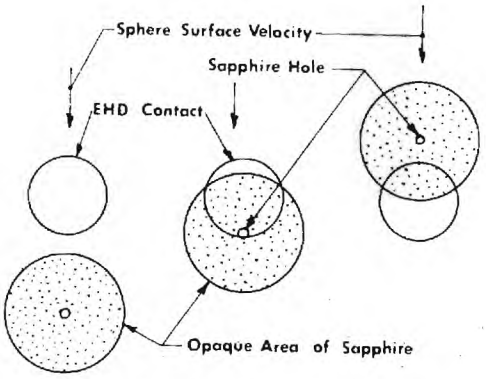

Fig. 2 Sapphire hole location sequence

check on the procedure, the viscosities of samples of an unsheared fluid were determined using both the microcapillary and standard capillary viscometers. Good agreement was found. The *MW*-viscosity correlation proposed by Barry [7] was then used to determine *MW* from the micro-capillary results for the siloxanes while the relation proposed by Wright and Crouse [8] was used for the PAMA solutions.

In addition to the microcapillary measurements, molecular weight distributions were obtained for the higher polymers (PAMA and silicones) using gel permeation chromatography (GPC). Lower molecular weight fluids were further analyzed using gas chromatography, IR spectroscopy or mass spectroscopy.

Experimental Results

The results of the tests are shown in Table 4. The first two columns are the measured viscosity and the percentage change in viscosity. The changes throughout Table 4 are calculated by subtracting the sheared quantity from the original and dividing by the original. The second two columns are the calculated viscosity average molecular weights and the percentage change in MW_v. The fifth and sixth columns are the weight average MW_s as determined by GPC and the change in this quantity. The seventh column is the number average *MW* also determined by GPC. The final column is the dispersity as calculated by dividing the weight average *MW* by the number average *MW* and is a measure of the spread of *MW*s found in the sample.

Table 2 Elastohydrodynamic operating conditions

Fluid	μ_o (25 deg C) Ns/m^2	Load N	Speed m/s	h_c μm	*TC*
P1	0.052	65	2.36	0.22	0.035
P2	0.112	67	2.34	0.25	0.033
P3	0.274	67	2.34	0.31	0.032
P6	0.240	67	2.34	0.25	0.038
S1	0.017	67	2.34	0.09	0.024
S5	0.175	69	1.45	0.43	0.068
S6	0.931	69	2.41	0.25	0.027
S7	1.200	67	2.34	0.19	0.035
S8	1.060	67	2.34	0.20	0.033
S9	0.056	67	2.34	0.30	0.042

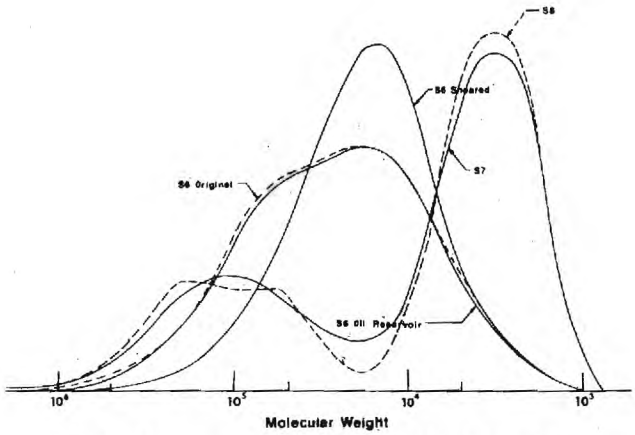

Fig. 3 Molecular weight distribution, fluids S6, S7 and S8

With the low *MW* silicone fluid S5, no degradation was detectable. This fluid was tested by the manufacturer using a gas chromatograph. No viscosity measurements were made because an insufficient sample was extracted during the EHD contact simulation.

Silicone fluid S6 exhibited marked degradation after shearing in the EHD contact. Both viscosity and GPC measurements were made on this fluid. The permanent viscosity loss was found to be 56.1 percent. The results of the GPC tests are shown in Fig. 3. The location at which each sample was extracted is noted on the figure. There is virtually no change in the molecular weight distribution *(MWD)* from the original fluid to the sample taken from the oil reservoir, however, there is marked change after the fluid has passed through the EHD contact. The viscosity loss was calculated from the *MW* found with the GPC and was found to be 61.4 percent.

Fluids S7 and S8, which were specifically blended to give an indication of a limiting MW for degradation, were not successfully tested. Although a fluid film could be established in the EHD contact for a period of time (less than 30 min), the film would collapse before any sample could be taken. This collapse resulted in direct contact between the sapphire and the sphere with subsequent scratching of both in most cases. Fig. 3 shows the *MWD*s for these two fluids and by comparison with the unsheared samples of fluid S6, it can be seen that they have a greater concentration of high *MW* fractions and are more disperse in makeup.

A very slight increase in viscosity and MW (as determined from gas chromatography by the manufacturer) was found in the sheared samples of fluid S9, the modified polyphenyl ether. However, these changes were both within experimental error. A very small amount of a very low boiling point substance was found in all of the samples except the original fluid. It is thought that this might be an indication of a small amount of degradation.

Fluids S1, the diester, exhibited a marked increase in viscosity, 4.3 percent, however, neither IR spectroscopy, gas chromatography nor mass spectroscopy could detect any change in the composition of the fluid. The increase in viscosity is typical of what has been found in extended service conditions [13].

The paraffinic base oil P1 was tested in a cone and plate viscometer and a 1.6 percent decrease in viscosity was found. However, this is within the experimental error (±2 percent) of this particular instrument. Because of its low *MW*, the other analytical techniques mentioned above could not be used to establish a molecular weight distribution.

The permanent viscosity decreases in the PAMA solutions, fluids P2, P3, and P6 were found to be extreme, up to 70 percent.

Table 3 Energy dissipation

Fluid	$\dot{\gamma} \times 10^{-6}$ s^{-1}	$\tau \times 10^{-6}$ N/m^2	$E \times 10^{-12}$ W/m^3	$\epsilon \times 10^{-15}$ J/kmol
P1	10.7	25.2	287	25
P2	9.4	24.8	211	1,080,000
P3	7.5	23.0	184	416,000
P6	9.3	27.4	267	2,240,000
S1	25.0	17.3	459	43
S5	3.4	49.0	176	34
S6	9.5	19.5	196	1950
S7	12.6	25.2	337	414
S8	11.5	23.8	290	1250
S9	7.8	30.2	251	23

In fact, all of these mixtures were reduced in viscosity to the region of the base oil, P1. The GPC molecular weight distribution curves for the polymer additives are shown in Fig. 4-6. These chromatographs were made by the PAMA manufacturer. It can be seen that only a small amount of shearing takes place in the oil reservoir and the entrance region of the EHD contact.

In order to determine if there is a general correlation between energy dissipated in the fluid ϵ and permanent viscosity loss or degradation, these quantities have been plotted in Fig. 7. The viscosity loss is given by the ratio of viscosity of a sheared sample to that of the original, unsheared sample. Similarly, the amount of degradation is shown as the ratio of viscosity average molecular weight for the sheared samples to that of the original. In the case of the polymer solutions all of the energy dissipated was assumed to go into the polymers and none into the base oil. A linear correlation coefficient of -0.89 was determined for the variable (μ_s/μ_o) on log ϵ and was found to be -0.993 for the equation $(MW_{vs}/MW_{vo}) = -.077 \log\epsilon + 3.92$. Attempts to correlate viscosity loss and degradation with the energy dissipated per unit volume E were not nearly as successful.

Discussion of Results

A significant change in viscosity was found in five of the ten lubricants tested, with a maximum decrease of seventy percent. Changes in molecular weight were found with a maximum decrease of ninety percent. This large amount of degradation indicates that the EHD contact may be the primary source of molecular degradation which has been found in earlier studies using automotive engines as the test apparatus. The permanent viscosity loss also may explain the disagreement that has been reported between experimental data and theoretical predictions of film thickness for these high MW fluids [10, 14].

The non-Newtonian behavior of certain fluids under high shear conditions has previously been given as the reason for the lack of agreement between theory and experiment in EHD lubrication.

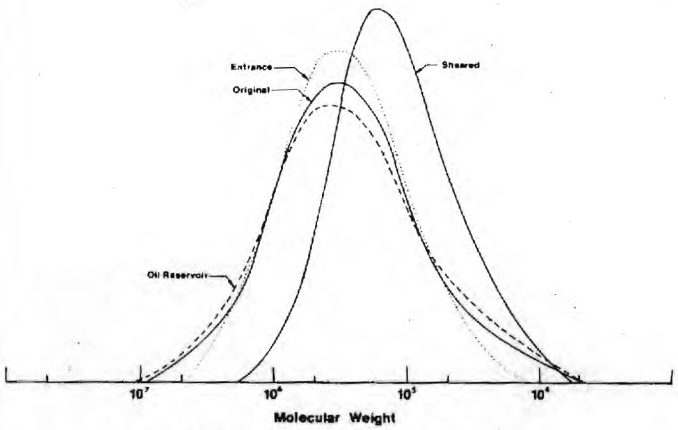

Fig. 4 Molecular weight distribution, fluid P2

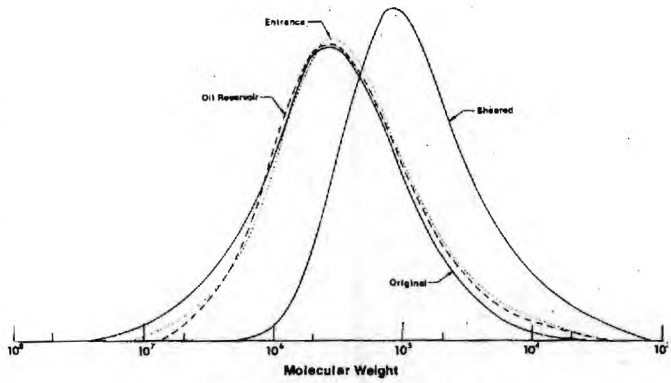

Fig. 5 Molecular weight distribution, fluid P3

For the hydrocarbon solutions tested in this study, this lack of agreement can be explained by permanent degradation of the fluid. In a previous publication [10], the authors determined an apparent viscosity loss S by estimating an effective viscosity μ_e which would bring the film thickness data for high MW fluids into agreement with data for Newtonian fluids. This apparent viscosity loss is defined by

$$S = 1 - \frac{\mu_e}{\mu_o} \tag{1}$$

By substituting the sheared fluid viscosity μ_s as measured using the microcapillary in this study for the effective viscosity, a comparable permanent viscosity loss S_p can be determined. Table 5 lists these values for the fluids which were studied in both works. The correlation is apparent. The quantitative differences are partially explained by the fact that the base viscosities were measured at different temperatures. Also, in the degradation studies, samples were extracted from near the contact centerline. The samples have, therefore, been subjected to the highest shear stresses in the EHD contact. The apparent viscosity loss determined on the basis of film thickness correlations would be influenced by degradation in the contact inlet, which has shear stresses somewhat lower than the maximum expected near the contact center.

Since a significant degree of correlation between energy dissipation and viscosity loss or molecular degradation has been found, it is possible that with proper development, this can be useful as a guide in formulating lubricants. For the present, the machine designer must assume that only the base oil viscosity is applicable to EHD lubrication conditions with polymer blends. With bulk polymers each fluid must be tested for each application.

The purpose of Fig. 7 is to graphically show the reduced data obtained during this investigation. Therefore, extrapolations should be avoided. The parameter ϵ has been defined in such a way that an increase in the mass flow rate of polymer through the

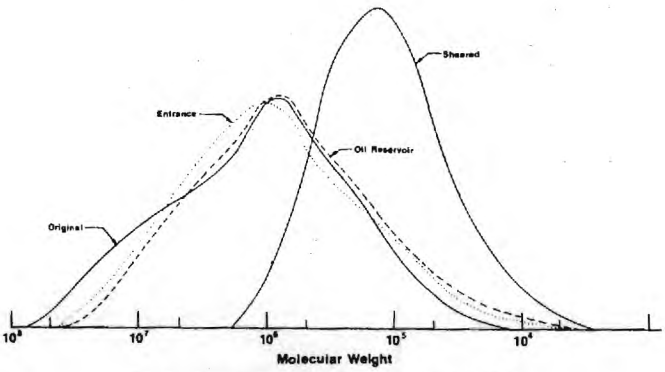

Fig. 6 Molecular weight distribution, fluid P6

Table 4 Summary of experimental results

Fluid	μ_o, μ_s Ns/m²	$\Delta\mu$ percent	MW_v	ΔMW_v percent	MW_W	ΔMW_W	MW_N	MW_W/MW_N
$P1_o$	0.0312		404		...	...	...	...
		1.6		0.0				
$P1_s$	0.0307[1]		404		...		...	...
$P2_o$	0.0130		560,000		610,000		140,000	4.5
		42.3		72.3		64		
$P2_s$	0.0075[2]		155,000		220,000		66,000	3.5
$P3_o$	0.0272		560,000		770,000		150,000	5.1
		61.0		80.2		79		
$P3_s$	0.0106[2]		111,000		160,000		23,000	6.7
$P6_o$	0.0306		1,650,000		3,200,000		390,000	8.3
		73.6		91.2		93		
$P6_s$	0.0081[2]		146,000		230,000		68,000	3.4
$S1_o$	0.0114		426		...		...	
		−4.3	...	...	...	...	...	...
$S1_s$	0.0119[3]						...	
$S5_o$	0.175		...		546			
	...		...	...		0.0	...	...
$S5_s$					546			
$S6_o$	0.931		26,000		45,600		10,300	3.0
		56.1		33.0		38.6		
$S6_s$	0.409[4]		17,400		28,000		9,280	
$S9_o$	0.0291		...		422			
		−0.7		...		−0.4		
$S9_s$	0.0293[3]		...		424		...	...

[1] Measured at 38 deg C with cone and plate viscometer
[2] Measured at 99 deg C with microcapillary
[3] Measured at 38 deg C with microcapillary
[4] Measured at 25 deg C with microcapillary

contact results in a decreased ϵ. The data shows that this results in a decrease in the amount of degradation. Although this appears to be a reasonable trend for a given amount of dissipated energy, there is some indication that this approach may be an over-simplification. Note for example that P2 and P3 experience essentially the same amount of degradation even though P3 has twice the polymer concentration of P2.

The inability to successfully test fluids S7 and S8 may be due to a near total degradation of the high MW ($>10^4$) component of each fluid as it enters the EHD contact. Elimination of the high MW component would leave a silicone lubricant of about 5×10^{-5} m²/s kinematic viscosity. Such a low viscosity lubricant has been successfully tested in this laboratory in previous experiments, but a continuous film could be maintained for only a short time. Therefore, although samples of S7 and S8 could not be obtained and analyzed, it appears likely that these fluids were also significantly degraded.

Conclusions

A new technique has been developed which allows the sampling of a lubricant directly from an EHD contact. Hydrocarbon fluids, synthetic bulk polymers, and polymer containing hydrocarbon solutions were tested. The viscosities of the fluids were measured and their molecular weight distributions were determined.

The fluids with low molecular weights (less than 1000) were not significantly degraded, although the viscosity of one fluid, the diester fluid S1, was changed. All fluids of larger molecular weight were significantly degraded and the corresponding viscosities altered. The viscosities of the polymer containing hydrocarbon solutions were reduced to the region of the base oil.

A significant degree of correlation was established between viscosity loss, degradation and energy dissipation. For PAMA solutions, it was shown that degradation increases both with increasing MW and increasing concentration.

Table 5 Apparent and permanent viscosity losses

Fluid	S [10]	S_p
P1	0.00	0.02
P2	0.26	0.42
P3	0.54	0.61
P6	0.63	0.74
S1	0.00	−0.04

Acknowledgments

The authors are indebted to Dow Corning Corporation and Rohm and Hass Company for their services in analyzing fluid samples. This research was supported by a grant from the National Science Foundation (NSF-GK-31154) and a grant-in-aid from Dow Corning.

References

1 Casale, A., Porter, R. S., and Johnson, J. F., "The Mechanochemistry of High Polymers," *Rubber Chemistry and Technology*, Vol. 44, No. 2.

2 Harrington, R. E., Zimm, B. H., "Degradation of Polymers by Controlled Hydrodynamic Shear," *Journal of Physical Chemistry*, Vol. 69, No. 1, Jan., 1965.

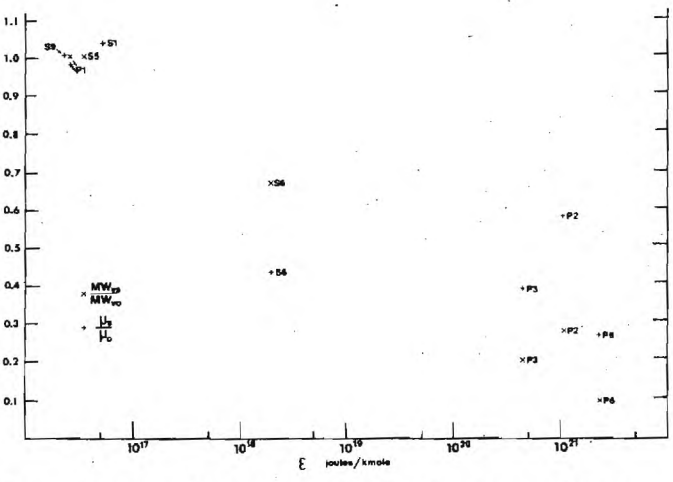

Fig. 7 Degradation and viscosity loss as a function of energy dissipation

3 Porter, R. S., Klaver, R. F., and Johnson, J. F., "Recording High Shear Viscometer for Measurement at Shear Rates Near 10^6 sec $^{-1}$," *The Review of Scientific Instruments*, Vol. 36, No. 12, Dec. 1965.

4 Porter, R. S., and Johnson, J. F., "Polyisobutene Degradation in Laminar Flow: Composition and Shear Variables," *Journal of Applied Physics*, Vol. 35, No. 11, Nov. 1964.

5 West, J. P., and Selby, T. W., "The Effect of Engine Operation on the Viscometric Properties of Multigrade Engine Oils," SAE Paper No. 650445, May 1965.

6 Johnson, R. H. and Wright, W. A., "The Rheology of Multigraded Motor Oils," SAE Paper 680072.

7 Barry, A. J., "Viscometric Investigation of Dimethylsiloxane Polymers," *Journal of Applied Physics*, Vol. 17, 1946, p. 1020.

8 Wright, W. A., and Crouse, W. W., "General Relationship for Polymer-Petroleum Oil Blends," *I and EC Product Research and Development*, Vol. 3, June 1964, p. 153.

9 Bly, D. D., "Gel Permeation Chromatography," *Science*, Vol. 168, No. 3931, May 1970.

10 Sanborn, D. M., and Winer, W. O., "Fluid Rheological Effects in Sliding Elastohydrodynamic Point Contacts with Transient Loading: I-Film Thickness," TRANS. ASME, JOURNAL OF LUBRICATION TECHNOLOGY, Vol. 93, 1971, p. 262–271.

11 Sanborn, D. M., and Winer, W. O., "Fluid Rheological Effects in Sliding Elastohydrodynamic Point Contacts with Transient Loading: II-Traction," TRANS. ASME, JOURNAL OF LUBRICATION TECHNOLOGY, Vol. 93, 1971, p. 342–348.

12 Walker, D. L., Sanborn, D. M., and Winer, W. O., "A Micro-capillary Viscometer," submitted as a Technical Brief to TRANS. ASME JOURNAL OF LUBRICATION Technology, 1974.

13 Gunderson, R. C., Hart, A. W., ed. *Synthetic Lubricants*, Rienhold New York, 1962.

14 Dyson, A., and Wilson, A. R., "Film Thickness in Elastohydrodynamic Lubrication by Silicone Fluids," *Proceedings of the Institution of Mechanical Engineers*, Vol. 180. Pt. 3K, pp. 97–112, 1965–66.

APPENDIX

Descriptive Data on Test Fluids and Additives

Petroleum oil: R-620-12	
Source: Sun Oil Company	
Supplier's designation	R-620-12
Type	Paraffinic
Symbol used in this study	P1
Viscosity at 38°C (m^2/s)	3.374×10^{-5}
Viscosity at 99°C (m^2/s)	5.402×10^{-6}
Viscosity index (ASTM D-2270)	103
Flash point (°C)	216
Fire point (°C)	246
Pour point (°C)	-15
Refractive index	1.4755
Density at 20°C(kg/m^3)	860.2
Molecular weight	404
%C atoms in aromatic rings	3.8
%C atoms in naphthenic rings	27.7
%C atoms in paraffinic rings	68.5
Average number of aromatic rings per molecule	0.18
Average number of naphthenic rings per molecule	1.66
Average number of total rings per molecule	1.84

Diester-Plexol 201 bis-2-ethyl hexyl sebacate:	PL-5159
Source: Rohm and Haas Company	
Manufacturer's designation	PL-5159
Symbol used in this study	S1
Viscosity at -54°C (m^2/s)	7.988×10^{-3}
Viscosity at 38°C (m^2/s)	1.141×10^{-5}
Viscosity at 99°C (m^2/s)	3.32×10^{-6}
Viscosity index (ASTM D-2270)	150
Neutralization number (ASTM D-974)	0.02
Cloud point (ASTM D-2500)(°C)	below -54

Polyalkylmethacrylate Additives:	PL-4521 and PL-4523	
Source: Rohm and Haas Company		
Manufacturer's designation	PL-4521	PL-4523
Percent polyalkylmethacrylate in solution	36.1	19.0
Viscosity at 99°C (m^2/s)	7.96×10^{-4}	7.73×10^{-4}
Viscosity average molecular weight	560,000	1,650,000
Gel permeation chromatograph molecular weight average	828,000	1,510,000

Pentaphenyltrimethyltrisiloxane:	DC-705
Source: Dow Corning Corporation	
Manufacturer's designation	DC-705
Symbol used in this study	S5
Viscosity at 25°C (m^2/s)	1.75×10^{-4}
Density at 25°C (kg/m^3)	1090
Molecular weight	546
Flash point (°C)	243
Refractive index	1.5790

Dimethylsiloxanes:	DC-200		
Source: Dow Corning Corporation			
Manufacturer's designation	DC-200	E1923-48	E1923-49
Symbol used in this study	S6	S7	S8
Viscosity at 25°C (m^2/s)	9.3×10^{-4}	1.2×10^{-3}	1.06×10^{-3}
Molecular weight (GPC)	45,600	43,000	160,000

Modified Polyphenyl Ether:	MCS-418
Source: Monsanto Reserach Corporation	
Manufacturer's designation	MCS-418
Symbol used in this study	S9
Viscosity at -18°C (m^2/s)	1.304×10^{-2}
Viscosity at 38°C (m^2/s)	2.5×10^{-5}
Viscosity at 99°C (m^2/s)	4.1×10^{-6}
Viscosity at 149°C (m^2/s)	2.0×10^{-6}
Density at 25°C (kg/m^3)	1195
Density at 38°C (kg/m^3)	1184
Density at 149°C (kg/m^3)	1101
Pour point (°C)	-29
Refractive index	1.6735

Printed in U. S. A.

Paper No.
74-Lub-28

J. Jakobsen
Lecturer,
Department of Machine Design,
The Technical University of Denmark,
Copenhagen, Denmark
Mem. ASME

W. O. Winer
Professor,
School of Mechanical Engineering,
Georgia Institute of Technology,
Atlanta Ga.
Mem. ASME

Traction of Elastohydrodynamic Contacts With Thermal Shearing Flow

The formulation and solution for the shear stress and temperature in heavily loaded sliding elastohydrodynamic contacts is presented. The solutions are presented in dimensionless design charts. Integration over the contact area will yield the traction. Accuracy is expected to be very good over the nearly flat part of the contact area where the majority of the sliding traction is generated. The procedure presented is not appropriate for thick film lubrication, for the inlet region, or for the rolling friction of elastohydrodynamic contacts.

Introduction

The high shear, high pressure flow in a sliding elastohydrodynamic contact of a lubricant with known pressure, temperature, shear, viscosity relation can be described by a general analysis which predicts the maximum temperature and the shear stress of the film. Other film quantities can be derived therefrom. The results are of interest for the determination of traction coefficients of sliding elastohydrodynamic contacts.

The study of thermal effects in lubricant films is not new. However, investigations of classical thick film lubrication where thermal effects are considered do not include high pressure and high shear as found in sliding elastohydrodynamic contacts. Numerical methods are often used to obtain solutions in the thick film thermal case except for highly simplified situations. Most of these earlier efforts were aimed at journal bearings and sliders and give insight in the thermal film behavior. The pressure gradient and the heat convection terms can not generally be neglected in the problem formulation. The theoretical work of Hunter and Zienkiewicz [1][1] 1960 may be regarded as typical. Their results showed that viscosity variations perpendicular to the film significantly reduce the load capacity. Nonconducting walls showed lower load capacity than conducting walls. The findings of Wilcock and Rosenblatt [2, 3], 1952, 1957, that the viscosity at the average outlet temperature adequately describes the bearing operation was confirmed in the case of heat conducting walls.

The works of Ezzat and Rohde [4], 1973, and of Sierig and Ezzat [5], 1973, comprehensively review the thermal thick film problem from the Beauchamp Tower observations and the Fogg-effect to Donaldson's [6] concept of an adiabatic transformation. The two works of Ezzat, et al. [4, 5] contain an extensive reference list on thermal thick film treatments. The aim of this group of investigations is to predict primarily film thickness or load capacity. Traction is seldom treated.

Some analytic presentations of thermal effects are available [7–11]. The solutions are given, in most cases, only for specific temperature viscosity relations, which often result in inadequate accuracy of the viscosity prediction if used for the relatively large temperature differences of a sliding elastohydrodynamic film.

Theoretical predictions of traction in elastohydrodynamic lubrication where thermal effects are included have relied on numerical methods as in the case of most thick film work. The computed solutions have been part of a greater investigation of thermal effects by Cheng and Sternlicht [12], 1965, Cheng [13, 14], 1965, 1967, and Dowson and Whitaker [15], 1965–1966. The main purpose of these works was to predict film thickness, pressure and temperatures. Only a few parameter combinations are calculated completely and line contacts are emphasized.

The analytic approach of Crook [16], 1961, is an attempt to predict a general friction behavior of a sliding line contact. The isothermal wall condition applied appears to be an oversimplification compared to reality. The analysis of Chiu [17], 1974, on rolling traction and sliding traction in the inlet and exit regions of a starved point contact gives dimensionless diagrams for direct determination of the traction. The analysis is not valid, however, for the unstarved condition. Some doubts have further been expressed because elastic deformations have not been included in the analysis. The simplified traction solution approach presented by Kannel and Walowit [18], 1971, appears primarily to be based on an extension of Crook [16]. Respectable agreement is found with the computer calculated results of Cheng [13] and with the data of Crook [16]. The Kannel and Walowit [18] solutions are developed with the shear rate as variable and use the isothermal wall condition $T = T_0\,(y = \pm h/2)$.

The available solutions intended for use in elastohydrodynamic lubrication appear not to possess the desirable direct accessibility

[1] Numbers in brackets designate References at end of paper.

Contributed by the Lubrication Division of THE AMERICAN SOCIETY OF MECHANICAL ENGINEERS for presentation at the ASME-ASLE Joint Lubrication Conference, Montreal, Canada, October 8-10, 1974. Revised manuscript received by the Lubrication Division, June 26, 1974. Paper No. 74-Lub-28.

Copies will be available until June, 1975.

to engineering use nor the generality of an analytic approach. More realistic boundary conditions may also improve the agreement with traction measurements.

A simplified, analytic method for shear stress determination in the high pressure area of a sliding elastohydrodynamic contact is presented. A general pressure-temperature-shear-viscosity relation for the lubricant is assumed. Solutions in terms of shear stress can be obtained directly with the use of dimensionless diagrams. Sliding speed and thermal conductivity of the lubricant must be known. Lubricant viscous properties, pressure distribution and film thickness of the high pressure part of the contact must be known from calculations or measurements. The Hertzian pressures can be used for a first estimation of the traction. A realistic model for the viscous behavior of many lubricants is also presented.

Problem Formulation

The change of film thickness over the major part of an elastohydrodynamic contact is small compared to the film thickness particularly for highly loaded contacts. The shear stress component generated by the pressure gradient is also small over a great part of the contact area compared with the shear stress component from the sliding action. The effect of convection along the film is small compared with the heat conduction perpendicular to the film. Therefore, a unidirectional laminar flow, with pointwise constant pressure and temperature between parallel surfaces may be assumed as a good approximation for the flow: $u_1 = u_1(x_3)$, $u_3 = 0$, $p = \text{const}$, $T = T(x_3)$. The flow model is shown in Fig. 1 which also shows the boundary conditions. Surface 2 is moving with constant velocity $u_1 = (UN)$ in the x_1 direction. Constant thermal conductivity is assumed. The assumptions are discussed further in [21].

The governing equations for conservation of momentum and energy, respectively, are reduced to:

$$\tau_{13} = \tau = \text{const} = \eta u_{1,3} \quad \text{and} \quad (kT_{,3})_{,3} + \eta(u_{1,3})^2 = 0 \tag{1}$$

The boundary conditions are

$$\begin{aligned} u_1(0) &= 0 & T_1 &= T_1(0) = \text{const} \\ u_1(h) &= (UN) & T_2 &= T_2(h) = \text{const} \end{aligned} \tag{2}$$

Although the analysis of these equations can be utilized with any general viscosity relation $F(p,T,\tau,\eta) = 0$, a particular form of this relation will be introduced which will be used in selecting parameters with which to nondimensionalize the governing equations. The so-called power exponential viscosity description [21]

$$ln\ln\frac{\eta}{\eta_0} = \pi_3(lnE - lnT)\Big|_{\tau,p} \tag{3}$$

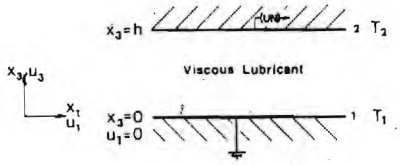

Fig. 1 Flow model

where E and π_3 are functions of pressure, has been found to give a reasonably accurate description of the viscosity behavior within a range of temperature of 39C–100C for many fluids. The range is of the same magnitude as the temperature difference often expected in elastohydrodynamic films. The temperature-viscosity relation (3) can be written as

$$\mu = \exp\left(\left(\frac{E}{T}\right)^{\pi_3}\right) \tag{4}$$

The introduction of this form will also permit the graphical presentation of the results to facilitate their utilization.

The expressions (4), (1), and (2) become in nondimensional form

$$\mu = \exp(\theta^{\pi_3}) \tag{5}$$

$$\mu u_{,z} = \pi_5 \tag{6}$$

$$\theta_{,zz} + 2\pi_4\pi_5 u_{,z} = 0 \tag{7}$$

$$\begin{aligned} u(0) &= 0 & \theta(0) &= \pi_1 \\ u(1) &= 1 & \theta(1) &= \pi_2 \end{aligned} \tag{8}$$

with the variables, dimensionless temperature, velocity and film thickness, introduced as

$$\theta = T/E \qquad u = u_1/(UN) \qquad z = x_3/h \tag{9}$$

and the operational parameters of the problem combined as the dimensionless quantities

$$\begin{aligned} \pi_1 &= T_1/E & \pi_2 &= T_2/E \\ \pi_4 &= \eta_0(UN)^2/2kE & \pi_5 &= \tau h/\eta_0(UN) \end{aligned} \tag{10}$$

The products π_4 and π_5 can be regarded as dimensionless velocity and shear stress parameters, respectively.

The Maximum Temperature and the Shear Stress

The assumptions imply that the film is convectionless and also that the direction of heat conduction is perpendicular to the film

Nomenclature

E = lubricant material parameter, the temperature (K) at which the viscosity is 2.718×10^{-3} Nsm^{-2}
h = film thickness, m
$I(i,j) \equiv \int_{\pi_i}^{\pi_j}(\mu(\xi,\pi_3))^{-1}d\xi$
k = thermal conductivity of lubricant, Wm^{-1}K^{-1}
p = pressure, Nm^{-2}
T = temperature, K
T_0 = arbitrary base temperature, I
UN = velocity of moving surface in x_1 direction, ms^{-1}
u_1 = velocity of fluid in x_1 direction, ms^{-1}
u = dimensionless velocity, u_1/UN
x_1, x_3 = dimensioned coordinates, m
x, z = dimensionless coordinates, $\frac{x_1}{h}$ and $\frac{x_3}{h}$, respectively
η = viscosity, Nsm^{-2}
η_0 = dimensional constant = 10^{-3} Nsm^{-2}
η_{38} = viscosity at 38C, Nsm^{-2}
η_{100} = viscosity at 100C, Nsm^{-2}
θ = dimensionless temperature = T/E
μ = dimensionless viscosity = η/η_0
π_0 = dimensionless base temperature = T_0/E
π_1 = dimensionless fixed wall temperature = T_1/E
π_2 = dimensionless moving wall temperature = T_2/E
π_3 = dimensionless lubricant material parameter
π_4 = dimensionless velocity parameter = $\eta_0(UN)^2(2kE)^{-1}$
π_5 = dimensionless shear stress parameter = $\tau h(\eta_0(UN))^{-1} = \mu u_{,z}$
τ = shear stress, Nm^{-2}
$,$ = subscript indicating differentiation with respect to the following variable.

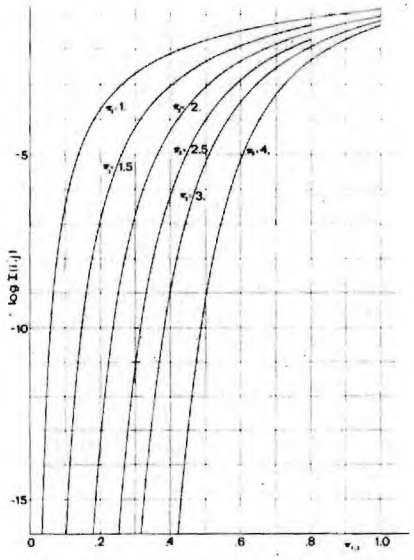

Fig. 2 Determination of $I(i,j)$ for maximum film temperature

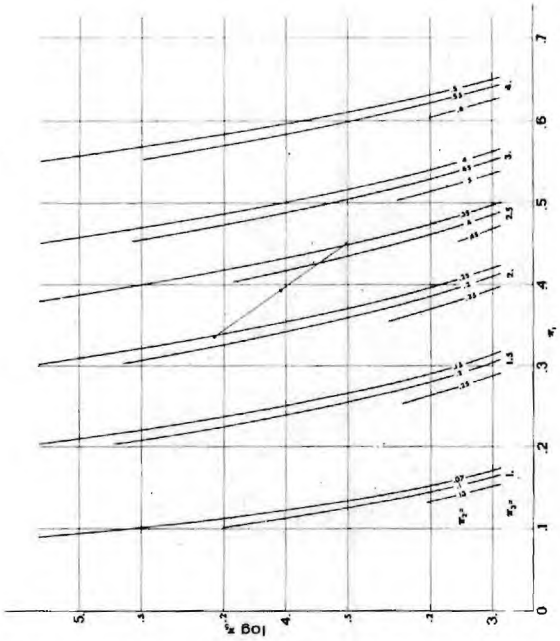

Fig. 3 Determination of π_5. The dimensionless shear stress

plane. Equation (1) shows that the shear stress, τ and hence π_5, is constant through the film, because $p_{,1}$ is assumed insignificant.

The local heat generation, due to viscous dissipation, is proportional with the shear rate, or film thickness, and the heat conduction is inversely proportional with thickness. The temperature distributions, and thereby the temperature extrema, are thus independent of the film thickness. The temperature profiles are symmetric about the adiabatic plane of the film. Considering the adiabatic plane located at the stationary surface is a good approximation for sliding elastohydrodynamic situations.

If we integrate equation (7) across the film from the stationary (adiabatic) surface to some arbitrary location in the film, we obtain

$$\theta_{,z}(z) + 2\pi_4\pi_5 u = 0. \tag{11}$$

Substituting π_5 from equation (6), rearranging and integrating across the film gives,

$$\pi_4 = \int_{\pi_2}^{\pi_1} \frac{d\theta}{\mu(\theta, \pi_3)} \equiv \mathrm{I}(1,2) \tag{12}$$

By introducing an arbitrary base temperature $\pi_0 < \pi_1$ or π_2 this can be written as

$$\pi_4 + \mathrm{I}(2,0) = \mathrm{I}(1,0) \tag{12a}$$

These integrals can be evaluated and graphically presented for a given viscosity function $\mu(\theta,\pi_3)$. For the particular viscosity function described above (equation (4) or (5)), these integrals are plotted in Fig. 2.

The integrals, from π_0 to π_i, are plotted in the figure for π_3 = 1.0, 1.5, 2.0, 2.5, 3.0 and 4.0. Entrance to the diagram is through the lower temperature π_2. Intersection of the vertical line π_2 with the appropriate interpolated π_3 value gives the value of the integral term $I(2,0)$. The value of π_4 is added to $I(2,0)$ which gives $I(1,0)$ as shown in equation (12a). Intersection of the horizontal line of $I(1,0)$ with the appropriate π_3 value gives the desired π_1 of maximum temperature.

The displacement of the adiabatic plane to the stationary surface does not reduce the generality primarily because the film behavior is symmetric about the adiabatic plane. The film thickness does not participate in the determination of the maximum temperature. The influence of the temperature π_2 of the moving, cold wall, $\pi_2 < \pi_1$, on the magnitude of the maximum temperature π_1 is found in many situations to be of only minor importance because the temperature dependent integrand is small at low temperatures compared with the magnitude of the integrand when the temperature is near the maximum temperature. The maximum temperature depends therefore mainly on the velocity parameter π_4, the power exponent π_3 and the characteristic temperature E.

Auxiliary diagrams to determine the material properties π_3 and E from viscosity data for the lubricant are presented in Appendix A. Approaches to the determination of the local temperature π_2 of the moving, colder bearing surface are found in Carslaw and Jaeger [22], 1962, which also contains further references to the original papers of Blok, 1937, and of Jaeger, 1942.

To obtain an expression for the shear stress in the case where the stationary wall is adiabatic we again substitute π_5 from equation (6) into (11) and integrate from the stationary wall to an arbitrary location in the film to obtain

$$\int_{\pi_1}^{\theta} \frac{d\xi}{\mu(\xi, \pi_3)} + \pi_4 u^2 = 0$$

which gives

$$u(\theta) = \frac{1}{\sqrt{\pi_4}} \left\{ \int_{\theta}^{\pi_1} \frac{d\xi}{\mu(\xi, \pi_3)} \right\}^{1/2} = \frac{1}{\sqrt{\pi_4}} \{\mathrm{I}(\pi_1, \theta)\}^{1/2} \tag{13}$$

Substituting (13) into (11) and integrating from one surface to the other and rearranging yields, (21),

$$\pi_5 = \frac{1}{2\sqrt{\pi_4}} \int_{\pi_2}^{\pi_1} \{\mathrm{I}(\pi_1, \theta)\}^{-1/2} d\theta = \pi_5(\pi_1, \pi_2, \pi_3) \tag{14}$$

which is the dimensionless shear stress.

The dimensionless shear stress, π_5, depends on three dimensionless parameters only, π_1, π_2, π_3. The dimensionless velocity parameter π_4 depends on the same set of parameters through equation (12).

Thus the shear stress π_5 of equation (14) depends on the same operational quantities as the maximum temperature of the film. The shear stress τ depends also on the film thickness h. Information about the thickness must be available, from measurements or from calculations, in order to determine the shear stress.

The dimensionless shear stress function, equation (14), can be evaluated and graphically presented for a given viscosity function

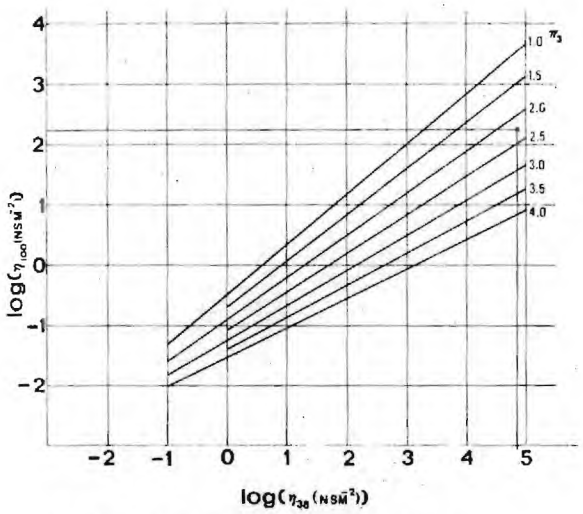

Fig. 4 The temperature viscosity coefficient π_3

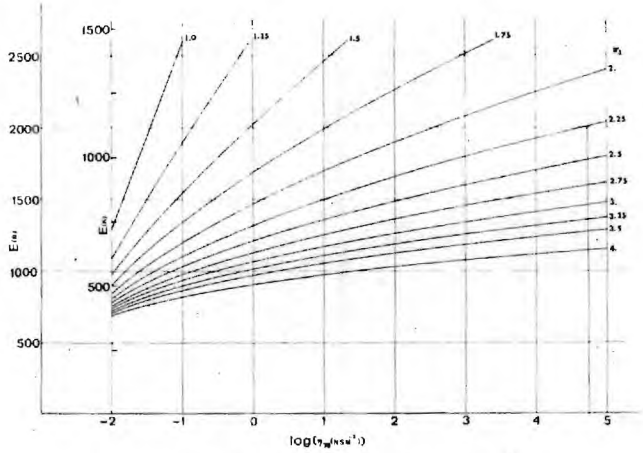

Fig. 5 The temperature E (R or K)

$\mu(\theta,\pi_3)$. For the particular abovementioned viscosity function (equation (4) or (5)), the function π_5 has been evaluated and plotted in Fig. 3. It shows the presentation for $\pi_3 = 1.0$, 1.5, 2.0, 2.5, 3.0 and 4.0, and for appropriate π_2 values. The range of π_5 in the figure covers the expected operation of elastohydrodynamic films.

The interpolation procedure can be carried out as shear stress determinations for two slope exponents, π_3, of the diagram values which are nearest to the π_3 exponent of the lubricant. A straight line between the two determined stress values, π_5, will intersect with the actual π_3 curve of the lubricant and give an approximation to the desired dimensionless shear stress π_5 of the film. The shear stress can then be calculated from equation (10).

The traction coefficient is determined as the summation of the shear stress distribution over the contact area. The traction coefficient may be determined also in the case of nonadiabatic walls using the symmetry properties of the film. The temperatures of the walls, Fig. 1, must be estimated, [22]. The dimensionless velocity of the adiabatic plane is found as $u_a = \frac{1}{2} + (I(2,1)/2\pi_4)$. The two parts of the film, divided by the plane, are considered individually assuming the relative velocity, with respect to the adiabatic plane, contained in two new velocity parameters. Iteration for the two parts of the film with the diagram, Fig. 3, may be continued until satisfactory agreement with the wall temperatures is achieved.

Conclusions

The shear stress and the temperatures in the high pressure part of a sliding elastohydrodynamic point or line contact can be determined directly with the presented design charts. The applicability is dependent on: 1) the ratio of the shear stress due to the pressure gradients to the shear stress due to sliding, and 2) the ratio of heat convection along the film to heat conduction perpendicular to the film plane. The accuracy of the procedure is best where these ratios are small, $\ll 1$. This is the case over 80–90 percent of the Hertzian area in elastohydrodynamic contacts where the major part of the sliding traction is generated. The procedure is not valid for thick film lubrication or to inlet-exit zones of elastohydrodynamic contacts.

Acknowledgments

The research reported herein was supported in part by the National Science Foundation (NSF GK-31154) and by NASA (NGR-11-002-133). The support is greatly appreciated.

One of the authors (J.J.) wishes to acknowledge the grant of leave from the Technical University of Denmark, the Department of Machine Design. The study and research were also supported by Statens teknisk-videnskabelige Fond (1959.M-158 and 2097.M-183) Denmark and Otto Monsteds Fond (1972 and 1973) Denmark. The support is greatly appreciated.

References

1. Hunter, W. B., and Zienkiewicz, O. C., "Effect of Temperature Variations across the Lubricant Films in the Theory of Hydrodynamic Lubrication," *Journal of Mechanical Engineering Sciences*, Vol. 2, No. 1, 1960.

2 Wilcock, D. F., and Rosenblatt, M., "Oil Flow, Key Factor in Sleeve Bearing Performance," TRANS. ASME, Vol. 74, 1952, pp. 849-866.

3 Wilcock, D. F., "Predicting Sleeve-Bearing Performance," *Proceedings of the Conference on Lubrication and Wear*, The Institution of Mechanical Engineers, London, October 1-3, 1957, Paper 48, pp. 82-92.

4 Ezzat, H. A., and Rohde, S. M., "A Study of the Thermohydrodynamic Performance of Finite Slider Bearings," TRANS. ASME, Series F, Vol. 95, No. 3, July 1973, pp. 298-307.

5 Sierig, A., and Ezzat, H. A., "Thermohydrodynamic Phenomena in Fluid Film Lubrication," TRANS. ASME, Series F, Vol. 95, No. 2, April 1973, pp. 187-194.

6 Donaldson, R. R., "Variable Viscosity Effects in Hydrostatic Films: The Adiabatic Transformation," TRANS. ASME, Series F, Vol. 93, No. 1, Jan. 1971, pp. 151-155.

7 Kingsbury, A., "Heat Effects in Lubricating Films," *Mechanical Engineering*, Vol. 56, 1934.

8 Hagg, A. C., "Heat Effects in Lubricating Films," TRANS. ASME, *Journal of Basic Engineering*, 1944.

9 Regirer, S. A., "The Influence of Thermal Effects on the Viscous Resistance of a Steady Uniform Flow of Liquid," *PMM*, Vol. 22, No. 3, 1958.

10 Bostandzhyan, S. A., Merzhanov, A. G., and Khudyaev, S. I.,

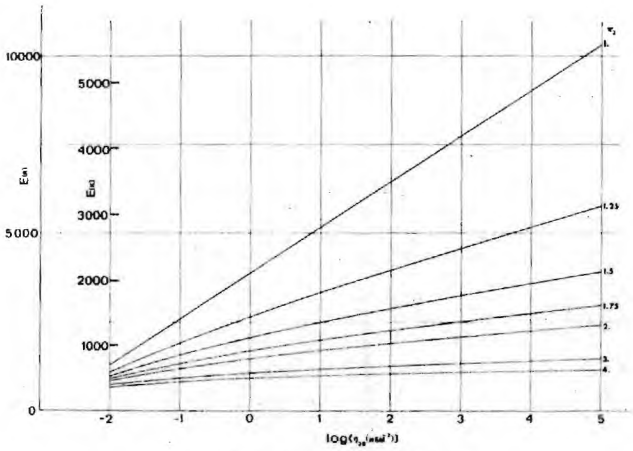

Fig. 6 The temperature E (R or K)

"Some Problems of Nonisothermal Steady Flow of a Viscous Fluid," *Zhurnal Prikladnoi Mekhaniki i Tekhnicheskoi Fiziki (Journal of Applied Mechanics and Technical Physics)*, No. 5, 1965.

11 Qvale, E. B., and Wiltshire, F. R., "The Performance of Hydrodynamic Lubricating Films With Viscosity Variations Perpendicular to the Direction of Motion," TRANS. ASME, Series F, Vol. 94, No. 1, Jan. 1972, pp. 44-48.

12 Cheng, H. S., and Sternlicht, B., "A Numerical Solution for the Pressure, Temperature, and Film Thickness Between Two Infinite Long, Lubricated Rolling and Sliding Cylinders, Under Heavy Loads," *Journal of Basic Engineering*, TRANS. ASME, Series D., Vol. 87, No. 3, 1965, p. 695.

13 Cheng, H. S., "A Refined Solution to the Thermal-Elastohydrodynamic Lubrication of Rolling and Sliding Cylinders," *ASLE Trans.*, Vol 8, No. 4, 1965, p. 397.

14 Cheng, H. S., "Calculation of Elastohydrodynamic Film Thickness in High Speed Rolling and Sliding Contacts," Technical Report, Mechanical Technology Incorporated, MTI-67TR24.

15 Dowson, D. and Whitaker, A. V., "A Numerical Procedure for the Solution of the Elastohydrodynamic Problem of Rolling and Sliding Contacts Lubricated by a Newtonian Fluid," *Symposium on Elastohydrodynamic Lubrication, Proceedings of the Institution of Mechanical Engineers*, 1965-66, Pt. 3B, 57, p. 180.

16 Crook, A. W., "The Lubrication of Rollers III. A Theoretical Discussion of Friction and The Temperatures in the Film," *Proceedings of the Royal Society of London*, A254, 1961.

17 Chiu, Y. P., "A Theory of Hydrodynamic Friction Forces in Starved Point Contact Considering Cavitation," TRANS. ASME, Series F, Vol. 96, No. 2, April 1974, pp. 237-246.

18 Kannel, J. W., and Walowit, J. A., "Simplified Analysis for Traction Between Rolling-Sliding-Elastohydrodynamic Contacts," TRANS. ASME, Series F, Vol. 93, No. 1, Jan. 1971, pp. 39-46.

19 Hersey, M. D., *Theory of Lubrications*, Wiley, London, 1938, second printing, pp. 115-118.

20 Hersey, M. D., *Theory and Research in Lubrication, Foundations for Future Developments*, Wiley, New York, 1966, pp. 70-71.

21 Jakobsen, J., "Lubricant Rheology at High Shear Stress," doctoral thesis, Georgia Institute of Technology, Sept. 1973, and University Microfilms, Ann Arbor, Mich., 1973.

22 Carslaw, H. S., and Jaeger, J. C., *Conduction of Heat in Solids*, Clarendon Press, Oxford, 1962.

APPENDIX A

Figs. 4, 5 and 6 are prepared in order to facilitate the determination of π_3 and E. Fig. 4 shows the slope parameter π_3 as a function of the viscosities $\eta_{39}|_p$ and $\eta_{100}|_p$. Entrance to the figure is the two viscosities measured at constant pressure, at the temperatures 39C and 100C, in the units of Nsm^{-2}. An ASTM chart (D 341-43) or similar charts may be used to determine the viscosities η_{39} and η_{100} if existing data were at other temperatures. Figs. 5 and 6 show the temperature E, in Rankine and Kelvin as function of η_{39} and π_3. Fig. 5 gives relatively high resolution for lubricants with the slope parameter π_3 in the range 1 to 2. Fig. 6 gives relatively high resolution for lubricants with the parameter π_3 in the range 2 to 4.

Printed in U. S. A.

74-LUB-40

an ASME publication

J. Jakobsen
Lektor,
Dept. of Machine Design,
The Technical University of Denmark,
Copenhagen,
Denmark. Mem. ASME

W. O. Winer
Professor,
School of Mechanical Engineering,
Georgia Institute of Technology,
Atlanta, Ga. Mem. ASME

Dissipative Heating Effects and End Corrections for Viscous Newtonian Flow in High Shear Capillary Tube Viscometry

The effect of dissipation heating on the apparent viscosity measured in capillary tube viscometry is described in this paper. Conditions of low Reynolds number and high shear are assumed. End corrections to the tube flow, found to be $3\pi/16$ times the diameter of the tube, are incorporated. The flow curves show decreasing apparent viscosity when the shear stress increases. The configuration of the flow curves plotted in logarithmic presentation are found to be identical for fluids with Newtonian behavior. Convection is the predominant mechanism in removal of the heat in short capillary tube. The estimated upper bound for the shear stress obtainable in short length capillary tubes appears to be of the order of magnitude of 10 MPa limited primarily by the pressure drop associated with the constant end correction from the flat ended inlet and exit of the tube.

Introduction

The measurement of the viscosity of liquid lubricants is of importance from an engineering point of view and hence has received a great deal of attention and work. The dependency of the viscosity on pressure, temperature and shear is of particular interest for elastohydrodynamic lubrication.

The ASME Pressure Viscosity Report, 1953 [1] is the most extensive single experimental work on pressure viscosity relations of lubricants found in the literature. The report documented large viscosity increases of all investigated lubricants at pressures of the same magnitude as the pressures reached in elastohydrodynamic contacts and showed large viscosity dependency on temperature at all pressures. The measurements were performed at low shear stress, in a falling body viscometer.

The elastohydrodynamic contact can be regarded as a high shear, high pressure viscometer. It has been used in sliding, rolling, or squeezefilm arrangements to measure lubricant behavior. Evaluation of traction data from elastohydrodynamic contacts is difficult, however, particularly for deduction of viscosity relations. Only the total traction is measured. The main objection to the use of an elastohydrodynamic contact as a viscometer seems to be that the parameters of primary interest pressure, temperature and shear cannot be varied independently of each other.

Vibrating crystal viscometers have been used to measure shear elasticity and viscosity of lubricants under conditions of high angular frequencies and small displacement amplitudes. The angular frequency is interpreted in these measurements as a quantity comparable with the shear rate in continuous shear. Some experimental results from high pressure work are available [2-3].

Capillary tube viscometry has been a preferred method of measurements of lubricant rheological relations particularly for high pressure investigations.

For a review of the work in this area prior to 1965 see Hersey [4]. High pressure, high shear measurements have been reported recently. Many types of lubricants, both mineral oils and synthetic lubricants, have been investigated by capillary viscometry in ranges of pressure, temperature and shear which are important for the understanding of elastohydrodynamic lubrication. Capillary tube viscometry offers conveniently an experimental situation where the effects of pressure, temperature and high shear stress on the viscous properties of lubricants can be independently investigated. High shear measurements can be performed in cylindrical capillary tubes with a small ratio of length and diameter with reasonably small pressure drop. Inlet and exit corrections must be evaluated properly. The high shear measurements can be carried out under experimental conditions of very low Reynolds numbers, $R_e \ll 1$, when the viscosity is of the same order of magnitude as the viscosity in the elastohydrodynamic film and a tube diameter 100 μm.

The viscous flow of a fluid through a capillary tube generates a

Contributed by the Lubrication Division of THE AMERICAN SOCIETY OF MECHANICAL ENGINEERS for presentation at the ASME-ASLE Joint Lubrication Conference, Montreal, Canada, October 8-10, 1974. Manuscript received by the Lubrication Division, July 8, 1974. Paper No. 74-Lub-40.

Copies will be available until June, 1975.

temperature increase, due to the dissipation heating, and a corresponding viscosity decrease of the fluid. The shear stress and the shear rate both reach their greatest value at the wall and are zero at the axis. The heat generation, which is the product of the shear stress and the shear rate, is greatest at the wall of the capillary tube and zero at the axis. The temperature after the inlet will therefore remain low at the axis and increase in radial direction with increasing distance from the axis till the cooling effect of the wall is noticeable. The temperature near the wall will remain low due to the relatively high heat conductivity of the wall material compared with the conductivity of the fluid. The temperature profiles are axisymmetric assuming an uniform inlet temperature. The radial temperature distribution immediately after the inlet is thus characterized by an annular maximum near the wall and low temperatures at the center and at the wall of the capillary tube. The temperature at the axis increases slowly in the downstream direction due to radial heat conduction towards the axis of the capillary tube. The radius of the annular maximum decreases with increasing distance from the inlet.

The viscous flow of a fluid into a cylindrical capillary tube from a reservoir also has associated with it a pressure drop originating from the velocity gradients in the contraction of streamlines before the inlet. The pressure drop ahead of the inlet is independent of the length of the capillary tube. The flow from the exit of the cylindrical capillary tube to a receiving reservoir generates an additional pressure drop. The stream lines of the exit flow will at sufficiently low Reynolds number be expected to assume a configuration equal to the configuration of the streamlines of the inlet flow because the stream function, at $R_e \simeq 0$, and the boundary conditions are symmetric with respect to the axial coordinate. The pressure drop at the exit and at the inlet are therefore identical under such conditions. The sum of the pressure drop outside the capillary tube cavity must be subtracted from the measured, total pressure change in order to calculate a correct shear stress in the fluid. The correction is often carried out as a number added to the geometrically determined ratio of capillary tube length and diameter. The magnitude of the correction may be found experimentally. The inlet and exit pressure drop generate temperature increases and corresponding viscosity decreases of the fluid due to dissipation heating, in the same manner as the changes that happen in the cylindrical capillary tube cavity.

High shear rate capillary viscometry has been the subject of several studies [cf., 4, 10–15]. The effect of temperature increase and resulting viscosity decrease have been studied by several authors [10, 13, 14, 15, 16]. However, they have not focused on the possible reduction of those effects and consequently increasing the upper limit of shear stress that can be attained in capillary viscometry. This is the purpose of the present research.

The purpose of this presentation is twofold. It is an attempt to establish criteria to distinguish dissipative heating effects from effects of non-Newtonian properties in capillary tube measurements. The purpose is also to indicate the possibility to attain, in capillary tube viscometry, fluid shear stresses approaching the average shear stress level experienced in an elastohydrodynamic film. The pressure level and temperature level are principally independent of the imposed shear stress in such an experiment. Time duration of shear load on a fluid particle is of the same order of magnitude as the contact time for the moving surfaces of an elastohydrodynamic contact. Rheological investigations of lubricant properties may thus be performed under simulated elastohydrodynamic conditions and under terms of mutual independency among the most important parameters pressure, temperature, and shear stress.

Problem Formulation—Flow in the Capillary Tube

The distribution of temperature increase over a uniform inlet temperature and the corresponding increase of flow rate are estimated for a highly viscous, high shear stress flow through a cylindrical capillary tube. The volume flow and the pressure drop over the capillary tube cavity are the measured quantities. The Reynolds number for the flow is sufficiently small so the entrance length, calculated according to the approach by Schiller [17], can be neglected in comparison with the total length of the capillary.

Fully developed flow is thus assumed to be present already at the inlet. Inertial forces are therefore zero. The flow is assumed to be steady laminar axisymmetric flow with the velocity a function of radius only. The velocity is zero at the wall and a maximum in the center. The pressure is assumed to be a linear function of distance down the axis of the tube. The fluid temperature is a function of radial and axial dimensions and is zero at the inlet and at the tube walls. Material properties, density, specific heat, and thermal conductivity are assumed constant.

Energy transport by axial convection and radial conduction only are considered. As will be seen, axial convection is the most important mode of energy transport with radial conduction important primarily near the tube wall. Axial conduction is small compared to convection and is also small compared to radial conduction unless $(L/D)^2 \leq 1$ and even then the convection term is more important than either radial or axial conduction.

First temperature distribution in the capillary tube due to dissipation is estimated for the case of axial convection and constant viscosity but no radial conduction. The deviation of the flow

Nomenclature

c = specific heat per unit mass
k = coefficient of heat conduction
p = pressure
$\hat{p}_{,\omega}$ = dimensionless pressure gradient $\hat{p}_{,\omega} = -(p_{,z})L/c\,\rho E$
q = volumetric flow rate
$\hat{q}$ = dimensionless volume flow rate $\hat{q} = -(p_{,z})R^4/4L\eta\kappa = -(2/\pi)\,(q/L\kappa)$
r = radius
r,θ,z = coordinates in cylindrical coordinate system
u_z = velocity in axial direction
D = diameter of the capillary tube $D = 2R$
E = a lubricant material parameter, the temperature (K) at which the viscosity is 2.718×10^{-3} Nsm^{-2}
L = length of the capillary tube
L_e = length equivalent with the end correction
R = radius of the capillary tube
R_e = Reynolds number
T = temperature
Δp = pressure drop
Δp_i = pressure drop ahead of the inlet area
Δp_{ie} = sum of pressure drop ahead of the inlet and after the exit area
Δp_t = total pressure drop over inlet, capillary tube and exit $\Delta p_t = \Delta p_{ie} + \Delta p$
η = viscosity
θ = dimensionless temperature $\theta = T/E$
κ = thermal diffusivity of the fluid $\kappa = k/c\,\rho$
μ = dimensionless viscosity
π_3 = a lubricant material parameter π_3
ρ = density
$\bar{\rho}$ = dimensionless radius $\bar{\rho} = r/R$
τ = shear stress at the wall of a cylindrical capillary tube $\tau = \Delta p/4(L/D)$
ψ = stream function
ω = dimensionless axial coordinate $\omega = z/L$
$'$ = index denoting differentiation with respect to the following symbol

curves will be evaluated assuming the estimated temperature distribution but using a temperature dependent viscosity function in the calculations of flow rates.

The procedure is then repeated incorporating radial conduction. The temperature distribution is estimated assuming axial convection, radial conduction and constant viscosity. The flow curves are then evaluated using the estimated temperatures but assuming temperature dependent viscosity in the calculations of flow rates.

The equation of mass continuity is satisfied identically and the equations of motion are reduced to

$$rp_{,z} = (\eta r u_{z,r})_{,r} \tag{1}$$

The energy equation reduces to

$$\rho c u_z T_{,z} = k(T_{,rr} + (1/r)T_{,r}) + \eta(u_{z,r})^2 \tag{2}$$

Integration of equation (1) and the condition of axisymmetric flow, $u_z, r(0) = 0$, give the equation (2)

$$\hat{q}\theta_{,\omega}(1 - \bar{\rho}^2) = \theta_{,\bar{\rho}\bar{\rho}} + (1/\bar{\rho})\theta_{,\bar{\rho}} + \hat{q}\hat{p}_{,\omega}\bar{\rho}^2 \tag{3}$$

where

$$\bar{\rho} = r/R \quad \theta = T/E \quad \omega = z/L \tag{4}$$

and

$$\hat{q} = (-p_{,z})R^4/4L\eta\kappa \quad \hat{p}_{,\omega} = (-p_{,z})L/c\rho E \tag{5}$$

The boundary conditions become

$$\theta(1, \omega) = 0 \quad \theta(\bar{\rho}, 0) = 0 \tag{6}$$

No Heat Conduction. The special case of no heat conduction in the fluid, is of interest because it gives an approximate description of the expected temperature profiles immediately after the inlet. This case also gives a particularly good description of the temperatures of the fluid following streamlines near the capillary axis. When heat conduction is absent, equation (3) reduces to:

$$\theta_{,\omega} = (\bar{\rho}^2/(1 - \bar{\rho}^2))\hat{p}_{,\omega} \tag{7}$$

with the solution

$$\theta = (\bar{\rho}^2/(1 - \bar{\rho}^2))\hat{p}_{,\omega}\omega \tag{8}$$

satisfying the condition $\theta(\bar{\rho},0) = 0$. The isothermal condition $\theta(1,\omega) = 0$ cannot be expected to be satisfied in this case.

The temperature in the capillary tube increases linearly with the axial coordinate when no conduction occurs. The temperature is zero along the axis and increases without bound when $\bar{\rho} = 1$. The temperature profiles as a function of the relative radius is shown in Fig. 1. The temperatures depend only on the pressure drop over the length L, the specific heat and on the location in the capillary. Fluid viscosity, shear rate or capillary tube diameter do not participate in determination of the temperatures. For a typical pressure drop of 3.45 MPa over the length L with a lubricant of 1.74 MPa/K specific heat per unit volume, equation (8) gives the temperature profile at the exit:

$$T \simeq 2.0(\bar{\rho}^2/(1 - \bar{\rho}^2)) \tag{9}$$

A temperature dependent viscosity can be introduced in order to estimate the character of the flow curves. The increase in volume flow, and thereby the decrease in apparent viscosity, due to heat dissipation, can be evaluated. Shear rates and fluid velocities can be determined when the temperatures as described by equation (8) are assumed. An increased flow rate can then be found direct by integration of the velocities. The decrease in apparent viscosity can be found by the ratio between pressure drop and increased flow rate. The assumption of an unchanged temperature profile represents an approximation which can be justified only within a certain interval of applied pressure drop. It is shown in the following that the flow curves will be congruent in the range of interest of the experimental parameters when capillary tube configuration, viscosity level, and fluid type are varied.

The velocity profile determined by assuming the temperatures of equation (8) and an arbitrary temperature viscosity relation does not depend on capillary tube dimensions or materials. The relative increase in flow rate of the same fluid through different capillary tubes will therefore depend on the pressure drop alone over the capillary tubes. The flow curves, measured apparent viscosity, proportional with the ratio of pressure drop and volume flow rate, plotted as a function of shear stress, will consequently have the same configuration in a logarithmic presentation but will be displaced in the direction of the shear stress axis according to the actual length over diameter ratio for the capillary tube in question.

The temperature profiles are independent also of the viscosity of the fluid, equation (8). Distortion of the velocity profiles from the parabolic form, change in volume flow rate and the change in measured apparent viscosity are therefore also independent of viscosity level. The flow curves are thus of the same congruent form for different viscosity levels but are displaced through a translation along the viscosity axis alone. The flow curves for a fluid will thus have the same form independently of capillary tube dimensions and viscosity level of the fluid.

In comparison, between fluids different material properties must be assumed. An exponential temperature viscosity relation is of sufficient generality to describe properly the viscosity behavior of fluids for temperature changes of the order of magnitude 5 – 10 K which approximately is the range of interest for the temperature increase. The linear relation between temperature increase and the ratio of pressure drop and specific volumetric heat, equation (8), and the assumed exponential temperature viscosity dependency imply a constant ratio of pressure drop for two fluids when equal decreases in apparent viscosity are generated. Fluids with the smaller ratio of temperature viscosity coefficient and specific volumetric heat will show the same temperature profile in the capillary cavity as fluids with greater ratios but at greater pressure drop. The flow curves for different fluids will therefore have congruent forms in logarithmic presentation but will be positioned along the shear stress axis in accordance with actual temperature viscosity coefficients and specific heats per unit volume.

The conformity of the flow curves can be expected over a greater range of temperature differences. The exponential power temperature viscosity relation

$$(\mu = e^{\beta \cdot T^3})\big|_p \tag{10}$$

yields a more nearly accurate description of the viscosity behavior within a range of temperature change of 40 – 100 K for many fluids. The ratio of the local temperature increases for two fluids under comparison is approximately constant for relation (10), proportional with the ratio of the power exponents, in the range of interest of temperature increases and pressure drop. The ratio of pressure drop necessary to produce equal changes in apparent viscosity for two fluids is therefore also approximately constant. The conformity of the flow curves can thus be expected over greater range of temperature changes than approximately 10 K.

The flow curves of apparent viscosity will be of identical form irrespective of the dimensions of the cylindrical capillary tube, the viscosity level of the fluid and the type of fluid in the range of interest when no heat conduction is present.

Flow With Radial Conduction. It is clear from the foregoing that radial conduction will be important especially near the wall. The general form on the flow curves will be modified to some extent when heat conduction is present. The temperature profiles can be approximated through solution of equation (3) with the collocation method. The temperature of the fluid along the capillary tube axis will not increase discernibly during passage of a relatively short capillary tube. The centerline temperature is therefore assumed to remain nearly constant in the solutions. A series expansion of the form

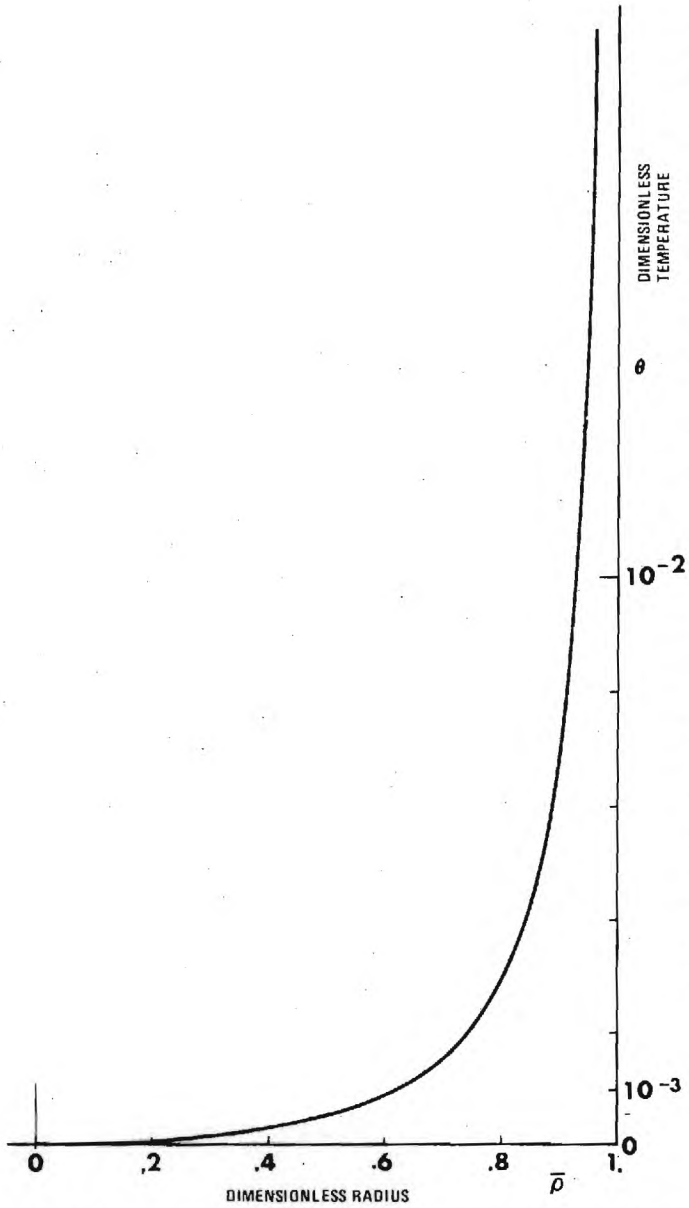

Fig. 1 Temperature distribution in capillary tubes for the case: no heat conduction in the fluid (ω = 1, Δp = 3.45 MPa, $C\rho$ = 1.63 MPa/K, E = 1111 K)

$$\theta - \theta_a \simeq \omega \sum_1^n a_n(1 - \bar{\rho}^{2n}) \quad n \text{ positive integer} \qquad (11)$$

has been selected. It satisfies the boundary conditions of zero temperature at the entrance and at the wall and gives a dimensionless temperature at the axis equal to the sum of the coefficients a_n. Eight radially and variably positioned collocation points were employed at each axial location. Temperature profiles for typical flow situations in a cylindrical capillary tube with a dia of 88 μm and a ratio of length and dia of 1.35 are shown in Fig. 2. The viscosity of the fluid is 3 Pas. The maximum temperatures are found at $\bar{\rho} \simeq .9$. The magnitude is 4.9 K at the exit for a pressure drop of 3.4 MPa over the capillary tube. This gives approximately 2.5 K average temperature increase and 5 – 10 percent decrease of viscosity at that location. The total change in apparent viscosity will however be much smaller. The figure shows also the temperature profile at ω = 0.5. The maximum temperature is 3.1 K at $\bar{\rho}$ = 0.93. The selected series expansion (11) gives the expected trend, in the solutions obtained via collocation, of decreasing radius of the annular maximum when axial distance from the inlet increases. It can also be seen from the figure that the magnitude of the temperature peak is not proportional with axial position ω. This is, in general, true at all radial positions, for $\bar{\rho}$ greater than about .7, where heat conduction is significant. Heat conduction is not significant in a center core $\bar{\rho} <$ ~0.7, and temperature increases are seen to be proportional to axial displacement in this region. The figure shows also the temperature profile for a pressure drop of 6.9 MPa over the capillary. Temperatures in the center core region is doubled compared to the temperatures for a pressure drop of 3.4 MPa. The temperature peak at Δp = 6.9 MPa is more pronounced with a maximum of approximately 12.7 K at $\bar{\rho} \sim .92$.

Fig. 3 shows the contribution from convection, conduction and dissipation from equation (3). The pressure drop is 6.9 MPa. The profiles are calculated at ω = 1. The dissipation profile is the same when ω = 0 as for ω = 1. The convection profile is a mirror picture about the $\bar{\rho}$ axis of the dissipation profile when ω = 0. Convection removes therefore the total amount of generated heat when ω = 0. The generated heat is seen to be removed primarily also by convection even at the exit, ω = 1. Conduction, in radial direction, sends an estimated 15 percent of the total dissipation heat to the capillary wall when ω = 1. This happens in the region $\bar{\rho} > 0.86$. The total amount of heat conducted away to the walls can be estimated to be of the order of 7.5 percent for the total capillary length assuming as an approximation that the conduction contribution increases linearly with ω position. It is seen, at ω = 1, that a small amount of heat is conducted inwards when $\bar{\rho}$ < 0.86. The heat conducted away to the walls is a relatively small proportion of the total generated heat. The generality of the flow curves when heat conduction is absent will, therefore, expectedly transfer to the case when heat conduction is present with some slight modifications. The small amount of heat conducted away suggests also that the capillary measurements are insensitive to the degree to which the desired condition of isothermal wall is satisfied.

The flow rate at ω = 1 can be estimated under the assumption that the shear rate from the constant viscosity case is modified by $\exp(\beta \Delta T)$ where β is the temperature viscosity coefficient for an exponential viscosity dependency of the fluid temperature and

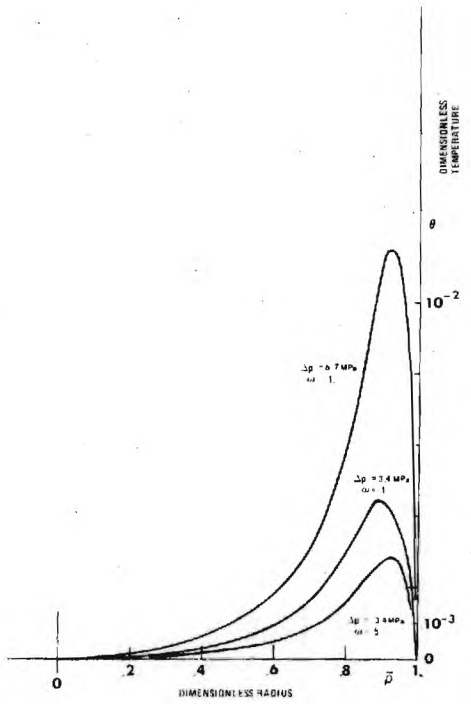

Fig. 2 Temperature distribution in a capillary tube: heat conduction present (D = 88μm, L/D = 1.35, η = 3 Pas, κ = 68 × 10^{-9} m^2/s, $C\rho$ = 1.63 MPa/K, E = 1111 K)

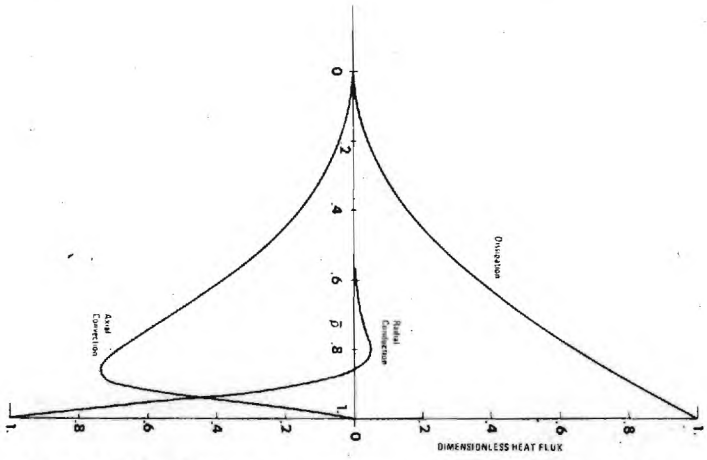

Fig. 3 Heat balance; contributions from convection, conduction and dissipation (L/D = 1.35, ω = 1, η = 3 Pas, $\kappa = 68 \times 10^{-9}$ m^2/s, $C\rho$ = 1.63 MPa/K, E = 1111 K, Δp = 6.7 MPa; quantities are nondimensionalized with respect to the dissipation at $\bar{p}$ = 1)

ΔT is the temperature increase determined previously. Expected flow curves of two model fluids synonymic with a known dimethyl siloxane and a known synthetic paraffinic oil have been determined for measurements in capillary tubes of ratios of length and dia of 14.9 and 1.35. Exponential temperature viscosity relations were assumed for both fluids with coefficients β = 0.027 for the Siloxane and β = 0.054 K^{-1} for the Synthetic Paraffinic Oil. Equal specific volumetric heats and equal exponential-power base temperatures E were assumed for the two fluids. Fig. 4 shows the expected behavior of the model fluids. The four flow curves are congruent in the range of obtained shear stress. The less temperature viscosity sensitive Siloxane shows a smaller drop in apparent viscosity than the Synthetic Paraffinic Oil at increasing, comparable shear stress. The curves from the shorter length capillary tube are located at higher shear stress than the curves from the longer capillary tubes. The gain in obtained shear stress with the use of the short capillary tube is less than expected from the length and diameter ratios of the capillary tubes. It might be speculated that the relatively better performance of the longer capillary tube can be ascribed to better cooling conditions.

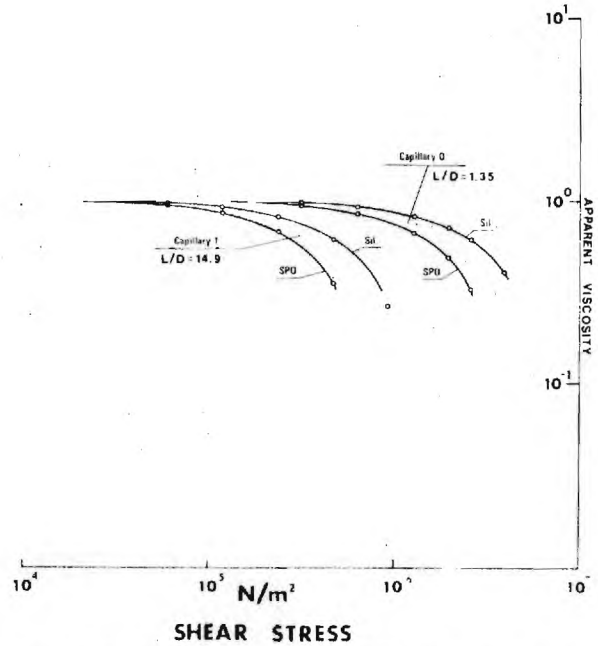

Fig. 4 Calculated flow curves for the model fluids (SPO = synthetic paraffinic oil, S = dimethylsiloxane, apparent viscosity normalized with respect to the low shear viscosities)

Pressure Drop for the Inlet and Exit Flow

The pressure drop associated with highly viscous laminar flow, $R_e \simeq 0$, from a semi-infinite reservoir to a cylindrical capillary, to a circular hole in a flat wall, can be expected to depend only on viscosity η, volumetric flow rate q and diameter D of the entrance. The pressure drop will, analogous with Poiseuille flow, $\Delta p = 128Lq\eta/\pi D^4$, be proportional with the viscosity and with the flow rate. Dimensional considerations lead to the expression.

$$\Delta p_t = \text{const } q\eta/D^3 \tag{12}$$

The investigations of Sampson, 1891 [18], Roscoe, 1949 [19], and Happel and Brenner, 1965 [20] gave this expression and the value 12 for the constant. Wurst, 1954 [21] estimated the constant to be slightly lower possibly due to the displacement of a numerical factor. The analyses are the solution approach for the differential equation of the stream function ψ, in oblate spheroidal coordinates. The boundary conditions are zero tangential fluid velocity at the wall and volume flow equal to -2π times the stream function at the wall. The stream function at the axis of rotational symmetry is zero. The solution, in terms of stream surfaces, is presupposed to be confocal hyperboloids of one sheet. The velocity distribution at great distance from the hole is similar to the velocity distribution for a point sink in the plane wall. The velocities over the inlet area of the hole are circularly distributed, proportional with $\sqrt{1 - \bar{r}^2}$. The pressure along the axis of rotational symmetry is a monotonically decreasing function with inflection point at the origin of the coordinate system. The pressure along the boundary wall is a steady increasing function with infinite slope at the edge of the hole. The edge is a singularity. The assumption of very small inertia terms compared with the viscous terms of the Navier-Stokes equations are thus not fulfilled in a certain small neighborhood of the edge, although the Reynolds number for the total flow is low.

Experimental verification in some respects of the expression (12) are given by Bond, 1921 [22], and 1922 [23]. A verification can also be deduced from the experimental work reported by Johansen, 1930 [24]. The measured values of the constant are near the analytic value 12. The determination by (24) of the value of the constant appears to be most nearly the analytic value although the orifice was bevelled at 45 deg which gave divergent flow. Proportionality between pressure drop and volumetric flow rate was found in both workers reports when Reynolds number for the total flow situation was below about 3.

Discussion

The inlet pressure drop, equation (12), the pressure drop from the Poiseuille flow in the capillary tube and the exit pressure drop amount to the total change of pressure measured in a capillary tube viscometric experiment. The inlet and exit flow have identical stream surfaces. The pressure drops are therefore of the same size. Their sum, $\Delta p_{te} = 24q\eta/D^3$, is equivalent to the pressure drop over a capillary tube of length

$$L_e = (24\pi/128)D = \frac{3\pi}{16}D \simeq 0.59D \qquad (13)$$

in Poiseuille flow, which can be seen by comparison of equation (12) with the expression for pressure drop of viscous flow in a tube. The expression (13) is the theoretical, total end correction to the length of a flat ended capillary tube viscometer in Newtonian flow.

The velocity distribution and pressure drop for inlet-exit flow and conical diffusor flow follow the same general expressions in the appropriate coordinate systems as those of Poiseuille flow in the cylindrical system. The heat generation will therefore have approximately the same effect on the flow curves from short length capillary tubes as the effect of an extension L_e on the capillary tube length. The flow curves from an actual, physical system and from a cylindrical capillary tube will therefore appear nearly identical.

The circularly distributed velocities at the inlet resulting from the flow from an semi-infinite reservoir do not fit the parabolic velocity profile of fully developed flow in a cylinder. The concept of an inlet length must therefore still be accounted for. The conditions are less severe than the conditions of a uniform, flat, inlet velocity profile usually assumed in the literature for flow at low Reynolds number. The exit flow will presumably impress a similar velocity profile upstream of the exit. The actual average shear rate at the wall will be slightly greater than the shear rate calculated from fully developed flow. The shear stress imposed on a fluid with a known viscosity will therefore also be correspondingly greater and interpretation of measurements in terms of parabolic velocity profiles will be a lower bound for the shear stress and shear rate.

The shear stress per unit pressure drop obtainable in a short cylindrical capillary can be evaluated as a function of the ratio of diameter and length of the capillary. The total pressure drop Δp_t over the inlet, capillary and exit system is the sum of the individual pressure drop. Equations (12), (13) and the expression for pressure drop in the capillary tube, $\Delta p = 128Lq\eta/\pi D^4$, give the ratio

$$\tau/\Delta p_t = 1/(4(L/D) + (3\pi/4)) \qquad (14)$$

where $\tau = \Delta p/4(L/D)$. The obtainable shear stress is in the range of 20–40 percent of the total applied pressure drop when ratios of diameter and length greater than one is used. The traditional concept of a capillary tube seems to vanish when the diameter approaches or exceeds the length. Neither the mechanisms nor the governing equations do, however, exclude such a parameter combination. Some experimental works report furthermore the use of short tubes in capillary viscometry, Bagley, 1957 [25] and Schnurmann, 1962 [12]. The expression (14) indicates the possibility to create experimental shear loads of the order of magnitude of 10 MPa on the fluid acting with pressure drop of only few times that over the measuring arrangement.

Conclusions

The highly viscous, steady laminar flow through a short cylindrical capillary tube has been investigated. Low Reynolds number conditions were assumed. A shear stress range with the upper limit approaching the average shear stress in a sliding elastohydrodynamic film was investigated, Fig. 4. The resulting flow curves, apparent viscosity as a function of shear stress, are plotted in logarithmic presentation.

The flow curves for Newtonian fluids will show constant viscosity at sufficiently low shear stress. An apparently lower viscosity due to dissipation heating will be measured at high shear stress. The decrease in apparent viscosity increases rapidly with increasing shear stress.

It was found that the flow curves will have an identical configuration for Newtonian fluids, independent of the parameters of the problem, shear rate, viscosity level, etc. An identical flow curve configuration cannot be expected for non-Newtonian fluids.

The location of the flow curves in the logarithmic presentation depends on viscosity level, the ratio of length and diameter of the capillary, the exponential temperature viscosity coefficient, the specific volumetric heat and to a minor degree on the coefficient of heat conduction of the fluid.

The boundary condition of no heat conduction in the fluid or isothermal wall appears to be of only moderate significance for high shear stress capillary viscometry under conditions of low Reynolds numbers because convection is the primary mechanism in removal of the dissipated heat.

Approximate temperature profiles in the capillary cavity show, for isothermal wall conditions, pronounced annular peaks near the wall, and low temperatures at the axis and at the wall. The peaks tend to move inwards as the axial location increases. The peaks remain, however, for short capillary tubes in the range 1.0 – 0.9 of dimensionless radius under actual operation.

Inlet and exit corrections for pressure drop over the capillary tube have been deduced for Newtonian behavior of the fluid. Only the flow from a semi-infinite reservoir into a circular hole in a flat wall has been considered. The inlet and exit pressure drop thus determined have the functional appearance of a Poiseuille flow situation. The correction can be expressed as the length, equation (13), of an equivalent, cylindrical capillary tube with diameter D. The heating effects are of the same character as the heating effects of the flow in the capillary tube cavity and do therefore not influence the flow curves.

Determination of end corrections enables an estimate to be made of an upper limit of shear stress attainable in high pressure capillary tube viscometry. The estimate shows a shear stress limit of the order of magnitude of 10 MPa. This is near the level of average shear stress experienced in a sliding elastohydrodynamic film. High pressure, high shear viscometry can therefore be useful in lubricant rheological investigations of interest for elastohydrodynamic lubrication.

Acknowledgments

The research reported herein was supported in part by the National Science Foundation (NSF GK-31154) and by NASA (NGR-11-002-133). This assistance is greatly appreciated.

One of the authors (J.J.) wishes to acknowledge the grant of leave from the Technical University of Denmark, the Department of Machine Design. The study and research were also supported by Statens teknisk-videnskabelige Fond (1959.M-158 and 2097.M-183) Denmark and Otto Mønsteds Fond (1972 and 1973) Denmark. The support is greatly appreciated.

References

1 Pressure-Viscosity Report, Vols. I and II, a report prepared by the ASME Research Committee on Lubrication, ASME, New York, 1953.

2 Appeldoorn, J. K., Okrent, E. H., and Philippoff, W., "Viscosity and Elasticity at High Pressures and High Shear Rates," 27th Midyear Meeting, API Division of Refining, San Francisco, Calif., May 14, 1962.

3 Barlow, A. J., Harrison, G., Irving, J. B., Kim, M. G., Lamb, J., and Pursley? W. C., "The Effect of Pressure on the Viscoelastic Properties of Liquids," *Procedures of the Royal Society of London*, A 327, 1972, pp. 403-413.

4 Hersey, M. D., *Theory and Research in Lubrication*, Wiley, New York, 1966.

5 Nowak, J. D., and Winer, W. O., "Some Measurements of High Pressure Lubricant Rheology," TRANS. ASME, JOURNAL OF LUBRICATION TECHNOLOGY, Vol. 90, Series F, No 3, July 1968, pp. 580-591.

6 Novak, J. D., and Winer, W. O., "The Effect of Pressure on the Non-Newtonian Behavior of Polymer Blended Oils," TRANS. ASME,

JOURNAL OF LUBRICATION TECHNOLOGY, Vol. 91, Series F, July 1969, 459–464.

7 Winer, W. O., Sanborn, D. M., Lee, D., Jakobsen, J., Carlson, S., and Bohn, M., "Investigations of Lubricant Rheology as Applied to Elastohydrodynamic Lubrication," NASA Report No. 11-002-133, Georgia Institute of Technology, Atlanta, Ga., June 1972.

8 Winer, W. O., Sanborn, D. M., and Jakobsen, J., "Simulation of Severe Shear Conditions in Lubrication," Paper 730482, the ASTM-SAE Symposium on Viscometry and its Applications to Automotive Lubricants, Detroit, Mich., May 14–18, 1973.

9 Jakobsen, J., "Lubricant Rheology at High Shear Stress," Doctoral thesis, Georgia Institute of Technology, Sept. 1973, and University Microfilms, Ann Arbor, Mich., 1973.

10 Philippoff, W., "Über das Fliessen in Kapillaren bei extrem hohen Schubspannungen," *Physikalische Zeitschrift*, 43 Jahrgang, Nr. 19/20, 1942.

11 Fritz, W., and Hennenhöfer, J., "Strömung zäher Öle in Kapillaren bei hohen Schergeschwindigkeiten und hohen Reibungsleistungen," *Angew. Chem. B*, 19 Jahrgang, No. 5/6, 1947.

12 Schnurmann, R., "Das Verhalten von Schmiermitteln bei hohen Schergefälen," *Erdöl und Kohle, Erdgas, Petrochemie*, No. 6, 15 Jahrgang, June 1962.

13 Gerrard, J. E., and Philoppoff, W., "Viscous Heating and Capillary Flow," *4th International Congress of Rheology*, Paper 51, 1963.

14 Gerrard, J. E., Steidler, F. E., and Appeldoorn, J. K., "Viscous Heating in Capillaries: The Adiabatic Case," ACS Petroleum Division Meeting, Chicago, Ill., Sept. 1964.

15 Gerrard, J. E., Steidler, F. E., and Appeldoorn, J. K., "Viscous Heating in Capillaries: The Isothermal-Wall Case," ACS Petroleum Division Meeting, Atlantic City, N.J., Sept. 1965.

16 Brinkman, H. C., "Heat Effects in Capillary Flow I," *Applied Science Research A2*, 1951, pp. 120–124.

17 Schiller, L., "Die Entwicklung der Laminaren Geschwindigkeitsverteilung," *Zeitschrift für Angewandte Mathematik und Mechanik*, Band 2, 1922.

18 Sampson, R. A., "On the Stoke's Current Function," *Phil. Trans. Roy. Soc.*, A182, 1891, pp. 449–518.

19 Roscoe, R., "The Flow of Viscous Fluids round Plane Obstacles," *Phil. Mag.* 40, 1949, pp. 338–351.

20 Happel, J., and Brenner, H., *Low Reynolds Number Hydrodynamics with Special Applications to Particulate Media*, Prentice-Hall, Englewood Cliffs, N.J., 1965.

21 Wurst, W., "Strömung durch Schlitz- und Lochblenden bei kleinen Reynolds-Zahlen, "*Ingenieur-Archiv*, XXII Band, Sechstes (Schluss-) Heft, 1954.

22 Bond, W. N., "The Effect of Viscosity on Orifice Flows," *Proceedings of the Physicists Society* 33, 1921, 225–230.

23 Bond, W. N., "Viscosity Determination by Means of Orifices and Short Tubes," *Proc. Phys. Soc.* 34, 1922, pp. 139–144.

24 Johansen, F. C., "Flow through Pipe Orifices at Low Reynolds Numbers," *Proc. Roy. Soc.* A126, 1930, pp. 231–245.

25 Bagley, E. B., "End Corrections in the Capillary Flow of Polyethylene," *Journal of Applied Physics*, 28, No. 5, 1957, pp. 624–627.

Printed in U. S. A.

J. Jakobsen
Lecturer,
Dept. of Machine Design,
The Technical University of Denmark,
Copenhagen, Denmark. Assoc. Mem. ASME

W. O. Winer
Professor,
School of Mechanical Engineering,
Georgia Institute of Technology,
Atlanta, Ga. Mem. ASME

High Shear Stress Behavior of Some Representative Lubricants

Shear stress independent behavior was observed for representative, synthetic, nonblended lubricants to about 4.8 × 10^6 N/m² (700 psi) shear stress in high pressure viscometric measurements. This shear stress is of the same magnitude as the shear stress in sliding elastohydrodynamic contacts. It is shown that dissipation heating is the only mechanism of importance in the generation of the deviations from constant viscosity as measured with capillary tube viscometric methods. The Newtonian end corrections for the capillary tubes were found to be constant for the nonblended, liquid lubricants. Newtonian behavior will be expected of the fluids in a high shear lubrication situation. Shear induced, nonliquid behavior was found for the silicone lubricant at about 10^6 N/m² and for the polymer-blended mineral oil at about 10^4 N/m² at a relatively low pressure level. The observations might provide a key to an understanding of the generation of the anomalous low elastohydrodynamic film thickness as found with these lubricants. The polymer-blended oil showed shear thinning effects. The apparent viscosity was found to increase (~30 percent) with increasing shear stress in the range of the second Newtonian viscosity level.

Introduction

This paper reports high pressure capillary tube viscometric measurements at shear stresses to 4.8 × 10^6 N/m² (700 psi) and reports the general observation of constant viscosity of the investigated unblended lubricants in the range of measurements. The purpose of the work is to develop a capillary tube viscometric method to determine the viscous properties of lubricants under elastohydrodynamic operating conditions in a laboratory experiment where the parameters of pressure, temperature and shear stress can be independently varied and to investigate the behavior of representative lubricants. The use of a short length capillary tube has been introduced in order to achieve high shear stress. The upper limit of shear stress attainable in capillary tube viscometry has been increased approximately 50 times over previously reported values of about 10^5 N/m². The increased shear stress limit is only 3–5 times less than the average shear stress experienced by the fluid during passage of a sliding elastohydrodynamic contact.

Capillary tube viscometers have been used in fluid rheological investigations [1–7][1] in the past. Large capillary tube lengths were a general characteristic of these works. The attainable shear stress level was therefore relatively low. A new type high pressure, high shear stress capillary tube viscometer was developed and used to investigate pressure temperature shear stress relations for lubricants, Novak, 1968 [8], Novak and Winer, 1968 [9], 1969 [10] and Winer, 1972 [11]. Shorter capillary tube lengths were used. The range of the ratio of length and diameter reported was 280 to 11.6. The maximum shear stress reported, [8], is 1.04 × 10^5 N/m², (15.1 psi). The measurements [8–10] of unblended base oils did not show significant deviations from a constant viscosity curve.

Theoretical works of Bondi, 1946 [12] and Smith, 1968 [13] have predicted nonlinear, shear thinning, behavior of lubricants under high shear stress. Both works are essentially based on the molecular behavior of liquids. Bondi predicts a viscosity drop to about 0.6 times the low shear viscosity at shear stresses of 10^5 N/m² for a liquid with molecular weight of 600. Smith predicts large rates of viscosity decrease with increase of shear rate. The shear rate where viscosity changes can be observed is highly temperature sensitive. These analytical predictions are not confirmed experimentally in the shear stress, shear rate ranges attained in this work.

The High Pressure Viscometer

The measurements were carried out with a high pressure capillary tube viscometer. The design and operation of the viscometer is described in detail by Novak [8] and Novak and Winer [9]. The viscosity is measured as the ratio of pressure drop and volume flow rate at the capillary tube. Shear stress is derived from the

[1] Numbers in brackets designate References at end of paper.

Contributed by the Lubrication Division of THE AMERICAN SOCIETY OF MECHANICAL ENGINEERS for presentation at the ASME-ASLE Joint Lubrication Conference, Montreal, Canada, October 8–10, 1974. Manuscript received by the Lubrication Division, July 8, 1974. Paper No. 74-Lub-41.

Copies will be available until June, 1975.

pressure drop and shear rate is determined from measurements of the volume flow rate. The viscometer consists essentially of two high pressure sections, cylinders with variable length, which are connected with piping to the ends of the small diameter capillary tube. A hydraulic pressure intensifier (50 times) can maintain constant pressure of the sample lubricant in the test section to a level of more than 7×10^8 N/m^2. A thermostat bath controls the constancy of the temperature of the capillary tube and the piping. The viscometer is operated by concurrent, continuous and opposite volume changes of the high pressure sections which generates pressure drop and flow through the capillary tube. Pressures are measured directly with strain gauge transducers.

The viscometer has been modified so the volume flow rate is measured with a velocity transducer. The flow is measured proportional with the speed of the moving end sections of the high pressure cylinders. An analog to digital converter and a multichannel magnetic tape recorder have been added to the equipment. The transducer signals are amplified and recorded on the tape. The collected data are processed with the aid of a computer. An infinitely variable, constant velocity drive has been incorporated to move the end sections of the high pressure cylinders during operation of the viscometer. The drive unit gives good reproducibility and steady and constant operation during measurements. Manual drive—hand pull—has been used at measurements of the highest shear stresses and flow rates because the capacity of the drive was limited. Satisfactory reproducibility was obtained at these higher velocities. Two high precision bourdon pressure gauges, 275 MPa (40 kpsi) and 700 MPa (100 kpsi), have been added in order to improve accuracy of the calibration procedure. The dimensions of the capillaries used are summarized in Table 1.

Table 1 Capillary tube dimensions and materials

	Length L, mm	Diameter D, mm	L/D
Capillary tube 4 stainless steel	76.1	0.2563	297
Capillary tube 1 stainless steel	2.97	0.1994	14.9
Capillary tube 0 sapphire	0.119	0.088	1.35

Calibration of the Transducers

The pressure drop over the capillary tube is obtained as the difference between the output of two high pressure transducers, of same type, which measure the total pressure at the end connections of the capillary tube. The input of a high gain amplifier for each transducer is balanced to zero output at each measurement before flow starts in the tube in order to bias the signal from the total pressure level and thereby to obtain sufficient resolution for the measurements of the pressure drop. The magnitude of the pressure drop is small compared with the total operational range, 0–700 MPa, of the viscometer. A high degree of accuracy and reproducibility is therefore required of the transducers in order to obtain satisfactory determination of the pressure drop. The transducers were calibrated with an approach involving summation of small increments of pressure in the test section and simultaneous recording of pressure level with precision bourdon gauges. The calibration procedure was found to be correct within less than one per cent of the full range.

The calibration of the velocity transducer and amplifier was carried out as measurements of displacement and corresponding time duration. The velocity of the traversing high pressure section was maintained constant with the drive unit during the calibration. The amplifier output was sampled by the appropriate channel on the analog-to-digital recorder. A typical calibration speed was 25 μm/sec (0.001 in./sec). Time was measured between the consecutive openings of two microswitches. A bracket on the traversing section activated the switches. These switches were connected to the inputs of two dummy channels on the converter. The opening times can, therefore, easily be assessed from a computer printout. The travelled distance between activation of the switches was measured with a precision dial indicator and was typically 0.25–0.50 mm (0.01–0.02 in.). The accuracy of the indicator is guaranteed to be better than 2.5 μm (100 μin.). This was confirmed in a series of measurements performed with parallel gauge blocks. The calibration procedure for the velocity transducer and amplifier was estimated to be correct within less than one percent of the full range of calibration.

Calibration of the Capillary Tubes

Two calibration fluids were used, a viscosity standard, S-60 from Cannon Instrument Company, and a diester/201 bis-2-ethyl hexyl sebacate. The fluid S-60 was used only at low shear stress calibrations. The diester was used over the total range of shear stress. Both fluids are assumed to be Newtonian liquids in the sense that the ratio between measured shear stress and shear rate is constant. Capillary tube 4 was used as the standard capillary tube for high pressure measurements. Calibration of capillary tube 4 was carried out at atmospheric pressure with diester and checked with the S-60 fluid. The diameter of capillary tube 4 was found to be 0.2563 mm, (0.01009 in.). Later calibrations confirmed this measurement within 0.125 μm (5 μin.). These statements about the diameter of capillary tube 4 assume the physical length of the capillary to be 76.1 mm ± .025 mm (2.996 in. ± .001 in.) as measured with a micrometre screw. Therefore, the diameter 0.2563 mm contains corrections originating outside the capillary tube cavity only for Newtonian liquids. The relative accuracy of the calibration of the capillary tubes is believed to be much better than the accuracy of the transducer calibrations. The total accuracy of a viscosity measurement is therefore determined primarily by the transducer accuracy and will be of the order of one percent.

Calibration measurements at high pressures for capillary tube 4 with the diester are given in Table 2. The table also gives a comparison with data for a diester reported as sample Al in the ASME Pressure Viscosity Report of 1953 (14). Calibration temperature was 0 deg C (32 deg F). This temperature was selected because the viscosity of the calibrating fluid for the applied pressures is then about 1 Ns/m^2 (10^3 cP), well within the expected viscosity range in the elastohydrodynamic lubrication film. The selected calibration temperature is also appropriate for comparison with previous work, notably ASME, 1953 [14]. Table 2 shows that the 1973 data deviate less than ±2 percent from the 1953 data. This small magnitude of deviation can be interpreted as a verification of the estimated measurement accuracy, of one percent. These data indicate that a search for further increase of

Nomenclature

A = lubricant material parameter
D = diameter of the circular capillary tube
L = length of the capillary tube
Q = lubricant material parameter
T = temperature (absolute)
Δp = pressure drop over the capillary tube
η = dynamic viscosity (Ns/m^2)
η_1 = viscosity measured at low shear
η_2 = viscosity, second Newtonian
τ = shear stress at the wall of the capillary tube

Table 2 Low shear pressure viscosity relations (diester) at °C(32F)

		Data 1973 Capillary tube 4	ASME 1953 Sample A1	Deviation of 1973 data from ASME 1953 data
MPa	kpsi	Ns/m²	Ns/m²	percent
0	0	0.0575	0.0568	+1.2
34.5	5	0.109	0.108	+0.9
69.0	10	0.196	0.194	+1.0
137.9	20	0.546	0.547	−0.2
206.8	30	1.400	1.420	−1.4
275.8	40	3.365	3.310	+1.7

measuring accuracy will be of limited value. The accuracy seems to be satisfactory for general investigations of high pressure properties of lubricants as long as the lubricants are no more well defined. The conclusions are not impaired by such an accuracy level of the measurements.

Calibration of capillary tube 1 was carried out as a comparison of low shear stress measurements with capillary tube 4 measurements. The diester was used as calibration fluid. The pressure range was 70–275 MPa (10–40 kpsi). The calibration was carried out at 0 deg C (31.9 deg F ± 0.1 deg F). The diameter of capillary tube 1 was found to be 0.1994 mm (0.00785 in.) for a measured physical length of 2.97 mm (0.117 in.). This diameter statement includes corrections originating outside the capillary tube cavity for Newtonian fluids.

The capillary with the ratio L/D = 1.35, capillary 0, is a sapphire ring embedded in stainless steel high pressure seals. Calibration of capillary 0 was carried out as a comparison of low shear stress measurements with capillary tube 1 and capillary tube 4 measurements in the same manner as described above for capillary 1. The diameter of the sapphire capillary was determined with a high power microscope (200X and 500X) to be 0.088 mm (0.0035 in.) with an estimated accuracy of 3 percent. The comparison with capillary tubes 1 and 4 measurements indicate the effective capillary length to be 0.119 mm, (0.0047 in.) which yields the ratio L/D = 1.35. This calibration will give a correct shear stress determination according to the expression $\tau = \Delta pD/4L$.

No directional effects were found for the capillaries during the calibration measurements. Reversal of flow direction gave consistently identical results within the measurement accuracy. This observation is consistent with the symmetry of the equations and the boundary conditions for viscous, Stoke's, flow, [15].

Fluid Measurements

Five lubricants have been investigated: the diester, a 50 cs dimethyl silicone oil, a polyalkyl aromatic plus additive (DN 600 + additive), a synthetic, paraffinic oil (XRM 177 F4) and a mixture (B3J) of paraffinic, mineral oil with 11.5 percent polyalkylmethacrylate with an average molecular weight of 2×10^6. A detailed description of each fluid is found in [16].

The high shear measurements are reported as flow curves of measured, apparent viscosity plotted as a function of shear stress. The pressure level and the temperature were maintained constant during collection of data for a flow curve. The number of data points for each lubricant and parameter combination of pressure, temperature and dimensions of capillary tube was in most cases too great to give space on the diagrams for a proper graphical presentation of each point. The flow curves are therefore assessed mean values at each coordinate location and are presented as smooth, uninterrupted curves through the assembly of data points.

Diester. The calibration lubricant, diester, was investigated at moderately high shear at the temperature level of 0 deg C, (32 deg F). Fig. 1 shows the viscosity measurements. The figure illustrates the calibration comparison at low shear for the capillaries. The high shear measurements show an apparent shear thinning behavior of the diester for both capillary 0 and capillary 1. The fluid is presumably subject to dissipation heating in the capillary tube. A series of measurements with only one capillary tube cannot easily discern shear thinning effects from dissipation heating. Comparison between measurements with different L/D ratios will allow a differentiation of these effects. The flow curves of Fig. 1 show at each pressure level consistently lower viscosity values for capillary tube 1 in the overlap zone of shear stress ranges of the capillary tubes 1 and 0. This holds whatever shear stress or shear rate are used as a basis of comparison. The decreasing viscosity values of capillary 1 measurements are found where the fluid exhibits Newtonian behavior as measured with capillary 0. The diester behaves, therefore, as a Newtonian liquid to at least 10^5 N/m², Fig. 1. Shear thinning effects cannot explain the high shear viscosity decrease measured with capillary tube 1. The configuration and the location of the flow curves from capillary tube 1 are consistent with the dissipation heating effects described in

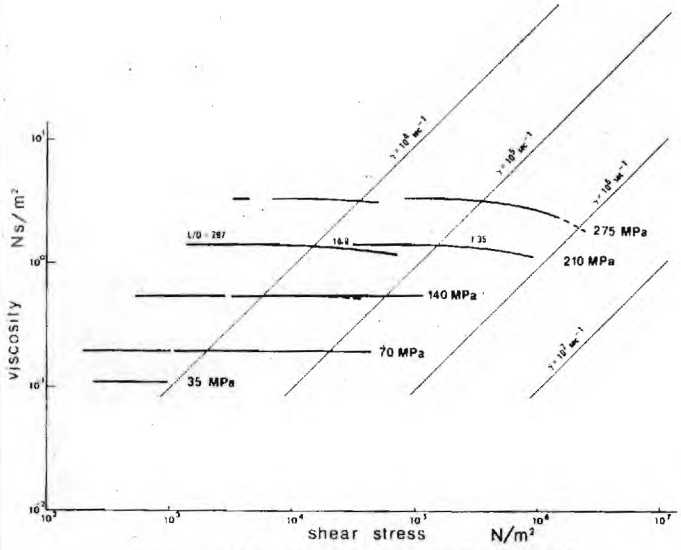

Fig. 1 Flow Curves for Diester, Calibration, T = 0°C

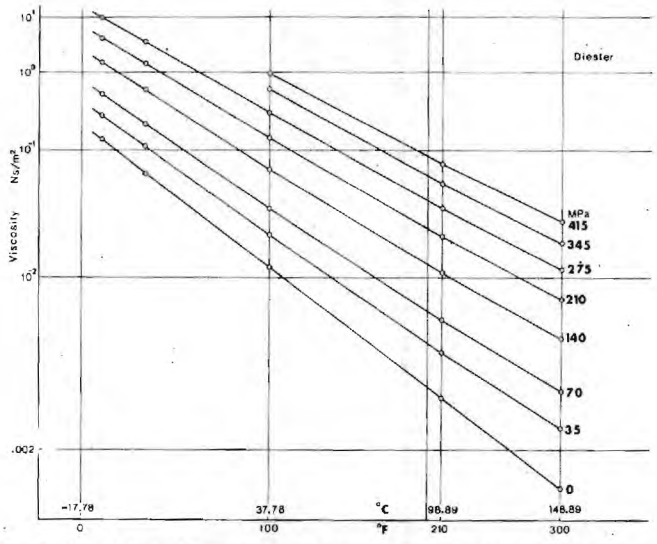

Fig. 2 Low SXHEER Temperature Pressure Viscosity Relations for Diester

[15]. The deviation of the flow curves from constant viscosity can therefore be assumed to depend on dissipation heating effects alone. The diester thus has shear independent properties up to 2 $\times 10^6$ N/m^2, (about 300 psi) shear stress.

The calibration lubricant was investigated also at higher shear loads. Greater viscosity levels were obtained by applying a low temperature of −12.2 deg C (10 deg F) and maintaining the pressure levels at 70–140–210–275 MPa, (10–20–30–40 kpsi). The flow curves at −12.2 deg C were found to be congruent with the curves at 0 deg C. The fluid can therefore be assumed to have Newtonian properties to the maximum applied shear stress, 3 $\times 10^6$ N/m^2, (435 psi).

Measurements with the standard high pressure capillary tube 4 were not performed at −12.2 deg C because the limiting low shear viscosities obtained with both capillary 0 and capillary 1 showed consistency with previously obtained low shear data for diester when interpreted through mapping as straight line temperature viscosity characteristics on rectifying diagrams, of the type of ASTM D 341-43. The calibration performed at 0 deg C, (32 deg F), is thus confirmed and the criteria of constant end correction for Newtonian liquids, proposed in [15], is satisfied.

Fig. 2 shows a summary of the low shear measurements of the diester over the temperature range covered. The rectifying diagrammatic presentation of Fig. 2 is essentially that of the ASTM Standard Temperature Viscosity Charts (D 341-43). The generating formula for the charts can be written as $\ln\ln(\nu + c_0) = \ln A - Q\ln T$, where ν is the kinematic viscosity, centiStoke, at the absolute temperature T and c_0, A and Q are constants. The usefulness of these rectifying charts is based on the observation that mineral oils plot as straight lines, presumably, however, only at atmospheric pressure. Hersey [17] states that fair results can be obtained by plotting the values of dynamic viscosity directly using the scale of kinematic viscosity. Fig. 2 is generated with such a simplified plotting method. The error that arises from the simplified method is not significant for use in elastohydrodynamic investigations. The density varies at most from about 900 kg/m^3 to 1100 kg/m^3, (0.9 g/cm^3 to 1.1 g/cm^3), (14) in the pressure and temperature ranges of interest. This is a change in density of ±10 percent, but the relative error, deviations from straight line characteristic, is smaller. The constant c_0 (0.6 cS) can be discarded for the use at elastohydrodynamic viscosity levels >1 Ns/m^2. The generating formula can therefore be regarded as having the form: $\ln\ln\eta = \ln A - Q\ln T$ which conveniently is a formula with two constants. The constant A stands for some defined base viscosity. The constant Q expresses the change of viscosity with temperature such that a large Q value represents great changes in viscosity for a given temperature change.

Fig. 2 shows that the diester has straight line characteristics in the rectifying diagram for viscosities above 0.1 Ns/m^2 (100 cP). It is also seen that the characteristics are straight for the ranges 0–275 MPa, (0–40 kpsi), and −12.2 deg C to 37.8 deg C, (10 deg F to 100 deg F), as well as for atmospheric pressure and −12.2 deg C to 148.9 deg C, (10 deg F to 300 deg F). There is a minor curvature at all reported pressure levels above atmospheric pressure and above 37.8 deg C, (100 deg F), when the viscosity is less than 0.1 Ns/m^2, (100 cP).

Dimethyl Siloxane (DC-200-50). One outstanding property of silicone oil is the relatively small decrease of viscosity with increasing temperature. The Q-exponent is in the range of 2–4 times less than the exponent for diester. The flow curves for siloxane will therefore be expected to show considerably less deviation from the constant viscosity characteristic than the diester flow curve at the same shear stress. This expectation was confirmed by the measurements.

High shear stress measurements of the siloxane fluid were carried out at 23.9 deg C, (75 deg F). The results are shown in Fig. 3. The flow curves for capillary tube 1 measurements deviate downward from the constant level curves of capillary 0 in the shear range covered by both capillaries. This shows that shear thinning, if it exists, are not present for dimethyl siloxane at stresses to at least 4 $\times 10^5$ N/m^2, (~57 psi). This is particularly well illustrated by the flow curves at 210 MPa, (30 kpsi), where the overlap zone is more than a decade wide, 10^4–10^5 N/m^2. The flow curves for both capillaries are of congruent form. This shows that dissipation heating is the cause of the devitions from constant viscosity, as was the case for the diester, and suggests further that the range where shear thinning effects are absent extends to the highest stress reported in Fig. 3, which is 4 $\times 10^6$ N/m^2, (~570 psi). End corrections are constant.

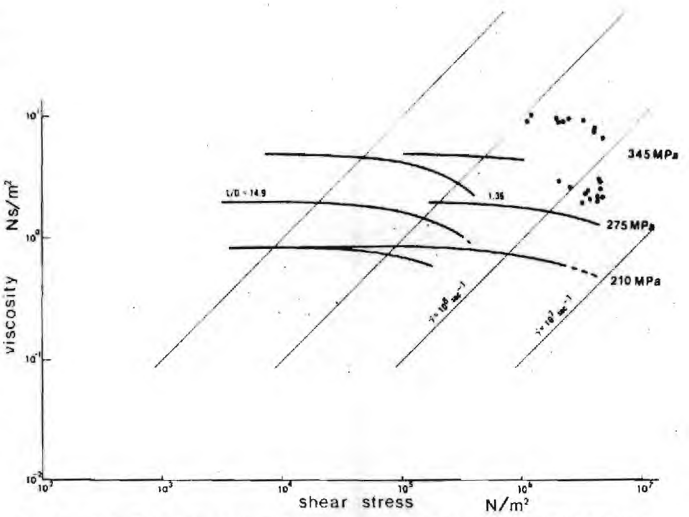

Fig. 3 High Shear Measurements of Dimethyl Siloxane DC-200-50, T = 4C 27C. Measurements with Partially Blocked Capillary Tube are Included.

Partial blockage of the capillary 0 occurred occasionally during the high shear experiments: The resulting data points showed apparent viscosities significantly higher than would be expected for liquid behavior, Fig. 3. The plotted results are grouped in the flow curve diagrams in an apparently meaningless pattern. The higher values of the viscosities and the scattered grouping of the data points possibly indicate partial solidification of the lubricant. Nonliquid behavior was observed above approximately 2 $\times 10^6$ N/m^2, (~285 psi), at 275 MPa, (40 kpsi), and above 10^6 N/m^2 at 345 MPa, (50 kpsi). Complete blockage was observed at 415 MPa,

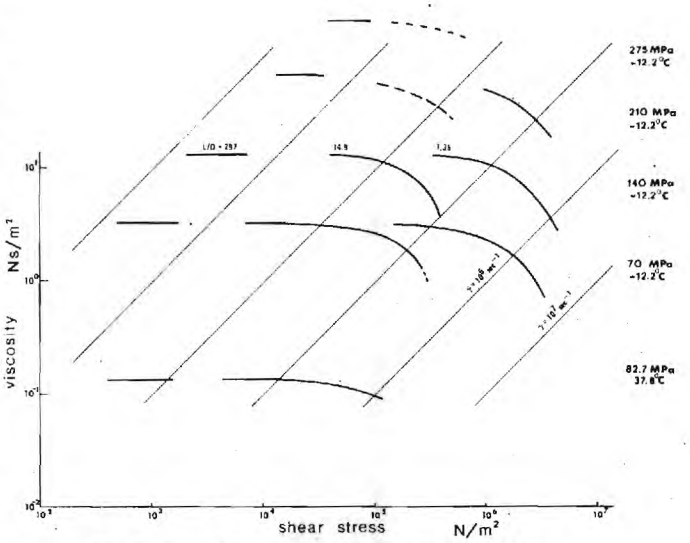

Fig. 4 Flow Curves for Polyalkyl Aromatic + Additive

Table 3 Viscosities at atmospheric pressure paraffinic mineral oil with 11.5 percent polyalkylmethacrylate $MW = 2 \times 10^6$

	η_1 Capillary no. 400 $\simeq 6$ N/m²	η_2 Capillary tubes 4 and $1.10^3 - 10^4$ N/m²
23.89°C (75°F)	—	1.000 Ns/m²
37.78°C (100°F)	1.010 Ns/m²	0.420 Ns/m²
65.56°C (150°F)	0.384 Ns/m²	0.155 Ns/m²
87.78°C (190°F)	0.221 Ns/m²	0.100 Ns/m²

(60 kpsi). The effect appears to be shear induced. The capillary was inspected in a microscope after such experiments. No damage was ever found. The capillary maintained its calibration.

Polyalkyl Aromatic + Additive (DN 600 + Additive). High shear measurements of the synthetic lubricant DN 600 plus an antiwear additive are found in Fig. 4. The flow curves show constant apparent viscosity up to at least 3×10^5 N/m² (~44 psi). The congruent form of the flow curves suggests that Newtonian behavior persists up to the maximum employed stress of 4.2×10^6 N/m², (~610 psi). The limiting low shear viscosity measurements with both capillary 0 and 1 show consistency with viscosities extrapolated from low shear data obtained with the standard high pressure capillary tube 4. The end corrections for capillaries 0 and 1 are thus constant for this fluid.

Nonliquid behavior was possibly encountered at 210 MPa, (30 kpsi), and certainly at 275 MPa, (40 kpsi). Previous measurements of DN 600 + Additive were carried out up to 165 Ns/m². Conditions were 700 MPa, (100 kpsi), and 37.8 deg C, (100 deg F). Non-liquid behavior was not experienced, presumably due to the higher temperature. The scatter at 210 MPa, (30 kpsi), and 275 MPa, (40 kpsi), may be explained as a partial solidification caused by low temperature and high pressure but not necessarily due to high shear stress.

Synthetic Paraffinic Oil XRM 177 F4. The fluid XRM 177 F4 is a synthetic hydrocarbon lubricant with a base viscosity approximately ten times the base viscosities of the investigated dimethyl siloxane and the polyalkyl aromatic + additive. The XRM 177 F4 fluid is also blended with an anti-wear additive. Low shear pressure temperature viscosity characteristics were found to be nearly straight lines in the rectifying diagrams of Roelands, 1966, [18]. Low shear measurements of the XRM fluids did not show significant influence from the antiwear additive, [16]. High shear measurements were carried out for the XRM 177 F4 only. Fig. 5 shows the high shear measurements. The flow curves are of identical configuration for this fluid also. The limiting low shear measurements are consistent with the Newtonian end corrections for the capillaries 0 and 1. The highest shear stress measured was 4.78×10^6 N/m², (695 psi). Some of the flow curves for a capillary cover more than two decades of shear stress. The parts of the curves with constant viscosity are particularly far extended into the low shear region and show the good agreement with measured low shear data. The overlap zone is more than a decade wide. The heating effects of the curves of capillary tube 1 is distinctly seen.

The characteristic for the lubricant in an elastohydrodynamic contact is also shown in the figure. The vertical line is the estimated working conditions for the lubricant at a load of 66.7 N, (15 lbf), at 1.39 m/s, (54.8 in./s), sliding speed in a steel ball and sapphire disk contact. The figure shows clearly that capillary tube viscometry is not far from the situation where elastohydrodynamic conditions for a lubricant can be created in a laboratory experiment in which the parameters of interest can be varied independently of each other.

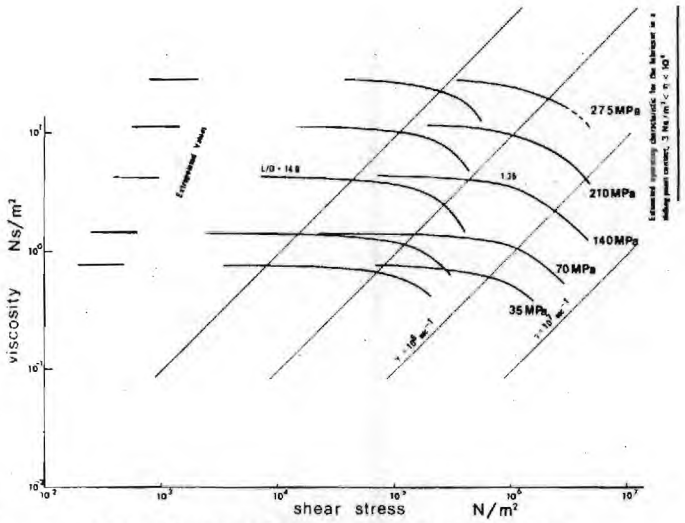

Fig. 5 High Shear Measurements of XRM 177 F4, 38C

B3J: Paraffinic Mineral Oil with 11.5 Percent Polyalkylmethacrylate. Polymer blended lubricants have long been used extensively in various engineering fields particularly in the automotive industry. High shear stress investigations of a polymer blended lubricant are therefore of interest. It was decided to select a high molecular weight polymer in a relatively high concentration with a straight paraffinic mineral base oil for such an investigation. The base oil as well as blends with a lower molecular weight polymer ($MW \sim .56 \times 10^6$) have been investigated before (8-10), however, only to about 10^5 N/m². The base oil was found to have completely Newtonian characteristics in the range investigated. The blends showed liquid response and some shear thinning effects.

The same base oil (R-620-12) was selected in this investigation. A polymer with considerably greater molecular weight (MW ~ 2×10^6) than used before, was used in order to produce extreme properties of the blend. The polymer was blended in a high concentration of 11.5 percent with the mineral base oil. High shear measurements with the throughly mixed blend were carried out with all three capillaries at 37.8 deg C and 35, 70 and 140 MPa, (100 deg F and 5, 10 and 20 kpsi). Meaningful measurements could not be carried out at higher pressures than 140 MPa, (20 kpsi). Fig. 6 shows the measurements, 35-140 MPa, (5-20 kpsi). It is seen from the figure that nonliquid response sets in for a relatively low magnitude of shear stress of about 3×10^4 N/m² (~4 psi) and continues to the highest stress ~3.5×10^6 N/m². A pronounced directional effect is found for capillary tube 1 measurements at 140 MPa. End corrections are not constant which further underlines the Non-Newtonian properties of the lubricant. Apparent viscosities differ by a factor 2-3 for capillary 0 measurements at 70 MPa for the same shear stress or the same shear rate. (The 70 MPa series from 2×10^5 N/m² to 10^6 N/m² was produced with the constant velocity drive unit. The 70 MPa data from 7×10^5 N/m² to 3×10^6 N/m² were produced manually.) A pronounced viscosity increase (~30 percent) occurs for increasing shear stresses before apparent nonliquid response sets in. Such viscosity increase as well as the non-liquid behavior were not observed in previous measurements [8-10] in the same shear stress range. The concentration of polymer and the molecular weight were, however, significantly lower.

The fluid, B3J, shows the expected shear thinning behavior when the material is in liquid state. The data from capillary tube 4 measurements may be regarded as second Newtonian viscosities. Table 3 gives atmospheric viscosities η_2 extrapolated from

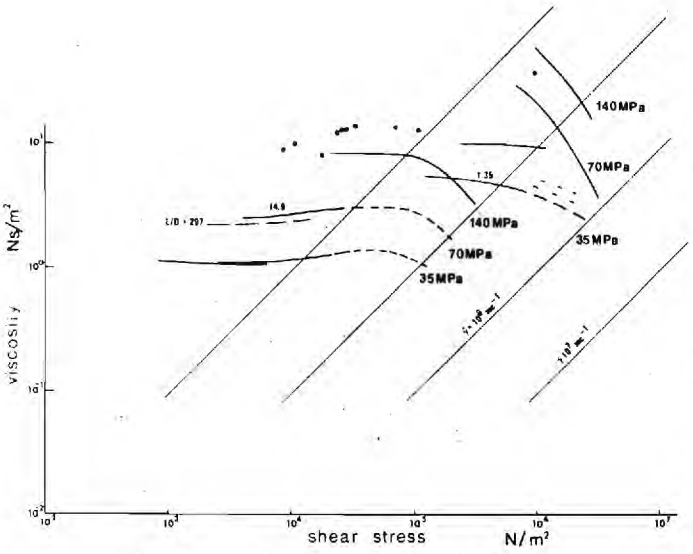

Fig. 6 High Shear Measurements of Fluid B3J

capillary tube 4 and 1 data of the second Newtonian range, 10^3–10^4 N/m². Table 3 gives also atmospheric viscosities η_1 measured with a glass capillary tube viscometer at estimated shear stress of 6 N/m². The ratio η_1/η_2 is found to be approximately 2.5. The second Newtonian viscosity η_2 never approaches the viscosity, η_b, of the base oil. The ratio η_2/η_b is of the order of 10. It is significant that non-liquid behavior appears at stresses which are 10^3 times smaller than the average shear stress in a moderately loaded elastohydrodynamic point or line contact. The shear stresses where transition to nonliquid behavior appears for the lubricant B3J are found far out in the inlet zone of an elastohydrodynamic contact. The pressures are low and the temperatures are very nearly equal to ambient temperature at this location. The experimental situation reported in Fig. 6 can thus be regarded as representative of the initial conditions of the inlet zone. The low shear transition to nonliquid behavior at great film thickness far out in the inlet zone can be expected to influence the creation of sufficient centerline film thickness significantly.

Summary and Discussion

Newtonian Behavior. The reported flow curves of the four unblended lubricants have been shown to be congruent with one general standard flow curve regardless of the fluid type and the dimensions of the capillaries 1 or 0, in all cases where liquid behavior was displayed. Deviations from the master curve are of the same magnitude as the experimental error. This observation of generality indicates that dissipation heating is responsible for the character of the flow curves thus eliminating the possibility of shear thinning properties of the lubricants in the range of investigated parameters. The standard flow curve configuration, determined experimentally, has been found to be congruent also with the general form of flow curves determined [15] in a simplified analytic approach which assumed Newtonian properties of the lubricant and flow curve configuration formed by heating alone. The congruity between experimentally and analytically determined flow curve shapes supports the presumption of Newtonian behavior of the lubricants. The established agreement of the Newtonian end correction for the three lubricants with the calibrated low shear end correction for the diester supports further the presumption that all four lubricants have Newtonian high shear characteristics in the range of investigation [15].

The flow curves are plotted with viscosity as a function of shear stress in a logarithmic presentation. Presentation of apparent viscosities plotted as a function of shear rate, as found often in the literature, was not used because this can make the distinction between heating effects and non-Newtonian effects difficult and may lead to incorrect evaluation of measurements of fluid properties.

Shear Induced Nonliquid Behavior. Silicone oils and polymer blended oils do not readily generate elastohydrodynamic film thicknesses as large as predicted by existing theory. The shear induced nonliquid behavior of these lubricants, at conditions which are found relatively far out in the inlet region, may possibly explain the difference.

Shear Thinning of the Polymer Blended Mineral Oil. The fluid consisting of a blend of polymer and mineral oil shows pronounced non-Newtonian behavior. A shear thinning effect reduces the viscosity approximately 2.5 times when the shear stress increases from about 6 N/m² to 10^3 N/m². The two viscosity levels can be characterized as the first and the second Newtonian viscosity levels respectively. The reduction in viscosity is nearly constant in the investigated temperature range 23.9 deg C–87.8 deg C, (75 deg F–190 deg F).

Observations of Time Independent Lubricant Behavior. The average residence time for the fluid in a capillary tube was in a typical series of measurements in the range from about 4 μsec to about 10^5 μsec. The relaxation time for a lubricant with a viscosity of 1 Ns/m² is of the order of 3×10^{-3} μsec to 3×10^{-2} μsec, respectively, [19]. The relaxation time at this viscosity level is thus 10^2 to 10^3 times smaller than the lowest residence time. Time dependent phenomena in the fluid behavior cannot, therefore, be expected to appear with any significance. The consistency of the measured flow curves with one common flow curve configuration irrespective of viscosity level, fluid type or capillary tubes confirms this.

Conclusions

The unblended hydrocarbon lubricants display Newtonian behavior up to a shear stress of about 4.8×10^6 N/m², (700 psi). This load is only a factor of 3–5 below the average shear stress which is experienced by the lubricant during passage of the high pressure zone of an elastohydrodynamic contact. High shear stress capillary tube viscometry is thus not far from the elastohydrodynamic conditions.

Dimethyl siloxane shows shear induced nonliquid behavior at relatively high shear stress levels. The lubricant shows Newtonian properties when liquid behavior is displayed.

The polymer blended lubricant shows distinct non-Newtonian properties at low shear, below a stress of 10^4 N/m², and shear induced nonliquid behavior at loads above this limit.

The nonliquid behavior of the lubricants is possibly of importance for the ability to create a sufficient centerline film thickness in elastohydrodynamic contacts.

No significant time dependent effects, for times >4 μsec, were observed in the high shear measurements when the lubricants under investigation showed liquid behavior.

Acknowledgments

The research was supported in part by the National Science Foundation (NSF GK-31154) and by NASA (NGR-11-002-133). The help is greatly appreciated.

One of the authors (JJ) wishes to acknowledge the grant of leave from the Technical University of Denmark, the Department of Machine Design. The study and research were also supported by Statens tekniskvidenskabelige Fond (1959.M-158 and 2097.M-183) Denmark and Otto Mønsteds Fond (1972 and 1973) Denmark. The support is greatly appreciated.

References

1 Hersey, M. D., and Snyder, G. H. S., "High-Pressure Capillary Flow," *Journal of Rheology*, Vol. 3, No. 3, 1932.

2 Hersey, M. D., and Zimmer, J. C., "Heat Effects in Capillary Flow at High Rates of Shear," *Journal of Applied Physics*, Vol. 8, May 1937.

3 Norton, A. E., Knott, M. J., and Muenger, J. R., "Flow Properties of Lubricants under High Pressure," TRANS. ASME, Vol. 63, No. 7, 1941.

4 Fritz, W., and Hennenhöfer, J., "Strömung zäher Öle in Kapillaren

bei hohen Schergeschwindigkeiten und hohen Reibungsleistungen," *Angew. Chem. B.*, 19 Jahrg., No: 5/6, 1947.

5 Gerrard, J. E., and Philippoff, W., "Viscous Heating and Capillary Flow," 4th International Congress of Rheology, 1963, Paper 51.

6 Gerrard, J. E., Steidler, F. E., and Appeldoorn, J. K., "Viscous Heating in Capillaries: The Adiabatic Case," ACS Petroleum Division Meeting, Chicago, Ill., Sept. 1964.

7 Gerrard, J. E., Steidler, F. E., and Appledoorn, J. K., "Viscous Heating in Capillaries: The Isothermal Wall Case," ACS Petroleum Division Meeting, Atlantic City, N. J., Sept. 1965.

8 Novak, J. D., "An Experimental Investigation of the Combined Effects of Pressure, Temperature and Shear Stress Upon Viscosity," Doctoral thesis, University of Michigan, Ann Arbor, Mich., 1968.

9 Novak, J. D., and Winer, W. O., "Some Measurements of High Pressure Lubricant Rheology," TRANS. ASME, JOURNAL OF LUBRICATION TECHNOLOGY, Vol. 90, Series F, No. 3, July 1968, pp. 580–591.

10 Novak, J. D., and Winer, W. O., "The Effect of Pressure on the Non-Newtonian Behavior of Polymer Blended Oils," TRANS. ASME, JOURNAL OF LUBRICATION TECHNOLOGY, Vol. 91, Series F, July 1969, pp. 459–464.

11 Winer, W. O., "A Viscometer for High Pressure Use, and Some Results," TRANS. ASME, *Journal of Basic Engineering*, Vol. 94, Series D, Sept. 1972, pp. 586–588.

12 Bondi, A., "Flow Orientation in Isotropic Fluids," *Journal of Applied Physics*, Vol. 16, Sept. 1945.

13 Smith, F. W., "Some Aspects of Nonlinear Behavior in Lubricants under Extreme Stress," TRANS. ASME, JOURNAL OF LUBRICATION TECHNOLOGY, Vol. 90, Series F, July 1968, pp. 549–552.

14 Pressure-Viscosity Report, Vol. I, II, a report prepared by the ASME Research Committee on Lubrication, ASME, N. Y., 1953.

15 Jakobsen, J., and Winer, W. O., "Dissipative Heating Effects and End Corrections for Viscous Newtonian Flow in High Shear Capillary Tube Viscometry," ASME-ASLE Lubrication Conference, Montreal, Canada, October 8–10, 1974.

16 Jakobsen, J., "Lubricant Rheology at High Shear Stress," Doctoral thesis, Georgia Institute of Technology, Sept. 1973, and University Microfilms, Ann Arbor, Mich., 1973.

17 Hersey, M. D., *Theory and Research in Lubrication*, Wiley, New York, 1966.

18 Roelands, C. J. A., "Correlational Aspects of the Viscosity-Temperature-Pressure Relationship of Lubricating Oils," Doctorate of Engineering dissertation, Delft, 1966, and University Microfilm, OP Books, Ann Arbor, Mich., 1969.

19 Lamb, J., "Physical Properties of Fluid Lubricants: Rheological and Viscoelastic Behaviour," Paper 18, *Proceedings of the Institution of Mechanical Engineers*, 1967–68, 182, Pt. 3A, p. 293.

Printed in U. S. A.

74-Lub-15

an ASME publication

Stephen F. Carlson
Graduate Student.

Ward O. Winer
Professor.

Georgia Institute of Technology,
School of Mechanical Engineering
Atlanta, Ga.

The Viscous Lubrication of Rolling and Sliding Rigid Cylinders

The general viscous lubrication of rolling and sliding rigid cylinders is examined. The flow is assumed isothermal and the fluid rheology is assumed completely defined by its compressibility as a function of pressure and by its viscosity as a function of pressure and shear stress. A general problem formulation and a general solution technique are developed. The solution technique is based on the iterative solution of a discrete representation of the problem formulation. These results are specialized for a viscosity function of the form

$$\mu = \mu_0 e^{\beta p}(1 + a^2(k\tau)^2)\ (1 + (k\tau)^2)^{-1}$$

Typical solutions are obtained and discussed. A dimensionless survey of design parameters is presented for the above viscosity function with (a) = 0.0. The use of such nonlinear general viscous fluids results in a significant loss of load capacity.

Introduction

The viscous lubrication of rolling and sliding rigid cylinders is a well-known and classical application of fluid mechanics to machine design. The basic theory of viscous lubrication was developed by Reynolds [1][1] and Sommerfeld [2] in the late nineteenth century. The first solutions for rolling and sliding cylinders were obtained almost simultaneously in 1916 by Guembel [3] and Martin [4] for different boundary conditions. The cavitation condition used by Martin has since become standard. A thorough review of the problem was made by Peppler [5] in 1938 and his careful experimental investigations were in good agreement with the theory of linear viscous fluids. The pressure dependence of the viscosity function was treated by Gatcombe [6] in 1945, and in different forms by Cameron [7] and by McEwen [8]. A second review of the problem was made by Peppler [9] in 1957 and various effects such as the viscosity-temperature dependence, the viscosity-shear stress dependence and the viscosity-time dependence were proposed for consideration.

The general viscous lubrication of rolling and sliding rigid cylinders has subsequently, been treated in a piecemeal fashion. Only special cases, namely pure rolling, and special viscosity functions have been considered, and both the problem formulation and solution technique have proceded in an *ad hoc* manner. This is true of the work of Milne [10], of Tanner [11], of Bell [12] and of Dyson [13]. This is also true of the more recent work of Brazinsky [14] and of Reher [15]. The special treatment is occasionally justified, but it is not compelling. It is possible to unify and extend and improve these results. As is shown in the forthcoming, it is possible to develop a uniform problem formulation for general viscous fluids. A uniform solution technique is also developed which is applicable over a wide range of parameters. This problem formulation and solution technique are applied to several special viscosity functions of interest. Numerical results are obtained and discussed.

Fluid Rheology

The fluid rheology is determined by a scalar relationship among the thermodynamic variables and by a tensor relationship between the kinematic and dynamic variables. For the flow situation existing in the general viscous lubrication of rolling and sliding rigid cylinders, these relationships are considerably simplified. The system operation minimizes the normal stress terms of the dynamic equations much as it minimizes the inertial terms [12, 16]. Hence, these terms need not be specified in a first order analysis. The flow is also isothermal to a good approximation, if the slip is not excessive. Thus, the fluid rheology can be represented by a nonlinear compressibility function of pressure alone relating the pressure and density and by a nonlinear scalar viscosity function of pressure and the xy component of deformation rate alone relating the xy components of deformation rate and stress. This viscosity function is most conveniently considered as a function of the xy component of the stress. Fluids whose rheology is so defined for this flow situation will be referred to as general viscous fluids.

[1] Numbers in brackets designate References at end of paper.

Contributed by the Lubrication Division of THE AMERICAN SOCIETY OF MECHANICAL ENGINEERS for presentation at the ASME-ASLE Joint Lubrication Conference, Montreal, Canada, October 8-10, 1974. Manuscript received by Lubrication Division, July 18, 1974. Paper No. 74-Lub-15.

Copies will be available until June, 1975.

Discussion on this paper will be accepted at ASME Headquarters until November 11, 1974

Let (ρ) be the fluid density and let (μ) be the fluid viscosity. Let (p) be the local pressure and let (τ) be the local xy stress component. Then the density and viscosity functions of the fluid are expressible in the form

$$\rho = \rho_0(1 + \hat{\rho})^{-1} \tag{1}$$

$$\mu = \mu_0 e^{\beta p}(1 + \hat{\mu})^{-1} \tag{2}$$

where (ρ_0) and (μ_0) are the base density and base viscosity, respectively, (β) is the ln-viscosity-pressure coefficient, and $(\hat{\rho})$ and $(\hat{\mu})$ are the density and viscosity deviation functions. It is assumed that $(\hat{\rho})$ is a function of (p) only and that $(\hat{\mu})$ is a function of (τ) only. Adherence of the fluid to the boundaries is also assumed. This specification is quite general and includes all the previous specifications of fluid rheology applied to the viscous lubrication of rolling and sliding cylinders.

The forms of $(\hat{\rho})$ and $(\hat{\mu})$ are not obtainable *a priori* and must be experimentally determined. Typical observations are of the form shown in Fig. (1) and (2). These curves are well-fitted by assigning the following forms to (ρ) and (μ)

$$\hat{\rho} = ep(1 + fp)^{-1} \tag{3}$$

$$\hat{\mu} = (1 - a^2)|k\tau|^m(1 + a^2|k\tau|^m)^{-1} \tag{4}$$

and adjusting the parameters *(e), (f), (a), (k)* and *(m)*. These parameters are all readily interpretable. *(e)* and *(f)* are reciprocal characteristic pressures. *(e)* is a measure of the initial slope of $(\hat{\rho})$ while *(e/f)* is a measure of the ultimate change in $(\hat{\rho})$. *(k)* is a reciprocal characteristic shear stress and is a measure of the initiation of change in $(\hat{\mu})$. *(a)* is a dimensionless constant and is a measure of the ultimate change in $(\hat{\mu})$. The exponent *(m)* is a measure of the maximum rate of change of $(\hat{\mu})$ and can be conveniently given the value 2. This choice is in accordance with *a*

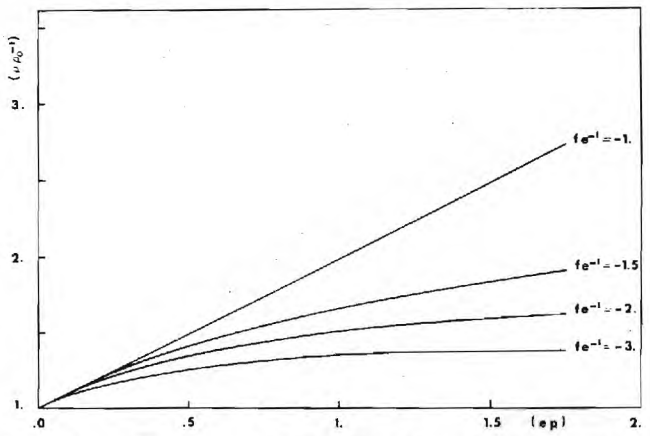

Fig. 1 Dimensionless density as a function of dimensionless pressure

Nomenclature

a = shear thinning coefficient [−]
e = first reciprocal characteristic pressure [m²/N]
f = second reciprocal characteristic pressure [m²/N]
$G1$ = dimensionless operations parameter [−]
$G1^*$ = maximum dimensionless operations parameter [−]
G_2 = dimensionless slip parameter [−]
G_3 = first dimensionless fluid parameter [−]
G_4 = second dimensionless fluid parameter [−]
h = local surface separation [m]
HT = dimensionless expansion parameter [−]
I_1 = first integral [N/m²]
I_2 = second integral [N/m²]
k = reciprocal characteristic shear stress [m²/N]
m = shear thinning exponent [−]
n = number of grid points [−]
p = local pressure [N/m²]
Q = mass flow rate per unit length [kg/msec]
QT = dimensionless flow rate parameter [−]
R = equivalent radius [m]
s = local shear stress on the lower surface [N/m²]
s_0 = function determining (s) for a linear viscous fluid [N/m²]
$\hat{s}$ = nonlinear function correcting (s_0) for a general viscous fluid [N/m²]
S = function determining (s) for a general viscous fluid [N/m²]
t = local product of (h) and derivative of (p) with respect to (x) [N/m²]
t_0 = function determining (t) for a linear viscous fluid [N/m²]
$\hat{t}$ = nonlinear function correcting (t_0) for general viscous fluid [N/m²]
T = function determining (t) for a general viscous fluid [N/m²]
TR = traction on the lower surface per unit length [N/m]
TRC = traction coefficient [−]
TRT = dimensionless traction parameter [−]
u = local x component of velocity [m/s]
u_1 = translational velocity of lower surface [m/s]
u_2 = translational velocity of upper surface [m/s]
U = rolling velocity [m/s]
v = local y component of velocity [m/s]
W = load capacity per unit length [N/m]
WT = dimensionless load capacity parameter [−]
x = horizontal coordinate [m]
y = vertical coordinate [m]
α = relative slip [−]
β = ln-viscosity-pressure coefficient [N/m²]
$\dot{\gamma}$ = local xy component of deformation rate [1/s]
ξ = dummy variable of integration [−]
μ = viscosity function [N·s/m²]
μ_0 = base viscosity [N·s/m²]
$\hat{\mu}$ = viscosity deviation function [−]
ρ = density function [kg/m³]
ρ_0 = base density [kg/m³]
$\hat{\rho}$ = viscosity deviation function [−]
τ = local xy component of stress [N/m²]
$(\ )_a$ = refers to quantities evaluated at the point of inlet of the fluid (for $x < x_a$, $s = 0$ and $p = 0$)
$(\ )_b$ = refers to quantities evaluated at the point of cavitation of the fluid (for $x \geq x_b$, $p = 0$)
$(\ )_c$ = refers to quantities evaluated at the point of exit of the fluid (for $x > x_c$, $s = 0$)
$(\ )_0$ = refers to quantities evaluated at the point of origin
$(\ )_s$ = refers to quantities evaluated at the point of splitting
$(\ )_{Ie}(\ )_{Je}$ = indices running from point of splitting to point of cavitation
$(\ )_{Ii}(\ )_{Ji}$ = indices running from point of inlet to point of splitting

(a) $(a^2) = 0.0$, $(k) = 0.0$ m²/N
(b) $(a^2) = 0.0$, $(k) = 0.1$ m²/N
(c) $(a^2) = 0.5$, $(k) = 0.1$ m²/N

1 $(U) = 2.54$ m/s, $(\alpha) = 0.0$
2 $(U) = 2.54$ m/s, $(\alpha) = 0.1$

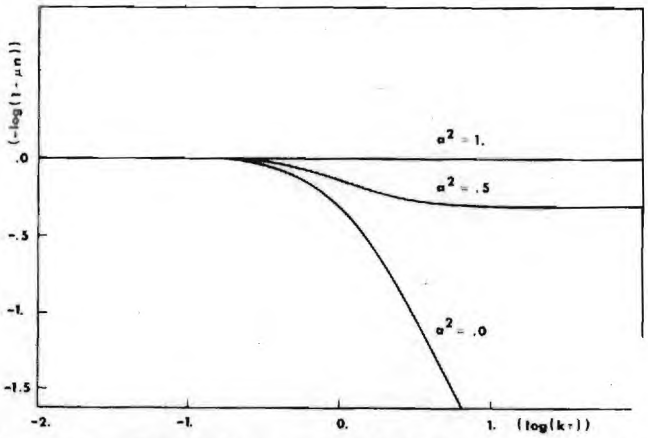

Fig. 2 Log_{10} dimensionless viscosity ($-\log(1 + \mu n)$) as a function of $\log_{10}$ dimensionless shear stress ($\log(k\tau)$)

priori considerations which require the exponent to be an even power. It is also in agreement with *a posteriori* correlations [17]. This specification results in some consequent mathematical simplification. However, these manipulations can be modified to consider other values of *(m)* if necessary.

The density deviation function is not of particular interest in this investigation since the pressure does not reach the relatively high levels at which the density deviation function becomes significant. The shear stress will, however, reach relatively high levels and several subclasses of fluids can be distinguished by their viscosity behavior at relatively high shear stress levels (i.e., $|k\tau| > 1$ in Fig 3).

(a) If *(a)* = 1.0 or if *(k)* = 0.0 m²/N, the viscosity function has the form

$$\mu = \mu_0 e^{\beta p} \tag{5}$$

and the fluid is linear. Such fluids are known as Newtonian fluids. Many fluids of simple molecular structures such as paraffinics are found in this class.

(b) If *(a)* = 0.0, but $k \neq 0.0$ m²/N, the viscosity function has the form

$$\mu = \mu_0 e^{\beta p}(1 + (k\tau)^2)^{-1} \tag{6}$$

and the fluid is nonlinear with zero ultimate viscosity. Many fluids of complex molecular structure, such as bulk polymers, are found in this class.

(c) If $(a) \neq 0.0$, $(a) \neq 1.0$ and $(k) \neq 0$ m²/N, the viscosity function has the form

$$\mu = \mu_0 e^{\beta p}(1 + a^2(k\tau)^2)(1 + (k\tau)^2)^{-1} \tag{7}$$

and the fluid is nonlinear with a nonzero ultimate viscosity. Such fluids are known as Reiner-Philippoff fluids. Many fluids of intermediate or mixed molecular structure, such as bulk polymer solutions are in this class.

Problem Formulation

The problem formulation is similar to that based on the rheology of linear viscous fluids. Emphasis is placed on the special assumptions necessary for the class of general viscous fluids defined in the foregoing. Again it should be pointed out that this term is relative to the flow situation and that the general viscous fluid may have a much more complex specification in other flow situations. The assumptions common to the linear viscous lubrication of rolling and sliding rigid cylinders [5, 9] such as steady, laminar and isothermal flow, neglect of inertial terms, and film geometry will not be discussed.

The system geometry and kinematics are shown in Fig. (3). Let *(x,y)* be a conventionally oriented system of Cartesian coordinates. Let *(R)* be the equivalent radius of the cylinders and *(h)* be the local surface separation. Let (h_0) be the centerline separation. Then the local separation is given by

$$h = h_0 + \frac{1}{2}R^{-1}x^2 \tag{8}$$

Let (x_a) be the inlet coordinate and (x_b) be the caviation coordinate of the film. Let *(u)* and *(v)* be the local velocity components of the film and $(\dot{\gamma})$ be the local xy component of the deformation rate. Let (u_1) and (u_2) be the velocities of the lower and upper surfaces, respectively.

Under the usual assumptions common to the problem formulation of the linear viscous lubrication of rolling and sliding rigid cylinder, the kinematic, and dynamic equations reduce to

$$\dot{\gamma} = \partial u/\partial y \tag{9}$$

$$\tau = \mu\dot{\gamma} \tag{10}$$

$$\partial(\rho u)/\partial x + \partial(\rho v)/\partial y = 0 \tag{11}$$

$$0 = -\partial p/\partial x + \partial\tau/\partial y \tag{12}$$

$$0 = -\partial p/\partial y \tag{13}$$

Let *(s)* be the value of (τ) on the lower surface and $(s + t)$ be the value of (τ) on the upper surface. Using the erit condition

$$\left.\frac{dp}{dx}\right|_b = 0 \tag{14}$$

these equations may be integrated to give

$$Q = \int_0^h (\rho u)dy = U\rho_0 h_b \tag{15}$$

$$\tau = s + y\frac{dp}{dx} = \mu\partial u/\partial y \tag{16}$$

where *(Q)* is the mass flow rate per unit length and *(U)* is the rolling velocity of the system and (h_b) is the film thickness at the cavitation coordinate. Let (α) be the relative slip. Then

$$U = \frac{1}{2}(u_1 + u_2) \tag{17}$$

$$\alpha = \frac{1}{3}(-u_1 + u_2)(u_1 + u_2)^{-1} \tag{18}$$

Substitution of the general density and viscosity functions given by equations (1) and (2), and subsequent integration and manipulation yields the following set of equations

$$S(s, p, t, x_b) = s - s_0 - \hat{s}(s, t) = 0 \tag{19}$$

$$T(s, p, t, x_b) = t - t_0 - \hat{t}(s, t) = 0 \tag{20}$$

$$t = h\frac{dp}{dx} \tag{21}$$

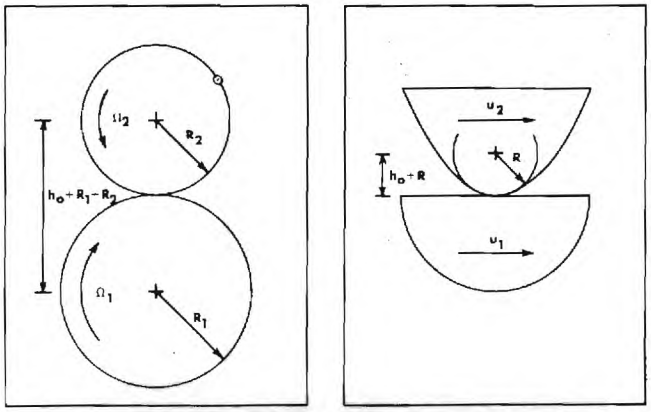

Fig. 3 System geometry and kinematics; *(a)* origlial geometry and kinematics, *(b)* equivalent geometry and kinematics

subject to the boundary conditions

$$p_a = 0 \tag{22}$$

$$p_b(x_b) = 0 \tag{23}$$

where

$$s_0 = 6U\mu_0 e^{\beta p}(-(1-\alpha)h + (1+\hat{p})h_b)h^{-2} \tag{24}$$

$$t_0 = 12U\mu_0 e^{\beta p}(h - (1+\hat{p})h_b)h^{-2} \tag{25}$$

$$\hat{s}(s,t) = -4I_1(s,t) - 6I_2(s,t) \tag{26}$$

$$\hat{t}(s,t) = 6I_1(s,t) + 12I_2(s,t) \tag{27}$$

$$I_1(s,t) = t^{-1}\int_s^{s+t} \xi\hat{\mu}(\xi)d\xi \tag{28}$$

$$I_2(s,t) = t^{-2}\int_s^{s+t} (s-\xi)\xi\hat{\mu}(\xi)d\xi \tag{29}$$

These are familiar equations in the case of a linear viscous fluid when $(\hat{\mu}) = 0.0$. The equations (19) and (24) yield the shear stress on the lower surface and the equations (20), (21) and (25) together with equations (22) and (23) yield the pressure on the lower surface and the exit coordinate. For the general viscous fluid these equations represent a coupled system of equations for these distributions and the exit coordinate. However, in the case of pure rolling when $(\alpha) = 0.0$

$$s = -\frac{1}{2}t \tag{27}$$

and equations (19) and (20) are uncoupled and identical and I_1 is identically zero. This is a considerable simplification and has been recognized by previous investigators [10, 11, 12, 13].

If the special viscosity deviation function given by equation (4) is substituted in equations (28) and (29) the integrals can be expressed as a combination of elementary functions. The forms of *(sn)* and *(tn)* for cases *(a)*, *(b)* and *(c)* are given in Appendix 1.

Solution Technique

The above system of equations (19), (20) and (21) together with equations (22) and (23) define a nonlinear first order differential equation for *(p)* as a function of *(x)* with an auxiliary condition for (x_b). An approximate solution of this system can be obtained as the solution of a related system of finite difference equations. These are nonlinear algebraic or transcendental equations and may be solved, in principle, by a variety of well-known iterative methods. The approximate solution approaches the true solution as the grid becomes increasingly dense.

The finite difference equations are obtained by constructing a variable grid of *(n)* points along the x axis from (x_a) to (x_b) and replacing the derivative of *(p)* with respect to *(x)* at (x_1) by the slope of a parabola running through (x_1) and the neighboring grid points. This results in a system of $(2n + 1)$ nonlinear equations for the $(2n + 1)$ unknowns (s_1), (p_1) and (x_b). A direct application of Newton-Raphson method to these equations is ineffective and a modified iteration method is shown schematically in Appendix 2. The inlet and outlet regions are separated at (x_a) and solved separately. The variables (p_1) and (x_b) are treated separately from (s_1) and equations (20) and (23) are solved for (p_1) and (x_b) and equation (19) is then solved for (s_1). These modifications reduce computational time and do not affect the accuracy of the solution of the system of finite difference equations.

Starting solutions (s_1, p_1, x_b) can often be obtained from the corresponding solution for the linear viscous fluid (i.e., with $(k) = 0.0$ m²/N). If this starting solution does not produce a convergent solution for the current value of *(k)*, a sequence of solutions can be generated beginning with $(k) = 0.0$ m²/N and arriving at the current value of *(k)* by using the previous convergent solution of the sequence as a starting solution for the next value of *(k)* in the sequence.

Results

Two objectives are pursued in this investigation. The first is to

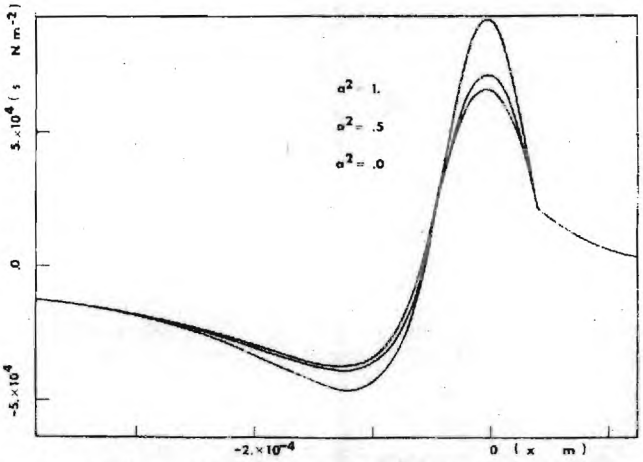

Fig. 5 Distribution of shear stress on the lower surface for 0.1 relative slip

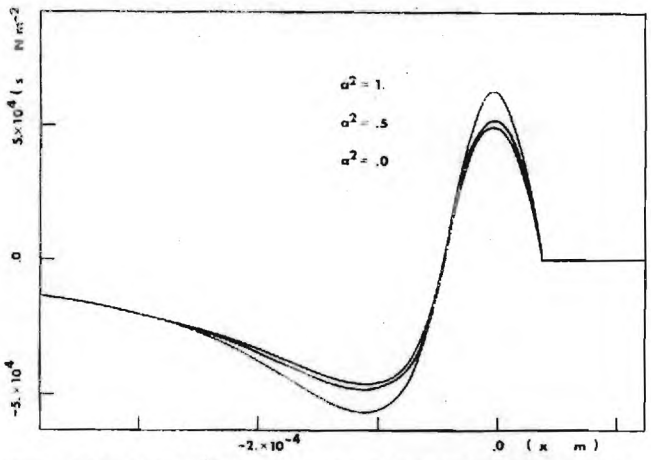

Fig. 4 Distribution of shear stress on the lower surface for 0.0 relative slip

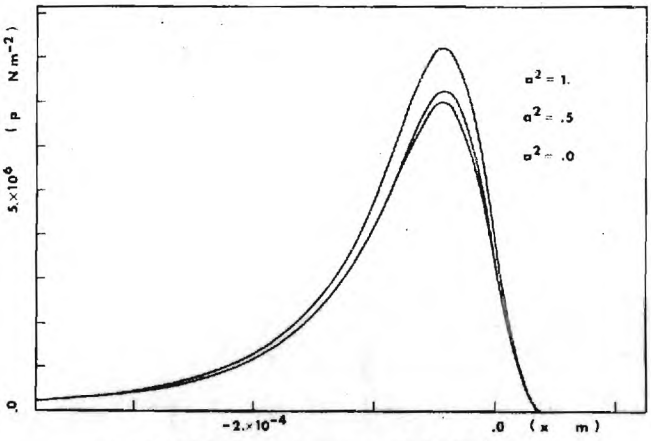

Fig. 6 Distribution of pressure of 0.0 relative slip

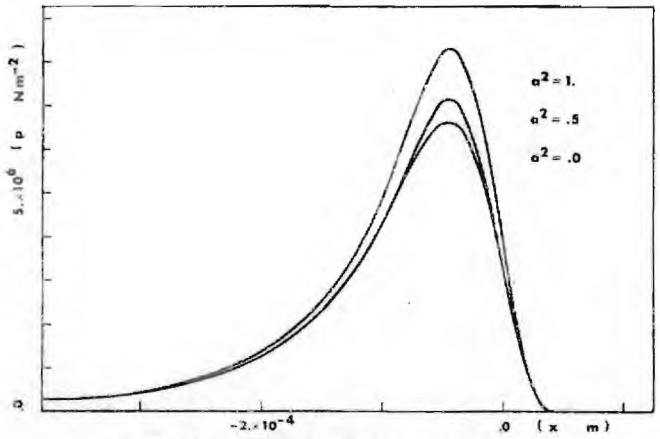

Fig. 7 Distribution of pressure for 0.1 relative slip

determine the details of the distribution of shear stress on the lower surface and the distribution of pressure for typical fluids of each of classes *(a)*, *(b)* and *(c)* in a typical operation. The second objective is to map out the system parameters over a wide range of fluids and operations and to correlate useful design information.

Pursuant to the first objective, a fluid is chosen with $(\rho_0) = 8.9 \times 10^2$ kg/m^3, $(\mu_0) = 1.4 \times 10^{-2}$ N·s/m^2, $(\beta) = 0.0$ m^2/N and *(e)* = *(f)* = 0.0 m^2/N. The fluid is further specified by

Case *(a)* is that of a linear fluid such as hydrocarbon lubricant, case *(b)* is that of a general viscous fluid with zero ultimate viscosity such as a silicone lubricant, and case *(c)* is that of a general viscous fluid with an ultimate viscosity at 25 percent of the base viscosity such as a polyisobutene dissolved in a hydrocarbon lubricant. These fluid specifications are chosen to eliminate the effects of pressure on both the density and viscosity functions. An operation is chosen with $(R) = 5.1 \times 10^{-2}$ m, $(h_0) = 7.6 \times 10^{-6}$ m and $(x_a) = 1.9 \times 10^{-2}$ m. The operation was finally specified by

Case 1 is that of an operation with pure rolling with no relative slip and Case 2 is that of an operation with the same rolling velocity and 0.1 relative slip. Thus, a total of six cases are considered. The resulting distributions of shear stress on the lower surface are shown in Figs. (4) and (5). The corresponding distributions of pressure are shown in Figs. (6) and (7).

Pursuant to the second objective, a number of dependent variables of interest must be introduced. Thus, let *(TR)* be the traction on the lower surface per unit length and *(W)* be the load per unit length. In accordance with standard conventions, *(TR)* is positive when it acts in the positive x direction in Fig. (4). These quantities can be obtained as simple integrals of *(s)* and *(p)* over the interval (x_a) to (x_c) where (x_c) is the exit coordinate of the film. For convenience and economy of display, the following dimensionless parameters are introduced

$$G1 = \beta(2Rh_0^{-1})^{1/2}(\mu_0 U h_0^{-1}) \quad \text{(operations parameter)}$$

$$G2 = \alpha \quad \text{(slip parameter)}$$

$$G3 = k(\mu_0 U h_0^{-1}) \quad \text{(first fluid parameter)}$$

$$G4 = \alpha^2 \quad \text{(second fluid parameter)}$$

$$TRT = \frac{1}{2} TR\, R^{-1}(\mu_0 U h_0^{-1})^{-1} \quad \text{(traction parameter)}$$

$$WT = \frac{1}{2} WR^{-1}(\mu_0 U h_0^{-1})^{-1} \quad \text{(load parameter)}$$

$$TRC = TRW^{-1} \quad \text{(traction coefficient)}$$

$$HT = h_b\, h_0^{-1} \quad \text{(expansion parameter)}$$

$$QT = Q(U\rho_0 h_0)^{-1} = HT \quad \text{(flow rate parameter)}$$

The dimensionless parameters *(HT)* and *(QT)* are of primary interest to the process engineer and will not be further considered here. Curves for *(TRC)* and *(WT)* as a function of $(G1)$ with $(G2)$ and $(G3)$ as parameters and $(G4) = 0.0$ are Presented in Figs. (8) and (9). These curves were calculated for fluids with *(e)* = *(f)* = 0.0 m^2/N (i.e., for a fluid with constant density). Estimates of dimensionless parameters for nonzero values of $(G4)$ can be obtained by vertical interpolation with respect to $(G4)$ between the bounding values of the parameter for $(G4) = 0.0$ as given by the current value of $(G3)$ and for $(G4) = 1.0$ as given by the zero value of $(G3)$.

Discussion

The solution of the system for a given set of data requires 30 to 90 sec of CPU time on the Univac 1108. The accuracy of these solutions is adequate for all practical purposes and these solutions are indistinguishable from the limiting solutions when comparison is possible. The maximum relative error for computation of the iterates was set at 0.1 percent for (s_1) and (p_1) and at 0.01 percent for (x_b). The roots are generally accurate to 4 or 5 significant figures. Comparison of the finite difference solutions based on a variable grid of 50 points with the analytic solution for a linear viscous fluid in case *(a)* indicates that the relative error for (s_1), (p_1) and (x_b) is less than 1.0 percent. Similar agreement would be expected for the general viscous fluid in cases *(b)* and *(c)*. A comparison of solutions for increasingly dense grids confirms this.

The solution technique is stable for values of the operations parameter $(G1)$ which are reasonably below its limiting value $(G1^*)$. This limiting value cannot be easily calculated except for the linear fluid of case *(a)*. In general, $(G1^*)$ is that value of $(G1)$ for which *(WT)* becomes infinite. For the linear fluid with $(G1^*) = 6.58$, stable solutions are easily obtained for all values of $(G1)$ less than 90 percent of $(G1^*)$. As $(G1^*)$ is approached, the pressure distribution becomes quite steep. This occasions an instability in the distribution which is attributable to the second order finite difference representation of the pressure gradient. Hence, the problem can be avoided by a modification of this representation. Such a modification is not necessary for this investigation since the maximum pressure is maintained at relatively low levels (under 1.5×10^7 N/m^2) so as not to validate the assumption of rigid cylinders. At these pressure levels, the effects of fluid compressibility are also negligible since typical values of *(e)* and *(f)* are on the order of 1.5×10^{-10} m^2/N.

An examination of Figs. (4) and (5) reveals a large reduction in peak shear stress for general viscous fluids as compared with linear viscous fluids. The distributions are similar in form. Comparison of Fig. (4) with Fig. (5) indicates a significant dependence of the distributions on the relative slip. The discontinuity in slope of the shear stress distribution at the cavitation coordinate is associated with the creation of fluid streamers there. Examination of Figs. (6) and (7) reveals a similar reduction in peak pressure for general viscous fluids are compared with linear viscous fluids. This results in a loss of load capacity *(WT)* which is particularly significant at large values of the operations parameter. It should also be noted that general viscous fluids with decreasing values of *(a)* have increasingly larger values of the cavitation coordinate (x_b). Comparison of Fig. (7) with Fig. (6) indicates a significant dependence of the pressure distribution for a general viscous fluid on the relative slip. For a linear viscous fluid the pressure distribution is independent of relative slip.

The behavior of a general viscous fluid with zero ultimate viscosity as given by equation (6) is represented in Figs. (8) and (9). These curves are strictly true only for incompressible fluids, but most fluids are incompressible at the pressure levels considered. These curves should be of interest to the machine designer, as

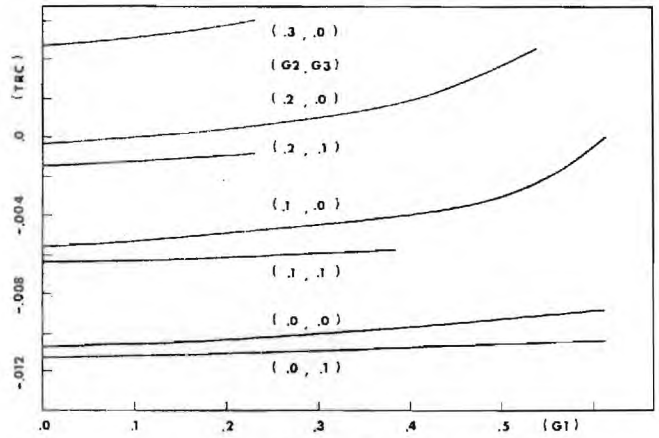

Fig. 8 Traction coefficient *(TRC)* as a function of operation parameter (G1) for given slip parameter (G2) and first fluid parameter (G3)

well as the researcher, working with fluids of class *(b)*. The upward turn of the curves in Fig. (9) should be noted. This indicates the existance of a limiting value of $(G1)$ as a function of $(G2)$ and $(G3)$. Generally, this limiting value $(G1^*)$ becomes larger as $(G2)$ and $(G3)$ increase. As this limit is approached, the peak pressure becomes infinite.

It is also interesting to note the large range of negative traction coefficients in Fig. (8). These values indicate conditions under which cylinder 2 cannot drive cylinder 1. Fig. (9) also allows the determination of the characteristic reciprocal shear stress *(k)* for fluids of class *(b)* by a correlation of the measured load capacity *(WT)* and the operations parameter $(G1)$. Previously published information [5, 18] has been confined to zero values of the operations parameter $(G1)$ and fluid parameters $(G3)$ and $(G4)$.

The problem formulation presented here is independent of the specification of the viscosity function for the general viscous fluid. As such it can be applied to viscosities of the Ree-Eyring type, Maxwell-Milne-Burton type, or the Maxwell-Zaremba-Tanner type. To obtain solutions by the solution technique presented, it is only necessary that the integrals and their partial derivatives be tractable. The integrals need not be in closed form, and, in fact, the viscosity function need not be expressible as a combination of elementary functions. The integral evaluations can be handled numerically with sufficient accuracy for solutions to converge. The solution technique is thus, adequate for the general problem formulation for rigid cylinders. Finally, the basic problem formulation and solution technique can also be retained when the assumption of rigid cylinders is replaced by the assumption of elastic cylinders.

Conclusions

Much of the previous work in the viscous lubrication of rolling and sliding rigid cylinders has been unified in this investigation. Building upon the specialized results of others, a general problem formulation has been obtained which encompasses the general viscous fluid as well as the linear viscous fluid. It is only required that the fluid rheology be defined by the density and viscosity deviation functions alone. A uniform solution technique has also been developed which is adequate for the general problem formulation. Results have been obtained for three special classes of viscosity functions. These indicate the feasibility of this approach. The above results are of practical interest and are valid under lightly loaded conditions.

Acknowledgments

The authors wish to acknowledge the support of NASA Grant NGR 11-002-133, the encouragement of Mr. R. L. Johnson of NASA-Lewis and the National Science Foundation (NSFGK-31154) in connection with their research. The support is greatly appreciated.

References

1 Reynolds, O., "On the Theory of Lubrication and its Application to Mr. *Beauchamp Tower's* Experiments, Including an Experimental Determination of the Viscosity of Olive Oil," *Philosophical Transactions of the Royal Society, London*, Vol. 177, Pt 1., 1886 pp. 157–235.

2 Sommerfeld, A., "Zur hydrodynamischen Theorie der Schmiermittelreibung," *Zeit. f. Math. u. Phy.*, Vol. 50, 1904, pp. 97–155.

3 Guembel, "Ueber geschmierte Arbeitsraeder," *Zeit. f.d. gesamte Turbinenwesen*, Vol. 13, 1916 pp. 205–223, 226–228, 239–241, 245–248, 258–262, 268–272.

4 Martin, H. M. "The Lubrication of Gear-Teeth," *Engineering*, Vol. 102, 1916 pp. 119–121.

5 Peppler, W., "Druck Uebertragung an geschmierten zylindirschen Gleit-und Waelzflaechen," *V.D.I. Forschungsheft*, Vol. 391, 1938, pp. 1–24.

6 Gatcombe, E. K., "Lubrication Characteristics of Involute Spur Gears—a Theoretical Investigation," TRANS. ASME Vol. 67, 1945, pp. 177–188.

7 Cameron, A., "Hydrodynamic Theory in Gear Lubrication," *Journal of the Institute of Petrol.*, Vol. 38, 1952, pp 614–622.

8 McEwen, E., "The Effect of the Variation of Viscosity with Pressure on the Load-carrying Capacity of the Oil Film between Gear-teeth," *Journal of the Institute of Petrol.* Vol. 38, 1952, pp. 646–650.

9 Peppler, W., "Die Theorie der hydrodynamischen Schmierung unter besonderen Beruecksichtigung physikalischer Erweiterungen," *V.D.I. Berichte*, Vol. 20, 1957, pp. 13–30, 182–183.

10 Milne, A. A., "A Theory of Rheodynamic Lubrication for a Maxwell Fluid," *Proceedings of the Conference on Lubrication and Wear*, 1957, pp. 66–71.

11 Tanner, R. I., "Full Film Lubrication Theory for a Maxwell Liquid," *International Journal of Mechanical Science*, Vol. 1, 1960, pp. 206–215.

12 Bell, J. C., "Lubrication of Rolling Surfaces by a Ree-Eyring Fluid," *ASLE Trans.*, Vol. 5, 1962, pp. 160–171.

13 Dyson, A., and Wilson, A. R., "Film Thickness in Elastohydrodynamic Lubrication by Silicone Fluids," *Proceedings of the Institution of Mechanical Engineers* Vol. 180, 1965–66, Pt. 3K, pp. 97–112.

14 Brazinsky, I., Cosway, H. F., Valle, C. F., Jr., Jones, R., and Story, V., "A Theoretical Study of Liquid-Film Spread Heights in the Calendering of Newtonian and Power Law Fluids," *Journal of Applied Polymer Science*, Vol. 14, 1970, pp. 2771–2784.

15 Reher, E. O., and Grader, L., "Zur Berechnung einer isothermer Doppelwalzen-Kalenderstroemung nichtlinear-plastischer Medien," *Plaste u. Kautschuk*, Vol. 18, 1971, pp. 597–601.

16 Williams, G., and Tanner, R. I., "Effects of Combined Shearing and Stretching in Viscoelastic Lubrication," TRANS. ASME, Series F, Vol. 92, 1970, pp. 216–219.

17 Philippoff, W., "Zur Theorie der Strukturviskositaet. I.," *Kolloid Zeit.*, Vol. 71, 1935, pp 1–16.

18 Cameron, A., *Principles of Lubrication*, Wiley, New York, 1963, pp. 155–185.

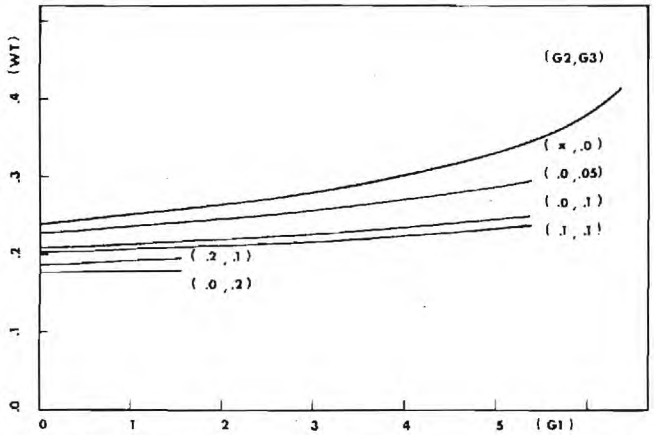

Fig. 9 Load parameter *(WT)* as a function of operation parameter (G1) for given slip parameter (G2) and first fluid parameter (G3) (when G3 = 0, G2 can take on any value)

APPENDIX 1

Case(*a*) $\mu = \mu_0 e^{\beta p}$

$$I_1 = (s, t) = 0.0$$

$$I_2 = (s, t) = 0.0$$

Case(*b*) $\mu = \mu_0 e^{\beta p}(1 + (k\tau)^2)^{-1}$

$$I_1(s, t) = k^2(s^3 + 1.5s^2t + st^2 + 0.25t^3)$$

$$I_2(s, t) = k^2(-0.5s^3 - s^2t - 0.75st^2 - 0.2t^3)$$

Case (*c*) $\mu = \mu_0 e^{\beta} p(1 + a^2(k\tau)^2)(1 + (k\tau^2)^{-1}$

$$I_1(s, t) = \frac{1}{2}(1 - a^2)a^{-2}(2s + t - a^{-2}k^{-2}t^{-1} \ln(1 + a^2k^2t(2s + t)(1 + a^2k^2s^2)^{-1}))$$

$$I_2(s, t) = \frac{1}{6}(1 - a^2)a^{-2}(-3s - 2t + 6a^{-2}k^{-2}t^{-1} +$$
$$- 3a^{-2}k^{-2}st^{-2} \ln(1 + a^2k^2t(2s + t)(1 + a^2k^2s^2)^{-1}) +$$
$$- 6a^{-3}k^{-3}t^{-2} \tan^{-1}(akt(1 + a^2k^2s(s + t))^{-1})$$

APPENDIX 2

Computational Flow Chart

(Subscript *(i)* refers to inlet region and subscript *(e)* refers to outlet region. (JAC) is the Jacobian of the set of equations in the first argument with respect to the set of variables in the second argument. (ERR) is the relative error function of the set of variables in the argument. (e) is the error criterion. (g.t.) is (greater than).

1 Read system parameters $(x_a, R, U, \alpha, p_0, e, f, \mu_0, \beta, k, a, p_a, p_b)$
2 Read state parameter (h_0)
3 Read grid spacing $(dx_I)^T = (dx_{Ii}, dx_{Ie})^T$
4 Read or calculate starting solution $(s_I{}^0, p_I{}^0, x_b{}^0)^T$
5 Set $(s_I{}^*, p_I{}^*, x_b{}^*)^T = (s_I{}^0, p_I{}^0, x_b{}^0)^T$
6 Calculate $(A_{Ii,Ji+1}) = (\text{JAC}(T_{Ii}{}^*, p_{Ji+1}{}^*)$
7 Solve $(T_{Ii}{}^*)^T = (A_{Ii,Ji+1})(p_{J+1} - p_{J+1}{}^*)$
8 Calculate $(s_{Ii})^T$
9 Set $(s_{Ii}{}^*, p_{Ii+1}{}^*)^T = (s_{Ii}, p_{Ii+1})^T$
10 If $(\text{ERR}((s_{Ii}{}^*, p_{Ii+1}{}^*)^T))$ g.t. (eps), go to (6)
11 Calculate $(A_{Ie,Je}) = (\text{JAC}((T_{Ie}{}^*, p_b{}^*), (p_{Je}{}^*, x_b{}^*)))$
12 Solve $(T_{Ie}{}^*, p_b{}^*)^T = (A_{Ie,Je})((p_{Je} - p_{Je}{}^*), (x_b - x_b{}^*))^T$
13 Calculate $(s_{Ie})^T$
14 Set $(s_{Ie}{}^*, p_{Ie}{}^*, x_b{}^*)^T = (s_{Ie}, p_{Ie}, x_b)^T$
15 If $(\text{ERR}((s_{Ie}{}^*, p_{Ie}{}^*, x_b{}^*)^T))$ g.t. (eps), go to (11)
16 Set $(s_I{}^0, p_I{}^0, x_b{}^0)^T = (s_I{}^*, p_I{}^*, x_b{}^*)^T$
17 If $(\text{ERR}(s_I{}^0, p_I{}^0, s_I{}^0)^T))$ g.t. (eps) go to (5)
18 Write $(s_I, p_I, x_b)^T$

Printed in U. S. A.

APPENDIX B

Thesis Abstracts

1. Jorgen Jakobsen, "Lubricant Rheology at High Shear Stress".

This thesis reports capillary viscometric measurements at shear stresses up to 700 psi (4.8×10^7 dyn/cm^2) and reports the general observation of constant viscosity of the investigated unblended lubricants in the range of investigation. The thesis also reports the development of a theory to predict the maximum temperature and the shear stress in elastohydrodynamic liquid films. Solutions can be obtained via dimensionless graphs and contain most other lubrication related quantities. Experimental observations are consistent with the theory.

The purpose of the work is to develop a method to determine the viscous properties of lubricants under elastohydrodynamic operating conditions in a laboratory experiment where the parameters of pressure, temperature and shear stress can be independently varied. The use of a short length capillary has been introduced in order to achieve high shear stress. Reliable entrance and exit corrections for highly viscous capillary flow appears to have been found. The upper limit of shear stress attainable in capillary viscometry has been increased approximately 50 times over previously reported values of about 10^6 dyn/cm^2 (~14.5 psi). The increased shear stress limit is only 3 - 5 times less than the average shear stress experienced by the fluid during passage of an elastohydrodynamic contact. A further increase in shear stress limit up to about 1.4×10^8 dyn/cm^2 (~2 kpsi) appears to be possible. This higher predicted level of shear stress is of the same order of magnitude as the average shear stress to which the fluid is subjected during passage of an elastohydrodynamic contact.

The work has shown that unblended synthetic hydrocarbon oils and a silicone oil tested have constant viscosity as function of shear stress in the investigated range, $\leq$ ~700 psi shear stress, when liquid behavior is displayed. The silicone fluid shows solidification at pressure above 50 kpsi and shear stress above about 10^7 dyn/cm^2, at 75°F. The polymer blended mineral oil shows non-liquid behavior at low stress (above about 10^5 dyn/cm^2, 1.4 psi). These observations of non-liquid behavior of a silicone oil and a ploymer blended mineral oil may possibly provide part of an understanding of the anomalous behavior of these types of lubricants with respect to the ability to create an elastohydrodynamic film. Existing theory for prediction of film thickness assumes implicitly liquid behavior of the lubricants. No discernible time dependent effects were observed for the liquid lubricants.

The thesis further deals with application of the viscosity measurements to determine liquid film behavior in the high pressure area of a point contact configuration. The purpose of this part of the work is to develop a general theory which will predict the elastohydrodynamic quantities of interest, particularly shear stress and maximum temperature, under physically reasonable assumptions. The theory has been developed to a

stage where the shear stress and the maximum attainable temperature each can be determined through a few graphical steps on a dimensionless diagram. Other related elastohydrodynamic quantities can be derived from the maximum temperature and the shear stress.

2. Valentin A. Turchina, "Pressure and Temperature Measurement Techniques in Elastohydrodynamic Contacts".

This research concerns the development of techniques to measure two parameters in elastohydrodynamic point contact lubrication. The measurement of lubrication parameters of pressure distribution, and temperature distribution for the very severe conditions of the contact can be an important tool in the design of the machine parts and in selecting the most efficient lubricant for them. The object of the research performed was to investigate the feasibility of both a proposed pressure measurement technique and a temperature measurement technique.

The pressure measurement technique employed a transducer which consists of a 9.0×10^{-5} m (.0035 in.) diameter piston attached to a cantilever load cell and allowed to move in a 9.0×10^{-5} diameter orifice in the sapphire bearing plate.

The temperature measurement system consists of an infrared micro-detector used to collect infrared radiant energy from the elastohydrodynamic contact and, thereby, allowing the deduction of the local temperature. The problem of separating the infrared radiance contributions from the ball, lubricant film and sapphire bearing plate has been solved by collecting the infrared radiation under three different conditions, two of them using steel spheres with different emissivities and, one using a filter consisting of a calibrated fluid sample "cell", placed between the infrared detector and sapphire bearing plate.

The research was entirely experimental in nature and, in each of the above two measurement systems (pressure and temperature) this thesis has the objective of simply showing the feasibility of the techniques. Therefore, the number of fluids examined and operating conditions used were limited.

3. David L. Walker, "Polymer Degradation in Sliding Elastohydrodynamic Contacts".

This investigation is a study of polymer degradation in sliding elastohydrodynamic lubrication. Elastohydrodynamic lubrication is typically found in highly loaded point contacts such as gears, certain cams and followers and rolling element bearings. The lubricant in this contact is subjected to extremely high pressures (150,000 psi) and very high shear rates (10^6 sec^{-1}). A variety of fluids were examined. These included bulk polymer lubricants, hydrocarbon lubricants, and polymer containing hydrocarbon solutions.

A technique was developed that allows small samples (10 microliters) of the test fluid to be extracted directly from the elastohydrodynamic contact. These samples were then analyzed to determine changes in viscosity and molecular weight distribution.

Severe degradation was found in fluids which had molecular weights of over 1000. This degradation resulted in viscosity losses of up to 70 percent. It is concluded that a designer should assume the base oil viscosity when designing mechanisms which are to use polymer containing hydrocarbon mixtures. When designing for bulk polymers each combination of fluid and mechanism should be tested.

4. Richard K. Kunz, "Thermal and Traction Behavior in Sliding Elastohydrodynamic Contacts".

An existing shear stress theory and lubricant rheological model were studied and evaluated by applying them to traction prediction in a sliding elastohydrodynamic point contact. A computer program was written to calculate shear stresses in the contact based on the theory, and to numerically integrate over the contact area to yield the traction. The results of such calculations, using measured film thicknesses and moving surface temperatures, were compared with measured tractions under several conditions of normal load and sliding speed. The comparison shows that the theory gives a relatively good traction prediction for high speeds, but that it appears to break down at lower speeds, where calculated tractions significantly exceed the measured values. Possible explanations for this disparity include the occurrence of asperity interactions at low speeds and thin films, and the onset of non-Newtonian lubricant behavior at the higher shear stresses which occur in the low speed range.

The effect of variations in the lubricant material properties on the traction was studied by varying the input parameters to the computer program. The traction was found to be increased by an increase in the inlet viscosity of the lubricant, and by a decrease in its temperature-viscosity dependence. A weaker increase in traction was obtained by increasing the fluid's pressure-viscosity dependence.

In order to make the theory applicable to engineering use, a formula for calculating the film thickness was applied, as well as an iterative method for determining the temperature of the moving surface. The film thickness calculation was found to yield satisfactory results for most hydrocarbon oils. The method for determining the temperature is adequate for use in traction calculations at high speeds, but becomes less satisfactory as the speed decreases.

5. Stephen F. Carlson, "The General Viscous Lubrication of Rolling and Sliding Elastic Cylinders".

The action of a fluid between rotating cylinders is examined, a general theory is proposed, a simplified model is derived, and a method of solution for the resultant pressure distribution is developed. The system is considered isothermal. The cylinders are considered smooth and elastic. The relative motion is considered steady and perpendicular to the line of centers. The fluid is considered generally compressible and viscous, that is, completely characterized by its density and viscosity functions. These functions are considered shear stress dependent. A mathematical model is derived, and a

method of solution is developed which yields the pressure distribution corresponding to a set of parameters defining the state of the system. All other information, such as the film thickness and shear stress distributions, can be obtained from this pressure distribution. The method of solution is effective over a wide range of system parameters for well-behaved density and viscosity functions. Solutions are obtained for several classes of fluids of technical importance, and applicable design charts are constructed. The isothermal assumption is reexamined. A thermal generalization of the theory is proposed.

6. Vernon K. Ausherman, "Infrared Temperature Mapping in Elastohydrodynamic Lubrication".

The research undertaken in this thesis develops and refines a technique for determining fluid and bearing surface temperatures in an elastohydrodynamic sliding point contact. The experimental technique utilizes a microdetector which collects and measures infrared radiation emitted at different locations in the Hertzian contact zone. Temperatures are calculated through an iterative procedure developed by an analysis of the bearing and fluid emissive and transmissive characteristics at two intervals in the infrared spectral range. Data obtained by subsequent experimentation using this technique is presented and discussed.